Semi-analytical buckling code development of stiffened and unstiffened plates with a free edge

by

Håkon Stenerud Andersen

THESIS

for the degree of

MASTER OF SCIENCE

(Master i Anvendt matematikk og mekanikk)

Faculty of Mathematics and Natural Sciences
University of Oslo

May 2010

Det matematisk- naturvitenskapelige fakultet
Universitetet i Oslo

Preface

This thesis is written at the University of Oslo (UiO) in collaboration with the Det Norske Veritas (DNV). I have been located at DNV for most of the thesis. Here I have been introduced to a good working environment in the section NTANO368 Advanced Structural Analysis. I would especially like to thank PhD Lars Brubak at DNV and UiO for continuous guidance during my thesis and for making his FORTRAN code available for me. I would also like to thank Professor Jostein Hellesland at UiO for valuable proposals and interesting discussions regarding the semi-analytical model and new possible strength criteria. Dr. Scient. Eivind Steen at DNV has provided valuable advices regarding the practical engineering aspects of the current study. Theoretical discussions with fellow students Jostein Fladby and Jarleiv Øie were much appreciated.

Oslo, 30$^{\text{th}}$ May, 2010.

Håkon Stenerud Andersen

Abstract

Criteria for estimating the ultimate strength, using a semi-analytical approach, of unstiffened and stiffened plates with a free edge are addressed. The semi-analytical approach is based on a Rayleigh-Ritz discretisation of the deflections, and the equilibrium equations are solved using an incremental perturbation technique with arc length control. Large deflection theory is used to include non-linear geometrical effects associated with slender cases. Development of ultimate strength criteria, accounting for plasticity, is an important part of the present work. The model is implemented in FORTRAN, and the ultimate strength estimates are compared to the strength found with ABAQUS. Testing of stiffened plates are performed for eccentric flat bar stiffeners parallel to the free edge. It is possible to include other types of stiffeners and stiffener orientations in the model. The first linear elastic buckling mode is used as imperfection when testing the criteria. Combined imperfections are also studied for the stiffened cases. Strength estimates produced with the final model are satisfactory when compared to ABAQUS results. These tests are performed for a wide range of plate cases. All important buckling modes for stiffened plates are then considered, except from local buckling of the stiffeners themselves. The latter is normally not a restriction, since design codes requires rather stocky stiffener sections.

Some model assumptions and principles with respect to boundary conditions, permanent plastic deformations and assumed imperfections were also investigated. These effects were studied using finite element analyses, for both unstiffened and stiffened plates. The tests were carried out for a small number of plate combinations, but the results presented indicated that the assumptions made in the semi-analytical model were reasonable.

Contents

Notation

Subscripts

x, y, z	Components in Cartesian coordinates
$,xy$	Differentiation with respect to x and y
f	Flange
w	Web
s	Stiffener
0	Initial

Superscripts

a	Component representing a plate with a free edge
b	Component representing a simply supported plate
c	Component representing linear variations of in-plane displacements
me	The location at the midlength of a free edge or of an edge stiffener
pb	Bending contribution of the plate
pm	Membrane contribution of the plate
L	Linear
NL	Nonlinear

Symbols

E	Young's modulus
J	Torsional constant
ν	Poisson's ratio
E_T	Hardening modulus
f_Y	Yield strength
L	Plate length
b	Plate width
t	Plate thickness
t_w	Web thickness
h_w	Web height (relative to the centre line of the plate)

h_s	Stiffener height (relative to the surface of the plate)
t_f	Flange thickness
b_f	Flange width
A_s	Area of the cross-section of a stiffener
N_{stiff}	Number of stiffeners
I	Moment of inertia about the middle plane of the plate
u, v, w	Displacements in a Cartesian coordinate system
Δx	End-shortening of the plate in x-direction
w_i^a, w_{ij}^b	Amplitudes for the out-of-plane displacements
u_i^a, u_{ij}^b, u^c	Amplitudes for the displacements in x-direction
v_i^a, v_{ij}^b, v^c	Amplitudes for the displacements in y-direction
w_0	Model imperfection
$w_t = w_0 + w$	Total displacements
w_{0i}^a, w_{0ij}^b	Amplitudes of the model imperfection
N_{dof}	Total number of degrees of freedom
σ_x, σ_y, τ_{xy}	In-plane stresses in a Cartesian coordinate system
ϵ_x, ϵ_y, γ_{xy}	In-plane strains in a Cartesian coordinate system
$S_x = P_x/A_{plate}$	External stress in the x-direction
P_x	Total force applied to the plate (in the x-direction)
A_{plate}	Cross sectional area of the plate surface perpendicular to the x-direction
$\bar{\sigma}$	Weighted average stress
Λ	Load factor
Π	Total potential energy
U	Strain energy
T	Potential energy of the external loads
β	Weight of bending stress in the combination plate criterion
B	Constant used in formulation of β
B_{mod}	Modified B dependent on total deflection w_t
$\Lambda = \sqrt{f_Y/S_E}$	Slenderness of the plate
S_E	Elastic buckling stress (minimum eigenvalue)
A	Surface area of the plate in the xy-plane

Chapter 1

Introduction

1.1 Background

In this thesis the ultimate capacity, ultimate strength limit (USL), of unstiffened and stiffened rectangular plates with a free edge, or a stiffened free edge is considered. The elastic buckling load of such plates was studied by Eiding [1] and a semi-analytical model for large deflection post-buckling analysis was developed by Brubak [2]. In this thesis the method develpoed by Brubak [2] will be studied further and the possibilities of improving and expanding it will be explored. This semi-analytical methods is developed as an alternative to the simplified calculations found in design rules, for instance DNV-RP-C-201 [3], or fully non linear finite element analysis. The semi-analytical method gives more accurate results than the design rule formulations and will be more computationally efficient and easier to use than a typical finite element program. One limitation of such models is the restrictions, on boundary conditions, geometry, loads etc, imposed during development of the theory. The semi-analytical method is based on an Rayleigh-Ritz formulation, with an assumed set of displacements, capable of modelling both global and local plate deformation shapes. The incremental solution procedure follows the method presented in Steen [4]. A similar semi-analytical formulation for simply supported plates, with irregular stiffeners, are developed by Brubak and Hellesland [5, 6]. This formulation utilizes Airy's stress function to relate in-plane displacements and out-of-plane deflection. In the current model the complete displacement field will, as in Brubak [2], be used, since an appropriate stress function was not found. The stiffeners are only modelled as beams in both Brubak and Hellesland [5, 6] and Brubak [2], and local stiffener buckling should be prevented by selecting suitable stiffener dimensions in accordance with for instance DNV-RP-C-201 [3].

A related type of semi-analytical incremental Rayleigh-Ritz approach, with corresponding buckling calculations, is the basis for the program PULS [7], Panel Ultimate Limit State, developed by DNV. The theory in Byklum [8] and in Brubak and Hellesland [5, 6] contains the current background for PULS, which is in constant development. Byklum [8] calculates global and local deformation separately instead of using a combined calculation as in Brubak and Hellesland [5, 6] and Brubak [2]. The global model developed by Byklum

[8] uses orthotropic plate theory to account for the overall (global) buckling of the plate and stiffeners. In the local model the stiffeners are included with a full set of deformations, and stiffener buckling is then included. Such local buckling of stiffeners was, as mentioned, not considered in Brubak [2], since the stiffeners are modelled as beams. It will also be neglected in the current model.

An alternative type of semi-analytical method for simply supported plates was developed by Paik at el. [9] for unstiffend plates and by Paik and Lee [10] for stiffened plates. These methods are based on an incremental Galerkin method, which instead of using the principle of stationary potential energy uses the partial differential equations for large deflection theory and an integration criterion to approximate the strenght.

Post-buckling capacity of plates

Post-buckling capacity of plates, or "overcritical strength", may be significant, and it is of great interest when estimating the ultimate capacity. The reason for this post-buckling capacity is the redistribution of stresses from the flexible parts with large deflections to the stiffer parts along the supported edges and, if present, along the stiffeners. If the ultimate capacity of the plate is reached, the plate will collapse. It will then no longer contribute to the overall strength of the structure, and might even lead to collapse of the entire structure if the global redundancy is limited.

Plate examples

Plates or girders with a free edge or a stiffened free edge may be encountered in many practical engineering applications like ships and bridges. Examples of such plates in ships can be longitudinal and transverse girders. Collapse of girders in ships may cause collapse of the entire ship. For ships in operation it is typical to experience hogging and sagging, which leads to bending and twisting of the entire structure. The global loads give considerable amounts of local in-plane loads, compression/tension and shear, for the plates. The plates may in addition to in-plane loads experience water pressure or pressure caused by internal cargo. Plates with a free edge will typically experience considerable loading parallel to the free edge. Shear loading and pressure, on the other hand, are not expected to be significant for plates with a free edge. Plates with free edges will usually be stiffened to avoid significant out-of-plane deflections. Figure 1.1 shows a typical girder profile.

Unstiffened plates with a free edge will typically be relevant for flange outstands etc, where one edge of the flange will be free. In such cases the flanges might experience local buckling, see Figure 1.2, and the current model will be able to estimate the capacity.

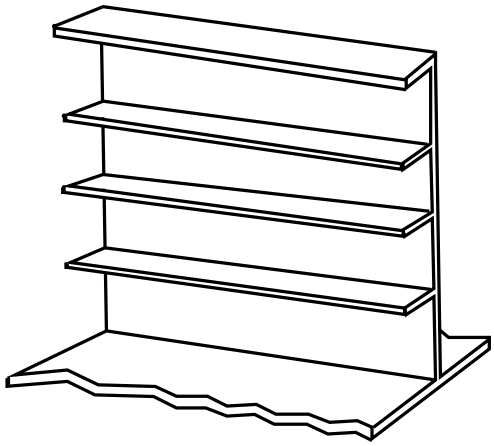

Figure 1.1: Typical girder with eccentric flat bar stiffeners.

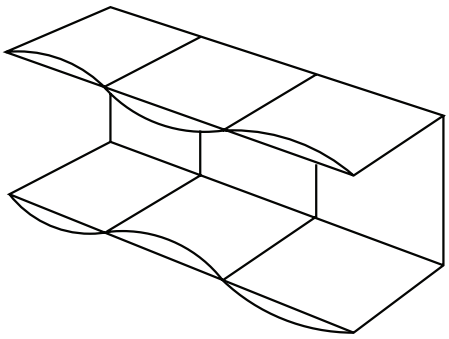

Figure 1.2: Channel section beam with local buckling of flange outstand.

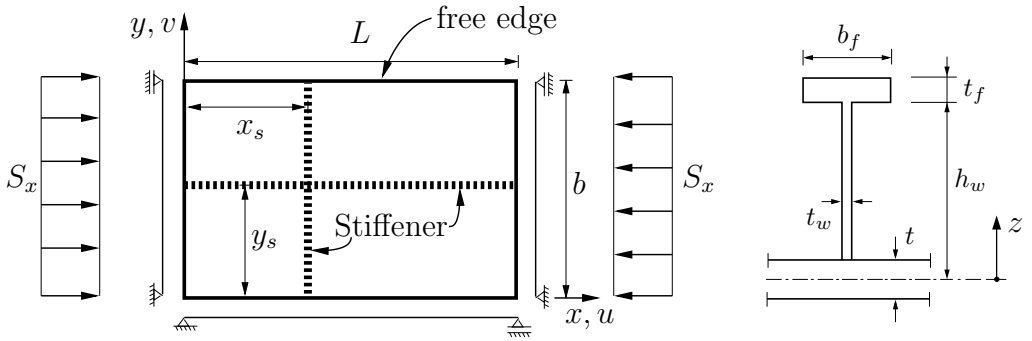

Figure 1.3: Shows (a) the general plate case, with uniaxial loading of a stiffened plate with a free edge and three simply supported edges, and (b) the cross section of an eccentric stiffener.

1.2 Problem formulation

Plate definition

A principle sketch of the rectangular plate studied is given in Figure 1.3a. This plate has three simply supported edges and one free, unsupported, edge. The externally applied stress, $S_x = P_x/A_{plate}$, is evenly distributed along the plate edges perpendicular to the free edge. Both stiffened and unstiffened plate cases will be studied in the current work. Figure 1.3b shows a principle sketch of an eccentric stiffener. In the current work only longitudinal[1] sniped eccentric flat bar stiffeners[2] will be considered. The free edge will always be stiffened when stiffeners are included.

The plates are assumed to be connected to other construction parts. Supported edges are assumed to be connected to other plates, and are therefore assumed to be straight in-plane. The loaded edges are assumed parallel, and a uniform end shortening of the plate, in the x-direction, will be present. Some remarks to the assumption of keeping the inner edge, parallel to the free edge, straight are given in Section 8.3.3. Aspects of assuming simply supported edges is discussed in Section 8.2.3. Mathematical definitions of boundary conditions etc. will be given in Chapter 3.

Scope

In Brubak [2] first yield of von Mises membrane stress is used as criterion, when estimating the ultimate plate strength. This criterion was tested for unstiffened plates and a non conservative deviation in ultimate strength limit estimates, when compared to finite element analyses, was observed for intermediate and rather thick plates. For unstiffened plates with

[1] In the x-direction

[2] $t_f = b_f = 0$

a free edge the deflection at the free edge will be considerable and large bending stresses in the plate should be expected. These bending stresses are not accounted for in the criterion used by Brubak [2]. Ultimate strength limits of stiffened plates are not considered in Brubak [2] but similar non conservative differences should be expected for small stiffeners, since such cases will be almost unstiffened. All expansions and modification of the orignal model, Brubak [2], will be done by modifying the FORTRAN code developed by Brubak.

Finding a suitable criterion, for unstiffened and stiffened plates, is the first, and main, scope in this thesis. A criterion for the unstiffened case will be developed first. This criterion will then be modified and combined with a suitable stiffener criterion to estimate the strength of stiffened plates. The proposed criteria will be tuned and compared with finite element analyses.

Torsional stiffness of stiffeners is not included in the original model developed by Brubak [2]. This contribution will be derived and included in the present model and the effect of torsional stiffness will be discussed.

PULS, see PULS manual [7], uses model imperfection when estimating the ultimate capacity of plates. Model imperfections are assumed to be in critical/preferred modes and do not necessarily reflect the real imperfection shape in welded structures. Such model imperfections are used to ensure conservative strength estimates of the plates. Imperfection amplitudes in PULS are given for the global and local imperfection separately. Similar global and local imperfections can be defined for stiffened plates with a stiffened free edge and the selected criterion will be tested for these imperfections. The global imperfection will be given by the deflection of an unstiffened plate and the local deflection will be given by deflection between stiffeners.

Some investigations of common uncertainties and assumptions will also be conducted. These studies are performed using finite element analysis, for selected unstiffened and stiffened cases. Assumptions regarding boundary conditions and imperfections are considered, in addition to the effect of permanent plastic deformation.

1.3 Presentation of chapters

The thoeretical background for the study will be given in Chapter 2 to 4. Chapter 2 includes the general theory and principles. In addition, it explains the principles of elastic buckling and ultimate strength. The development of the semi-analytical model is described in Chapter 3. An example of a snap-through problem is also included to illustrate the capabilities of the model. Principles of the finite element modelling is described in Chapter 4.

Improvements and modifications of the model will now be discussed in the second main part of this study. The improved ultimate strength (collapse) criteria are described and discussed in Chapter 5. This chapter contains two main parts, one for unstiffened and one for stiffened plates. The effect of torsional rigidity of stiffeners are studied in Chapter 6. Chapter 7 consists of two parts. The first part consideres the effect of local stiffener buckling with respect to formulations in DNV-RP-C-201 [3]. The second part includes a

study of combined imperfection, with reference to the imperfections used in PULS. Some aspects of the assumptions in the semi-analytical model are studied in Chapter 8. This chapter is also divided into one part for unstiffened and one part for stiffened plates.

Conclusions and further work proposals are given in Chapter 9.

Chapter 2

General Theory

2.1 Thin plates and large deflection

The following assumptions are made in the Navier-Kirchoff theory for thin plates with large deflections:

- In-plane deformations and rotations remain small during deformation.
- The thickness of the plate is much smaller than the length and width (breadth) of the plate.
- The plate consists of isotropic linear elastic materials.
- Lines that are normal to the middle plane remain normal to the middle plane after deformation of the plate. This implies that transverse shear deformations are neglected. In addition, the thickness of the plate is assumed constant meaning that lines normal to the middle surface maintain their initial length.
- The normal stress in the transverse direction is neglected.

The last two assumptions are called the Kirchhoff assumptions, see Bazant and Cedolin [11]. There is an inconsistency in these assumptions since the plate is assumed to both maintain its thickness and have zero normal stress in the transverse direction. This inconsistency can be seen from the general Hooks law, see Benham, Crawford and Armstrong [12], which is valied for isotropic linear elastic materials. If the stress in the transverse direction is zero then Hooks law implies that $\epsilon_z = -\frac{\nu}{E}(\sigma_x + \sigma_y)$, which is a contradiction to the assumption of constant thickness in the transverse direction. It is natural to conclude that this inconsistency can be neglected, since the Kirchhoff assumptions are well known and accepted.

For large deflection theory, as for common linearised theory, the strains can be divided into membrane strains and bending strains. The membrane and bending strain components will have the superscripts "pm" and "pb" respectively. Membrane strains will be considered first.

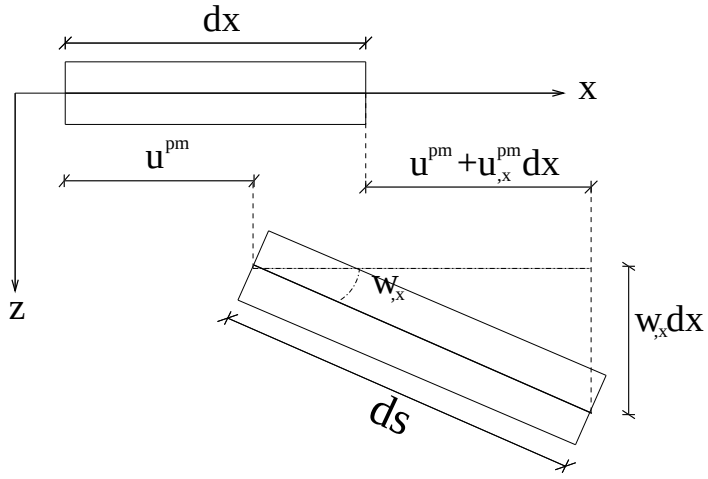

Figure 2.1: An infinitesimal segment of a plate viewed in the xz-plane for initial and deflected configuration when large deflection theory is used. Here u^{pm} and w denotes the displacement of the middle plane in the x- and z-direction respectively.

Membrane strains

In large deflection theory the membrane strains are given by the Green strains, which differ from the classical linearised theory. A derivation of the normal strain in the x- and y-direction for a plate without imperfection will be given here. The corresponding derivation of the shear component can be found in Bazant and Cedolin [11]. Figure 2.1 shows an infinitesimal segment of the plate in the xz-plane. The membrane strain in the x-direction, ϵ_x^{pm}, is defined as the relative change in length from initial configuration to deflected configuration. Mathematically this can be written as:

$$\epsilon_x^{pm} = \frac{ds - dx}{dx} = \frac{ds}{dx} - 1 \tag{2.1}$$

where ds and dx is defined in Figure 2.1. Using Pythagoras' theorem, the length after deflection can be written as:

$$ds^2 = (dx + u_{,x}^{pm}dx)^2 + (w_{,x}dx)^2$$

$$\Longrightarrow ds = dx\sqrt{1 + 2u_{,x}^{pm} + (u_{,x}^{pm})^2 + w_{,x}^2}$$

Putting this expression into Equation 2.1 gives:

$$\epsilon_x^{pm} = \sqrt{1 + 2u_{,x}^{pm} + (u_{,x}^{pm})^2 + w_{,x}^2} - 1$$

Using the known series expansion $\sqrt{1+x} = 1 + \frac{1}{2}x + O(x^2)$, see Rottmann [13], the expression above can be written as:

$$\epsilon_x^{pm} = \frac{1}{2}(1 + 2u_{,x}^{pm} + (u_{,x}^{pm})^2 + w_{,x}^2) + \dots$$

where "..." indicates the higher order terms. The first assumption made above indicates that $u^{pm}_{,x} << 1$, which implies that $(u^{pm}_{,x})^2 << u^{pm}_{,x}$. In addition, the large deflection assumption, implying large rotations and small in-plane strains, gives $w^2_{,x} >> (u^{pm}_{,x})^2$. In Figure 2.1, it is assumed that $\sin(w_{,x}) \approx w_{,x}$, which implies that $w_{,x} << 1$. Since we are looking at large deflection theory with small in-plane strains, it is implied that $w^2_{,x}$ is of the same order as $u_{,x}$. Given these assumptions the higher order terms in the series expansion and $(u^{pm}_{,x})^2$ can be neglected. The membrane strain will then be given by:

$$\epsilon^{pm}_x = u^{pm}_{,x} + \frac{1}{2}w^2_{,x}$$

Applying the same arguments for the yz-plane would result in the following strain expression:

$$\epsilon^{pm}_y = v^{pm}_{,y} + \frac{1}{2}w^2_{,y}$$

In both the strain expressions above the effect of in-plane rotations are neglected while out-of-plane rotations are considered. This is consistent with the first assumption given above. The in-plane shear strain γ_{xy}, see Bazant and Cedolin [11], is:

$$\gamma^{pm}_{xy} = u^{pm}_{,y} + v^{pm}_{,x} + w_{,x}w_{,y}$$

The semi-analytical model presented here includes initial out-of-plane imperfection. The Green strains without imperfections presented above are included to show the basic assumptions and steps. The Green strains with an initial out-of-plane imperfection, $w_0 = w_0(x, y)$, was developed by Marguerre in [14] and they are:

$$\epsilon^{pm}_x = u^{pm}_{,x} + \frac{1}{2}w^2_{,x} + w_{0,x}w_{,x} \tag{2.2}$$

$$\epsilon^{pm}_y = v^{pm}_{,y} + \frac{1}{2}w^2_{,y} + w_{0,y}w_{,y} \tag{2.3}$$

$$\gamma^{pm}_{xy} = u^{pm}_{,y} + v^{pm}_{,x} + w_{,x}w_{,y} + w_{0,x}w_{,y} + w_{0,y}w_{,x} \tag{2.4}$$

where $w = w(x, y)$ is the deflection relative to the initial imperfection.

Bending strains

The bending strains are the same as those used in regular linearised plate theory for bending of plates, and a result of the first Kirchhoff assumption presented above. Figure 2.2 shows the displacement component due to bending in the x-direction. A similar displacement component will be present in the y-direction. These displacement components are given by:

$$u^{pb} = -zw_{,x}$$
$$v^{pb} = -zw_{,y}$$

The first Kirchhoff assumption implies that the first order (linear) strain relations apply to the bending strains:

$$\epsilon^{pb}_x = u^{pb}_{,x} = -zw_{,xx} \tag{2.5}$$

$$\epsilon_y^{pb} = v_{,y}^{pb} = -zw_{,yy} \tag{2.6}$$

$$\gamma_y^{pb} = u_{,y}^{pb} + v_{,x}^{pb} = -2zw_{,xy} \tag{2.7}$$

The bending strain equations will not be influenced by an initial imperfection since w is defined as deflection relative to the imperfection. In Figure 2.2 this point can be illustrated by adding an initial rotation, $w_{0,x}$, to the initial plate segment. The rotation of the deformed segment will then be given by $w_{0,x} + w_{,x}$ and the displacement component due to bending will still be given by $-zw_{,x}$, implying the same strains in both cases.

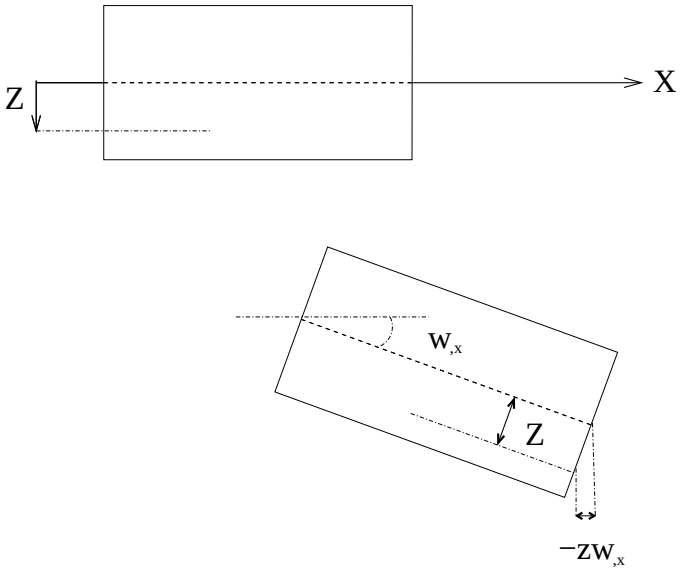

Figure 2.2: An infinitesimal segment of a plate viewed in the xz-plane. The displacement variation in the x-direction because of bending is illustrated.

Total strains

The total strains are then given by the sum of the bending and membrane strains:

$$\epsilon_x = \epsilon_x^{pm} + \epsilon_x^{pb} \tag{2.8}$$

$$\epsilon_y = \epsilon_x^{pm} + \epsilon_y^{pb} \tag{2.9}$$

$$\gamma_{xy} = \gamma_{xy}^{pm} + \gamma_{xy}^{pb} \tag{2.10}$$

where the strain contributions are given in Equation 2.2 to 2.4 and Equation 2.5 to 2.7.

2.2 Material assumptions

2.2.1 Material law

For thin plates it is common to assume a plane stress situation. This implies that, in addition to neglecting σ_z as assumed in Section 2.1, one also neglects the transverse shear stresses, τ_{xz} and τ_{yz}. The material in this model is assumed to be isotropic and linear elastic. Hooke's law for a isotropic linear elastic material with a plane stress condition can be found in Benham, Crawford and Armstrong [12] and is given by the following equations:

$$\sigma_x = \frac{E}{1-\nu^2}(\epsilon_x + \nu\epsilon_y) \tag{2.11}$$

$$\sigma_y = \frac{E}{1-\nu^2}(\nu\epsilon_x + \epsilon_y) \tag{2.12}$$

$$\tau_{xy} = \frac{E}{2(1+\nu)}(\gamma_{xy}) = G\gamma_{xy} \tag{2.13}$$

where the in-plane stresses are given by σ_x, σ_y and τ_{xy}, and the in-plane strains are given by ϵ_x, ϵ_y and γ_{xy}. The normal stresses and strains are defined positive in tension. In addition, the material properties are given by the Young's modulus E and the Poisson's ratio ν.

2.2.2 Yield criterion

Brubak [2] used first yield of the von Mises yield criterion applied to membrane stresses as a criterion for the ultimate strength limit. This section will give a general presentation of the von Mises yield criterion and some initial comments on the predictions of ultimate limit strength in Brubak [2]. In Cook, Malkus, Plesha and Witt [15], the von Mises yield criterion is given for a general state of stress as follows:

$$\sigma_e = \frac{1}{\sqrt{2}}\left[(\sigma_x-\sigma_y)^2 + (\sigma_y-\sigma_z)^2 + (\sigma_z-\sigma_x)^2 + 6\left(\tau_{xy}^2+\tau_{yz}^2+\tau_{zx}^2\right)\right]^{1/2} \leq f_Y$$

where f_Y gives the yield stress of the material, which is assumed to be elastic perfectly plastic. The assumption of plane stress presented above simplifies the yield criterion to:

$$\sigma_e = \sqrt{\sigma_x^2 + \sigma_y^2 - \sigma_x\sigma_y + 3\tau_{xy}^2} \leq f_Y \tag{2.14}$$

The von Mises criterion for membrane yielding will then be:

$$\sigma_e^{pm} = \sqrt{(\sigma_x^{pm})^2 + (\sigma_y^{pm})^2 - \sigma_x^{pm}\sigma_y^{pm} + 3(\tau_{xy}^{pm})^2} \leq f_Y \tag{2.15}$$

where the superscript "pm" indicates membrane stresses in the plate. Equation 2.15 is included here to give a consistent presentation of the theory developed by Brubak [2]. New possible strength criteria will be presented in Chapter 5.

2.2.3 Selected material properties

The following material properties are used to model the material:

$$E = 208000 \text{ MPa}$$

$$\nu = 0.3$$

$$f_Y = 235 \text{ MPa}$$

These material properties are quite typical for steel materials. Steel properties are selected since this is the common material in ship structures.

2.3 Principle of stationary potential energy

The total potential energy, Π, of a deformable body is defined as:

$$\Pi = U + T$$

where U denotes the internal strain energy and T denotes the potential energy of external forces. The principle of virtual work is a well known condition for equilibrium of systems and can be written as follows:

$$\delta W + \delta H = 0$$

where δW and δH denotes the virtual work of internal and external forces respectively. The virtual displacements applied to the system must satisfy the kinematic conditions. This principle can be applied to non-conservative systems and systems with inelastic material properties.

To simplify the principle of virtual work it is assumed that the system is conservative[1] and that the material is elastic. The expression for virtual work of internal forces will under these assumptions be equal to the strain energy of the system. This simplified version of the principle of virtual work is called the principle of stationary potential energy. In mathematical terms this can be written as:

$$\delta\Pi = \delta U + \delta T = 0$$

where $\delta\Pi$ gives the variation of the total potential energy.

The principle of stationary potential energy can also be stated on an incremental form:

$$\delta\dot{\Pi} = \delta\dot{U} + \delta\dot{T} = 0 \tag{2.16}$$

where $\dot{\Pi} = \frac{\partial\Pi}{\partial\eta}$ and η denotes a propagation (incrementation) parameter. In the following work, the rate form of the principle of stationary potential energy will be used, due to the non-linear contributions caused by large deflection theory.

[1] A conservative system is a system where the work done by internal and external forces is only dependent on the start and end configuration, and not how the loads are applied between these two configurations.

2.4 Expressions for potential energy

2.4.1 General overview

The theoretical expressions for potential energy of plates and stiffeners will be introduced in this section. These expressions are important in the development of the Rayleigh-Ritz approach presented in Chapter 3. The potential energy consists of two main contributions, as described in Section 2.3. The first is the potential strain energy and the second is the potential energy of external loads. Potential strain energy is the energy stored in a system with elastic material during deformation, while potential energy of external loads is defined as the negative work of external loads.

2.4.2 Potential strain energy of the plate

The potential strain energy for a plate can be expressed as follows, see for instance Cook, Malkus, Plesha and Witt [15] or Brush and Almroth [16]:

$$U^p = \frac{1}{2}\int_V \boldsymbol{\sigma}^T \boldsymbol{\epsilon}\, dV \tag{2.17}$$

where V denotes the volume of the plate, $\boldsymbol{\sigma} = [\sigma_x, \sigma_y, \sigma_z, \tau_{xy}, \tau_{xz}, \tau_{yz}]^T$ denotes the stress vector and $\boldsymbol{\epsilon} = [\epsilon_x, \epsilon_y, \epsilon_z, \gamma_{xy}, \gamma_{xz}, \gamma_{yz}]^T$ denotes the strain vector. The thin plate assumption in Section 2.1 simplifies the stress and strain vector to $\boldsymbol{\sigma} = [\sigma_x, \sigma_y, \tau_{xy}]^T$ and $\boldsymbol{\epsilon} = [\epsilon_x, \epsilon_y, \gamma_{xy}]^T$ respectively. The assumptions in Section 2.1 also implies no coupling between membrane and bending contributions for stresses and strains. This property makes it convenient to split the stress and strain vector into one contribution from membrane and one from bending. The total potential energy can then be written as:

$$U^p = \frac{1}{2}\int_V (\boldsymbol{\sigma}^{pm} + \boldsymbol{\sigma}^{pb})^T (\boldsymbol{\epsilon}^{pm} + \boldsymbol{\epsilon}^{pb})\, dV \tag{2.18}$$

where the subscript *pm* denotes plate membrane contributions and *pb* denotes plate bending contributions. By utilising the decoupling of bending and membrane contributions, Equation 2.18 simplifies to:

$$U^p = U^{pm} + U^{pb} \tag{2.19}$$

where

$$U^{pm} = \frac{1}{2}\int_V (\boldsymbol{\sigma}^{pm})^T \boldsymbol{\epsilon}^{pm} dV \tag{2.20}$$

and

$$U^{pb} = \frac{1}{2}\int_V (\boldsymbol{\sigma}^{pb})^T \boldsymbol{\epsilon}^{pb} dV \tag{2.21}$$

Potential membrane strain energy

Multiplying the vectors in Equation 2.20 gives:

$$U^{pm} = \frac{1}{2}\int_V \left[\sigma_x^{pm}\epsilon_x^{pm} + \sigma_y^{pm}\epsilon_y^{pm} + \tau_{xy}^{pm}\gamma_{xy}^{pm}\right] dV$$

Integrating over the thickness of the plate and introducing Hooke's law for a plane stress condition, see Section 2.2.1, simplifies this expression to:

$$U^{pm} = \frac{C}{2}\int_A \left[(\epsilon_x^{pm})^2 + (\epsilon_y^{pm})^2 + 2\nu\epsilon_x^{pm}\epsilon_y^{pm} + \frac{1-\nu}{2}(\gamma_{xy}^{pm})^2\right] dA \tag{2.22}$$

where A is the area of the plate in the xy-plane, $C = \frac{Et}{1-\nu^2}$ and t is the plate thickness. The constant C is called the extensional stiffness of the plate.

Potential bending strain energy

The potential bending strain energy can be written as:

$$U^{pb} = \frac{1}{2}\int_V \left[\sigma_x^{pb}\epsilon_x^{pb} + \sigma_y^{pb}\epsilon_y^{pb} + \tau_{xy}^{pb}\gamma_{xy}^{pb}\right] dV$$

In this case Hooke's law and bending strain expressions (Equations 2.5, 2.6 and 2.7) are introduced and the expression is integrated over the thickness. This gives the following expression:

$$U^{pb} = \frac{D}{2}\int_A \left[(w_{,xx} + w_{,yy})^2 - 2(1-\nu)(w_{,xx}w_{,yy} - w_{,xy}^2)\right] dA \tag{2.23}$$

where $D = \frac{Et^3}{12(1-\nu^2)}$ denotes the bending stiffness of the plate.

2.4.3 Potential strain energy of stiffeners

The stiffeners are included as beams with isotropic linear elastic material. This implies that the potential strain energy of a general stiffener can be written as follows:

$$U^s = \frac{1}{2}\int_{V_s} \sigma_s\epsilon_s dV$$

where V_s is the stiffener volume, σ_s is the stiffener stress and ϵ_s is the stiffener strain. The linear elastic material assumption for the stiffener implies that $\sigma_s = E\epsilon_s$, giving the following expression for the potential energy:

$$U^s = \frac{E}{2}\int_{V_s} \epsilon_s^2 dV \tag{2.24}$$

Potential strain energy of stiffener in the x-direction

For a stiffener in the x-direction, parallel to the free edge, the strain distribution is given by:

$$\epsilon_x = \epsilon_x^{pm} - z w_{,xx}$$

Introducing this expression into Equation 2.24:

$$U^{s,x} = \frac{E}{2} \int_0^L \int_{A_s} \left[\epsilon_x^{pm} - z w_{,xx}\right] dA_s dx$$

where A_s gives the cross-sectional area of the stiffener. Integrating over the cross section of the stiffener gives:

$$U^{s,x} = \left[\frac{EI}{2} \int_0^L w_{,xx}^2 \, dx - e_c E A_s \int_0^L \epsilon_x^{pm} w_{,xx} \, dx + \frac{E A_s}{2} \int_0^L (\epsilon_x^{pm})^2 \, dx \right]_{y=y_s} \tag{2.25}$$

where $I = \int_{A_s} z^2 dA_s$ is the second moment of inertia for the stiffener about the midplane of the plate (z = 0), $e_c = \frac{1}{A_s} \int_{A_s} z dA_s$ is the distance from the midplane of the plate to the stiffeners centre of area and y_s gives the y-coordinate of the stiffener.

The formulation above neglects the stiffeners torsional stiffness. This torsional stiffness might be important for cases with local buckling shapes, resulting in considerable torsional twisting of the stiffener which is resisted by torsional stiffness. Neglecting the torsional stiffness is a conservative approach since the total stiffness then is underestimated. The torsional stiffness can approximately be accounted for by using the contribution due to St. Vernant torsion:

$$U^{sT,x} = \frac{GJ}{2} \int_0^L \left[w_{,xy}^2 \right]_{y=y_s} dx \tag{2.26}$$

where $G = \frac{E}{2(1+\nu)}$ is the shear stiffness and J denotes the torsional constant.

Too conservative results might be present for cases with considerable torsional twisting if the torsional stiffness is neglected. This effect is studied further in Chapter 6.

Potential strain energy of stiffener in the y-direction

The expression for potential strain energy of stiffeners in the y-direction, perpendicular to the free edge, will be analogous to the expressions for stiffeners in the x-direction:

$$U^{s,y} = \left[\frac{EI}{2} \int_0^b w_{,yy}^2 \, dy - e_c E A_s \int_0^b \epsilon_y^{pm} w_{,yy} \, dy + \frac{E A_s}{2} \int_0^b (\epsilon_y^{pm})^2 \, dy \right]_{x=x_s} \tag{2.27}$$

where x_s gives the x-coordinate of the stiffener. The torsional stiffness can be approximated by:

$$U^{sT,y} = \frac{GJ}{2} \int_0^b \left[w_{,xy}^2 \right]_{x=x_s} dy \tag{2.28}$$

2.4.4 Potential energy of external loads

Potential energy for three typical load cases will be presented in this section. The presentation of the different load cases is based on the theory in Brubak [2].

Potential energy of external membrane loading of the plate in the x-direction

In-plane loading of the plate in the x-direction gives the following load potential:

$$T^{p,x} = -\Lambda S_{x0} t b \Delta u \tag{2.29}$$

where S_{x0} is the reference stress for the external load, $\Lambda = \frac{S_x}{S_{x0}}$ is the load factor and Δu is the plate shortening.

Potential energy of external lateral pressure load in the z-direction

The potential energy due to an external pressure load in the z-direction can be calculated by the following formula:

$$T^{p,z} = -\int_0^b \int_0^L p\, w\, dx\, dy \tag{2.30}$$

where p = p(x,y) represents the lateral pressure on the xy-plane. This load case is not considered further in the current work.

Potential energy of external load applied to stiffener in x-direction

End loading of stiffeners is generally a result of interconnections with other structural elements or continuous stiffeners over several spans. The expression for the load potential of stiffeners with end loading in the x-direction can be written as:

$$T^{s,x} = -P_{sx}\Delta u - P_{sx} e_c w_{2,x} + P_{sx} e_c w_{1,x} \tag{2.31}$$

where the resultant force (positive in compression) on the stiffener is denoted by P_{sx}, $w_{1,x}$ is the end rotation of the stiffener at $x = 0$ and $w_{2,x}$ is the end rotation of the stiffener at $x = L$. This load case is not considered further in the current work.

2.5 Buckling and post-buckling behaviour

The semi-analytical model presented here includes large deflection theory. This theory makes it possible to trace non-linear loading responses. When performing such analysis it is necessary to assume an imperfection. The imperfection causing the most flexible configuration should be chosen to ensure a conservative estimate of the ultimate capacity. For plates, the first elastic buckling shape, corresponding to the lowest elastic buckling load, is usually assumed to give the most flexible configuration.

Linear Elastic buckling

Linear elastic buckling, also denoted elastic buckling stress limit (ESL), is defined as the load causing out-of-plane deflection when a perfect plate[2] only is subjected to in-plane loads. To estimate the linear elastic buckling load, it is necessary to study equilibrium of the plate in deformed configuration. Out-of-plane deflections can only be present after reaching the buckling load, which represents a bifurcation point in the load-deflection path. Material yielding is not accounted for when finding the linear elastic buckling mode.

Linear elastic post-buckling behaviour

It is important to determine if the bifurcation point, represented by the linear elastic buckling load, is stable or unstable when utilising the post-buckling strength for a case with linear elastic materials. The system is stable if the external load can be increased after reaching the buckling load without causing failure. For plates, as considered in this model, the load-deflection and load-shortening curves are typically as given in Figure 2.3. As shown in this figure, the load can be increased above the buckling load without implying failure. Plates are therefore stable with respect to buckling behaviour. For curved shells, as in Figure 2.4, it is usually observed that the load must be decreased in the post-buckling range to avoid failure. Curved shells are therefore unstable when buckling behaviour is considered.

Figure 2.3 and Figure 2.4 also includes the behaviour when an initial imperfection is present. The load-shortening and load-deflection response of the imperfect plate is observed to resemble the response of the perfect plate, but with a reduced stiffness due to the imperfection. Based on these observations it is concluded that imperfect plates are stable, while imperfect curved shells are unstable. The stable behaviour of plates motivates the possibility of utilising post-buckling strength when estimating the ultimate capacity for in-plane loading. Curved shells will not be considered in the further work, but was included here for comparison.

[2] A perfect plate has no initial imperfection and represents the ideal case.

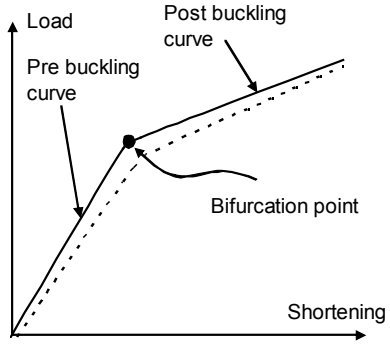

(a) load-shortening

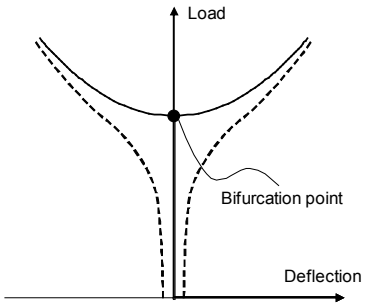

(b) load-deflection

Figure 2.3: Example of typical (a) load-shortening and (b) load-deflection curves for plates (stable buckling). The solid lines represent the path of a perfect plate while the dotted lines represent the path of an imperfect plate.

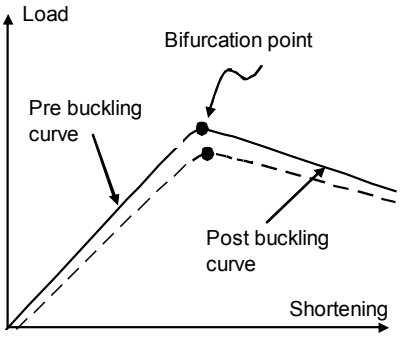

(a) load-shortening

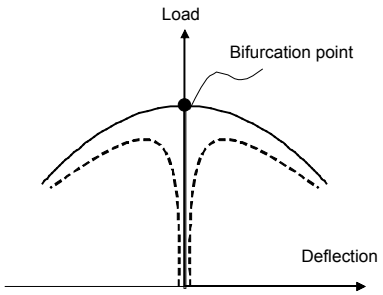

(b) load-deflection

Figure 2.4: Example of typical (a) load-shortening and (b) load-deflection curves for curved shells (unstable buckling). The solid lines represent the path of a perfect shell while the dotted lines represent the path of an imperfect shell.

Buckling and ultimate capacity

Ultimate capacity, also called ulitmate strength limit (USL), is the maximum load the system can carry without collapsing. Both material non-linearity, yielding, and large deflections must be accounted for when estimating the ultimate capacity of a system. The ultimate capacity is identified by the highest point in the load-shortening and load-deflection curves. Typical load-shortening and load-deflection curves for a system, with yielding and large deflections, are illustrated in Figure 2.5.

When estimating the ultimate capacity of slender plates the post-buckling capacity is very important. The stable behaviour in the post-buckling range gives the possibility of utilising the full potential for such plates. For plates with a lower slenderness, the ESL is significantly higher than the yield stress, implying that non-linear effects are small when estimating the ultimate capacity. This implies that the load-shortening and load-deflection paths for an imperfect plate, estimated by the semi-analytical model, will be almost linear for non-slender cases, while they will be non-linear for the slender cases. When plasticity is included, it is evident that the load-shortening and load-deflection curve will be non-linear for both cases due to yielding.

The ultimate capacity of plates is dependent of the post-buckling behaviour (if the plate is slender) and yielding of the material. In a fully non-liner analysis, with non-linear geometry and non-linear material properties, the interaction between these effects are included. This interaction should be accounted for in the semi-analytical model, by using a suitable strength (collapse) criterion.

It is important that the permanent plastic deformation is limited, when unloading from the ultimate capacity, if the ultimate capacity should be utilised in dimensioning of real structures. Significant permanent plastic deformations will change the stiffness properties of the plate, which might result in a considerably more flexible configuration when the plate is reloaded. The effect of permanent plastic deformations are further studied for some unstiffened plates in Section 8.2.4 and for some stiffener plates in Section 8.3.2.

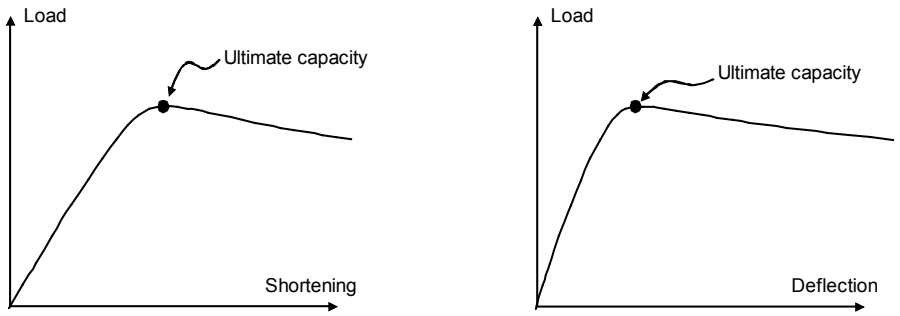

(a) load-shortening **(b)** load-deflection

Figure 2.5: Example of typical (a) load-shortening and (b) load-deflection curves for plates with imperfection when yielding and large deflection theory is included. The deflection and shortening are relative to the initial imperfection.

Characterisation of buckling and deformation shapes

When studying the buckling and deformation shape of stiffened and unstiffened plates with a free edge, two characteristic shapes are observed. These shapes are defined as follows:

- **Local shape**
  A local buckling or deformation shape, see Figure 2.6, is defined by the cases where the out-of-plane deflection along the free edge is limited, implying that the plate is almost simply supported along all edges. The deflections of the plate will only be significant in the interior of the plate between stiffeners. This kind of buckling(deformation) shape is only possible for plates with a stiffened free edge.

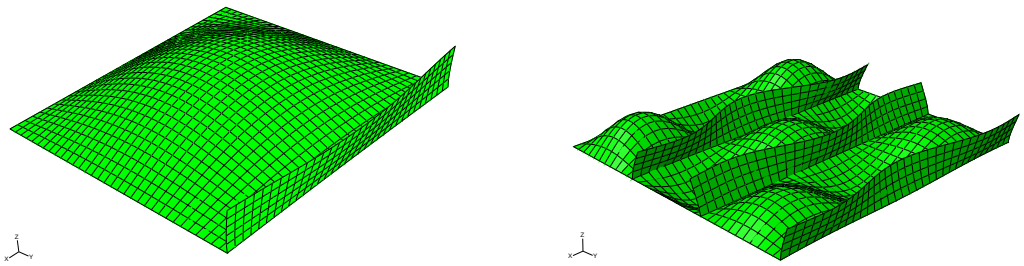

(a) One stiffener **(b)** Three stiffeners

Figure 2.6: Examples of local buckling (deformation) shape for a quadratic plate with (a) one stiffener or (b) three stiffeners. The edge stiffener is directed along the free edge.

- **Global shape**
  A global buckling or deformation shape, see Figure 2.7, is dominated by deflections along the free edge. This will always be the case for unstiffened plates. It will also occur for stiffened plates if the stiffeners are small.

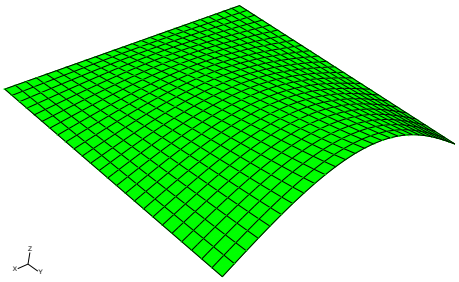

Figure 2.7: Example of global buckling (deformation) mode for an unstiffened plate with a free edge.

Buckling and deformation shapes with combinations of the two characteristic shapes will be possible for stiffened plates.

Chapter 3

The incremental Rayleigh-Ritz method and the semi-analytical model

3.1 General overview

In the expressions for potential energy (Section 2.4) the strains, curvatures and displacements are continuous functions. Using the principle of stationary potential energy directly to find these functions will be impossible for a general case. One way of finding an approximate solution to such problems is the Rayleigh-Ritz method. In the Rayleigh-Ritz method weighted sums of suitable shape functions are used to discretise the principle of stationary potential energy. This reduces a system with an infinite number of unknowns to a system with a finite number of unknowns. The unknowns will now be the weights of the shape functions, instead of the displacement values at all locations. In mathematical terms, the assumed displacements can be written as follows:

$$u = \sum_{i=1}^{N_u} u_i f_{u,i} \qquad v = \sum_{i=1}^{N_v} v_i f_{v,i} \qquad w = \sum_{i=1}^{N_w} w_i f_{w,i} \tag{3.1}$$

where u_i, v_i and w_i are the weights and $f_{u,i}$, $f_{v,i}$ and $f_{w,i}$ are the assumed shape functions. The selected shape functions must be continuous and satisfy the forced boundary conditions[1], but not the natural boundary conditions[2].

The expressions for potential energy of the plate and stiffeners, presented in Section 2.4, are dependent on the plate membrane strains. This will not be a problem in the discretisation since the membrane strains are related to the displacements through Equations 2.2, 2.3 and 2.4. All the potential energy contributions can then be expressed in terms of displacements and discretised by use of Equation 3.1.

[1]Forced boundary conditions are constraints on the system related to displacements and rotations.
[2]Natural boundary conditions are constraints on the system related to forces and moments.

The stationary potential energy on rate form, see Equation 2.16, can be written as follows for a discretised displacement field:

$$\delta\dot{\Pi} = \frac{\partial\dot{\Pi}}{\partial d_i}\delta d_i = 0 \tag{3.2}$$

where $\mathbf{d} = [u_1, \ldots, u_{N_u}, v_1, \ldots, v_{N_v}, w_1, \ldots, w_{N_w}]^T$ and δd_i is the variation of the displacement component d_i. Assuming $\delta d_i \neq 0$ and $\delta d_j = 0$ for all $j \neq i$ implies the following set of equations:

$$\frac{\partial\dot{\Pi}}{\partial d_i} = 0, \;\; \mathrm{i} \;\; = 1, 2, \ldots, (N_u + N_v + N_w) \tag{3.3}$$

Equation 3.3 gives the relation between the displacement amplitudes and the load factor. An extra equation will be necessary to solve the system, since the load factor also is unknown. This extra equation will be introduced together with the complete incremental system in Section 3.5.

Using discrete displacement assumptions, as in Equation 3.1, forces the system to deform as a combination of the assumed shape functions. This implies that the Rayleigh-Ritz approach overestimates the stiffness of the system. The stiffness will approach the actual value as the number of shape functions is increased. This implies that a regular convergence test, checking if the changes in estimates are small as the numbers of terms are increased, is a sound way of verifying the estimate.

Stress computations, based on the derivatives of the displacements found with Rayleigh-Ritz, will generally be less accurate than the displacement estimates. This is based on the fact that the derivatives of an approximate function will be less accurate than the approximate function itself. The derivatives will only be exactly the same if the assumed displacements are capable of modelling the exact shape, which is only likely for simple systems. This implies that a higher number of shape functions are necessary to get good stress estimates.

3.2 Assumed displacements

The assumed displacements used in the model consist of one contribution representing a global deformation shape and one representing a local deformation shape. In addition a linear variation, representing in-plane compression/elongation, is included for u and v. The displacement components representing a global deformation shape are:

$$u^a(x,y) = \sum_{i=1}^{M_{ua}} u_i^a \frac{y}{b}\sin(\frac{\pi i x}{L}) \tag{3.4}$$

$$v^a(x,y) = \sum_{i=1}^{M_{va}} v_i^a \frac{y}{b}\cos(\frac{\pi i x}{L}) \tag{3.5}$$

$$w^a(x,y) = \sum_{i=1}^{M_{wa}} w_i^a \frac{y}{b}\sin(\frac{\pi i x}{L}) \tag{3.6}$$

where u_i^a, v_i^a and w_i^a are the amplitudes of the relevant shape function.

The following displacements components are used to model the local deformation shape:

$$u^b(x,y) = \sum_{i=1}^{M_{ub}} \sum_{j=1}^{N_{ub}} u_{ij}^b \sin(\frac{\pi i x}{L}) \sin(\frac{\pi j y}{b}) \tag{3.7}$$

$$v^b(x,y) = \sum_{i=1}^{M_{vb}} \sum_{j=1}^{N_{vb}} v_{ij}^b \sin(\frac{\pi i x}{L}) \sin(\frac{\pi j y}{b}) \tag{3.8}$$

$$w^b(x,y) = \sum_{i=1}^{M_{wb}} \sum_{j=1}^{N_{wb}} w_{ij}^b \sin(\frac{\pi i x}{L}) \sin(\frac{\pi j y}{b}) \tag{3.9}$$

where u_{ij}^b, v_{ij}^b and w_{ij}^b are the amplitudes of the relevant shape function.

The contributions to in-plane displacements due to compression/elongation are:

$$u^c(x,y) = u^c \frac{x}{L} \tag{3.10}$$

$$v^c(x,y) = v^c \frac{y}{b} \tag{3.11}$$

where u^c and v^c are amplitudes of elongation.

A combination of these displacement components should be sufficient to model the loading response for all relevant cases of unstiffened and stiffened plates. The total displacement components are then:

$$w = w^a + w^b \tag{3.12}$$

$$u = u^a + u^b + u^c \tag{3.13}$$

$$v = v^a + v^b + v^c \tag{3.14}$$

Further discussions of the selected shape functions can be found in Brubak [2].

3.3 Imperfection

It is necessary to use an initial out-of-plane imperfection when performing a large deflection load-response analysis. The first linear elastic buckling mode with an imperfection amplitude of 5 mm will, as in Brubak [2], mainly be used as imperfection in the current work. A discussion of the effect of changes in the imperfection amplitude for unstiffened plates are given in Section 8.2.2. To include the possibility of both global and local buckling shapes, as well as combinations of the two, the imperfection is given by a combination of the following:

$$w_0^a(x,y) = \sum_{i=1}^{M_{wa}} w_{0i}^a \frac{y}{b} \sin(\frac{\pi i x}{L}) \tag{3.15}$$

$$w_0^b(x,y) = \sum_{i=1}^{M_{wb}} \sum_{j=1}^{N_{wb}} w_{0ij}^b \sin(\frac{\pi i x}{L}) \sin(\frac{\pi j y}{b}) \tag{3.16}$$

where w_{0i}^a and w_{0ij}^b are the weights of the appropriate shape function. The selected shape functions of the initial imperfection are analogous to the shape functions for out-of-plane displacements stated above, see Equations 3.6 and 3.9. The total imperfection will be:

$$w_0 = w_0^a + w_0^b \tag{3.17}$$

The first linear elastic buckling mode is found by a classical Rayleigh-Ritz approach presented in Brubak, Hellesland and Steen [17]. In Brubak, Hellesland and Steen [17] the case of a simply supported plate with arbitrary stiffeners is studied, using only the assumed displacement shape of $w_0^b = w_0^b(x, y)$ above. This implies a somewhat different system of equations in the current model, but the principles are the same. The system of equations, on matrix form, is given in Brubak [2].

The model is able to approximate any kind of imperfection by fitting the w_{0i}^a and w_{0ij}^b values. This possibility is utilised in Section 7.2 where a local and global imperfection will be combined. Some further remarks on the selection of imperfection and calculation of the linear elastic buckling mode can be found in Brubak [2].

3.4 Boundary conditions

All the supported edges of the plate is assumed to be simply supported, with the possibility of in-plane compression. This gives the following boundary conditions for the plate:

$$\left.\begin{array}{lll} u(0,y) = 0, & u(L,y) = u^c, & v(x,0) = 0 \\ w(0,y) = 0, & w(L,y) = 0, & w(x,0) = 0 \end{array}\right\} \tag{3.18}$$

where the coordinate system is defined in Figure 1.3.

The possibility of using other boundary conditions for the assumed displacement field is discussed in Brubak [2]. In Section 8.2.3 the possibility of using the ultimate capacity of a simply supported case as an estimate for cases with one or more clamped edges is investigated. These tests are carried out with the finite element method for an unstiffened plate. The effect of keeping the edge at $y = 0$ straight, $v(x, 0) = 0$, is discussed, for a stiffened plate, in Section 8.3.3.

3.5 Complete incremental form

3.5.1 Propagation parameter

The semi-analytical model uses the incremental propagation theory presented in Steen [4] to trace the load-response. This theory uses an arc length parameter to propagate the solution. Propagation with an arc length parameter makes it possible to trace complex load-responses as snap through, see Section 3.6, and snap back behaviour.

The relation between external load factor, Λ, and the displacement components, d_i, see Brubak [2], is given by:

$$\dot{\Lambda}^2 + \sum_{i=1}^{N_{\text{dof}}} \frac{\dot{d}_i^2}{t^2} = 1 \tag{3.19}$$

where $\dot{d}_i$ and $\dot{\Lambda}$ are the rates of the displacement amplitude d_i and the load factor Λ respectively. N_{dof} gives the total number of degrees of freedom defined by:

$$N_{\text{dof}} = M_{ua} + (M_{ub} \times N_{ub}) + M_{va} + (M_{vb} \times N_{vb}) + M_{wa} + (M_{wb} \times N_{wb}) + 2 \tag{3.20}$$

The displacement vector, $\mathbf{d}$, is defined as follows:

$$\begin{aligned} \mathbf{d} = [d_i] =& \Big[d_1, d_2, d_3, ..., d_{N_{\text{dof}}} \Big] \\ =& \Big[u_1^a, ..., u_{M_{ua}}^a, u_{11}^b, u_{12}^b, ..., u_{M_{ub}N_{ub}}^b, u^c, v_1^a, ..., v_{M_{va}}^a, v_{11}^b, \\ & v_{12}^b, ..., v_{M_{vb}N_{vb}}^b, v^c, w_1^a, ..., w_{M_{va}}^a, w_{11}^b, w_{12}^b, ..., w_{M_{wb}N_{wb}}^b \Big] \end{aligned} \tag{3.21}$$

A numerical procedure will be used to trace the incremental behaviour. This procedure is based on a Taylor exspansion of Λ and d_i as functions of the arc length η:

$$d_i(\eta + \Delta\eta) = d_i(\eta) + \dot{d}_i(\eta)\Delta\eta + \frac{1}{2}\ddot{d}_i(\eta)\Delta\eta^2 + O(\Delta\eta^3)$$

$$\Lambda(\eta + \Delta\eta) = \Lambda(\eta) + \dot{\Lambda}(\eta)\Delta\eta + \frac{1}{2}\ddot{\Lambda}(\eta)\Delta\eta^2 + O(\Delta\eta^3)$$

where $\Delta\eta$ is an arc length increment.

The solution space is then discretised with a finite arc length increment. Each step is given a number related to a point along the load-response curves. The end step of an increment can then be expressed by the following Taylor expansion:

$$d_i^{k+1} = d_i^k + \dot{d}_i^k \Delta\eta + O(\Delta\eta^2) \tag{3.22}$$

$$\Lambda^{k+1} = \Lambda^k + \dot{\Lambda}^k \Delta\eta + O(\Delta\eta^2) \tag{3.23}$$

where the indexes k and $(k+1)$ denotes the consecutive step numbers, $\dot{d}_i^k$ is the rate of the displacement amplitude i at step k and $\dot{\Lambda}^k$ gives the load factor rate at step k.

Only a first order approximation, neglecting the terms of order $\Delta\eta^2$ and higher in Equations 3.22 and 3.23, will be included in the following work. This implies that a small incremental arc length step, $\Delta\eta$, should be used to ensure sufficient accuracy. A further discussion with regards to accuracy and alternative propagation methods can be found in Brubak [2].

3.5.2 Complete incremental equation system

A complete system of equations can now be found by combining Equation 3.3 and Equation 3.19. This combined system of equation will then have the same number of unknowns as equations. The incremental form of Equation 3.3, expressed with Einstein's summation rule, is:

$$\frac{\partial \dot{\Pi}}{\partial d_i} = \frac{\partial}{\partial \eta}\frac{\partial \Pi}{\partial d_i} = K_{ij}\dot{d}_j + G_i\dot{\Lambda} = 0 \tag{3.24}$$

where the incremental stiffness matrix is defined by:

$$K_{ij} = \frac{\partial^2 \Pi}{\partial d_i \partial d_j} \tag{3.25}$$

and the vector G_i, in the inremental load vector $-G_i\dot{\Lambda}$, is defiend by:

$$G_i = \frac{\partial^2 \Pi}{\partial d_i \partial \Lambda} \tag{3.26}$$

As a result of using large deflection theory, some sub matrices of the incremental stiffness matrix, $\mathbf{K}$, will be non-linear in the sense that they are dependent on the displacement amplitudes. These non-linear contributions are a result of using Green strains for the membrane strains in the plate. The $\mathbf{K}$ matrix will be calculated based on the displacement amplitudes at the start of the step. This linearizes the equations for stationary potential energy resulting in a tangential stiffness matrix[3]. This simplification is used in the development of Equation 3.24 where $K_{ij} = \frac{\partial^2 \Pi}{\partial d_i \partial d_j}$ is assumed to be independent of changes in the displacement amplitudes over the increments. In reality $\mathbf{K}$ would change during the increment, as the displacement amplitudes changes, resulting in a more complex expression for the stationary potential energy of the system. Neglecting the change in $\mathbf{K}$ over the increments should give satisfactory results if the arc length increment is small, since this implies small incremental changes in the displacement amplitudes.

The G_i vector will, on the other hand, be independent of the displacements and load factor for the considered load case. Since all the expressions for potential strain energy is independent of the load factor, it is evident that G_i of Equation 3.26 simplifies to:

$$G_i = \frac{\partial^2 T^{p,x}}{\partial d_i \partial \Lambda}$$

for the current load case. Using the expression for $T^{p,x}$ from Equation 2.29 and the fact that the plate shortening in the x-direction (Δu) is $-u^c$, G_i simplifies to:

$$G_i = \begin{cases} S_{xo}tb, & \text{if } i = M_{ua} + (M_{ub}xN_{ub}) + 1 \\ 0, & \text{if } i \neq M_{ua} + (M_{ub}xN_{ub}) + 1 \end{cases} \tag{3.27}$$

which is not dependent on the load factor or the displacement amplitudes.

[3] A tangential stiffness matrix is the initial stiffness matrix of the system at the start of a given step.

The complete incremental system of equations, in matrix notation, are:

$$\mathbf{K}\dot{\mathbf{d}} + \mathbf{G}\dot{\Lambda} = 0 \tag{3.28}$$

$$\dot{\Lambda}^2 + \frac{1}{t^2}\dot{\mathbf{d}}^T\dot{\mathbf{d}} = 1 \tag{3.29}$$

The full expressions for $\mathbf{K}$ can be found in Brubak [2] and will not be repeated here.

3.5.3 Solution procedure

The load propagation is divided into steps as described earlier. Implying that Equations 3.19 and 3.24 must be solved for each increment k. Equation 3.24 is a linear system of equations giving the following expression for $\dot{d}_j^k$:

$$\dot{d}_j^k = -\dot{\Lambda}(K_{ij}^k)^{-1}G_i = \dot{\Lambda}Q_j^k \tag{3.30}$$

where

$$Q_j^k = -(K_{ij}^k)^{-1}G_i \tag{3.31}$$

There is no superscript on G_i since this vector is independent of the load factor and displacement amplitudes, see Equation 3.27, and it will remain the same for all increments. Introducing $\dot{d}_j^k$, from Equation 3.30, into Equation 3.19, and solving for $\dot{\Lambda}^k$ gives:

$$\dot{\Lambda}^k = \pm\frac{t}{\sqrt{t^2 + \sum_{j=1}^{N_{\text{dof}}}(Q_j^k)^2}} \tag{3.32}$$

Equation 3.32 has two possible solutions for the load factor rate. The solutions have opposite signs and the $\dot{\Lambda}^k$ value giving the smoothest curve will be used. A criterion for selecting the suitable arc length increment can be found in Steen [4]. This criterion is restated here for completeness, and states that the correct $\dot{\Lambda}^k$ must satisfy the following condition:

$$\sum_{j=1}^{N_{\text{dof}}}\dot{\Lambda}^k\left(\frac{Q_j^k\dot{d}_j^{k-1}}{t^2} + \dot{\Lambda}^{k-1}\right) > 0 \tag{3.33}$$

The solution at the next step, $(k+1)$, can now be found by the Taylor expansions presented earlier, see Equations 3.22 and 3.23, neglecting terms of second order and higher:

$$d_j{}^{k+1} = d_j{}^k + \dot{d}_j{}^k\Delta\eta \tag{3.34}$$

$$\Lambda^{k+1} = \Lambda^k + \dot{\Lambda}^k\Delta\eta \tag{3.35}$$

where $\dot{d}_j{}^k$ and $\dot{\Lambda}^k$ is given by Equations 3.30 and 3.32 respectively. This procedure can then be continued for each step until a suitable criterion is fulfilled, making it possible to trace the load-response behaviour of the system.

3.6 Snap through example

Using arc length increments, as presented in Section 3.5, makes the model capable of tracing any type of load-shortening behaviour. In this section the possibility of modelling snap through problems will be illustrated with an example. The estimates from the semi-analytical model will be compared to ABAQUS results.

Plate dimensions

In the following section an unstiffened plate with $L = 3000$ mm, $b = 1000$ mm and $t = 14$ mm will be studied. The applied imperfection of the plate will be the first buckling mode with an imperfection of 5 mm.

Selecting parameters

It is necessary to set $M_{wa} = 3$, to include the possibility of snapping. A deflection shape with three half waves in the x-direction can then be modelled. Such a deflection shape will be expected after snapping for the current plate. The number of terms for the other displacement contributions are the same as those used by Brubak [2] and the complete set of parameters is stated in Section 5.2.2. It is expected that a very small value for the arc length increment, $\Delta\eta$, will be necessary, since there is no method for equilibrium correction in the semi-analytical model. Results for $\Delta\eta = 0.04$ and $\Delta\eta = 0.005$ will be presented in this section.

Finite element model

The finite element model used in this example includes finite strain formulations and linear-elastic material properties. In addition it uses arc length increments, as the semi-analytical model. These properties make the ABAQUS model comparable to the semi-analytical model. The arc length solution procedure in ABAQUS, called the modified Riks method (see Section 4.3.2), is somewhat more refined and it includes equilibrium iterations and an automatic procedure for deciding increment size. The element model consists of 850 four node elements with reduced integration (S4R). A discussion of element types etc. can be found in Chapter 4.

Results

The load-shortening response for the selected $\Delta\eta$ values are presented together with ABAQUS results in Figure 3.1. Figure 3.2 shows the deflection shape before and after snap through.

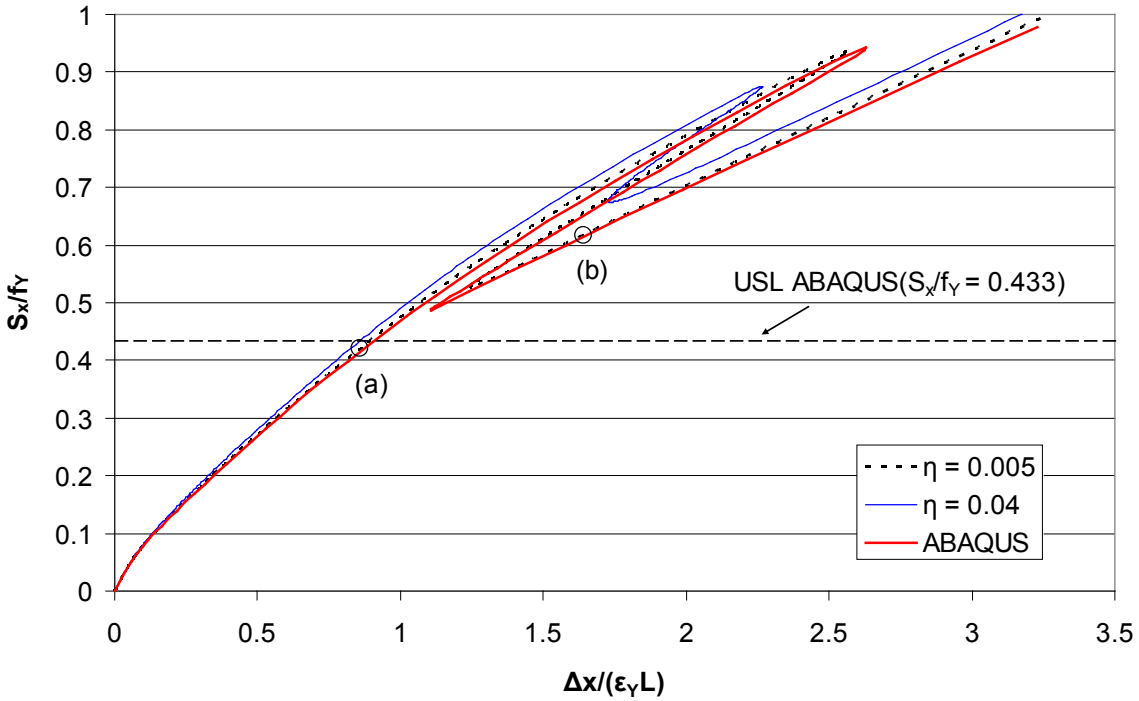

Figure 3.1: The load-shortening response as predicted by the semi-analytical model and ABAQUS. The ultimate strength prediction by ABAQUS, see Section 5.2.3, is also included as a referance value. Points (a) and (b) corresponds to the subfigures in Figure 3.2.

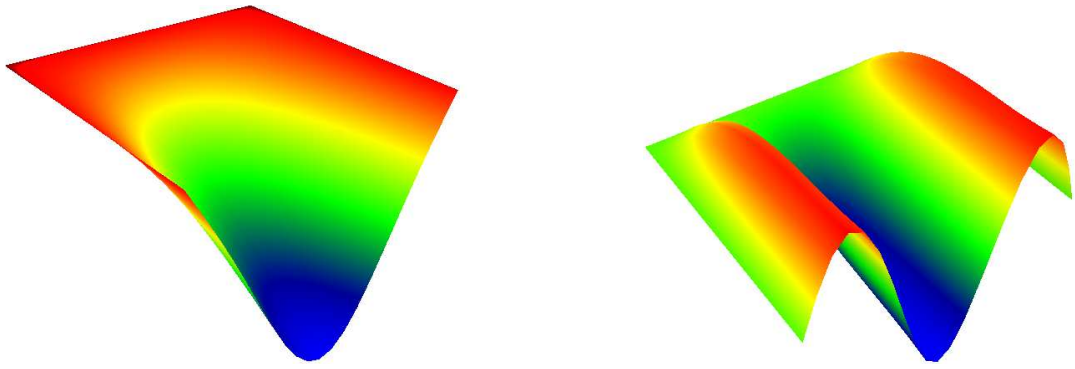

Figure 3.2: Deflection shape (a) before and (b) after snap through for an unstiffened plate with a free edge and three simply supported edges. The dimensions used for the plate are $L = 3000$ mm, $b = 1000$ mm and $t = 14$ mm. The deflections are calculated by the semi-analytical model with $\Delta\eta = 0.005$.

Conclusion and discussion

From Figure 3.1 it is seen that the semi-analytical model is fully capable of modeling cases with snap through behaviour. For $\Delta\eta = 0.04$, the response in the snapping region has a quite large deviation from the ABAQUS results. The response for $\Delta\eta = 0.005$, on the other hand, corresponds good with the response found with ABAQUS. This indicates that a small arc length increment, $\Delta\eta$, is needed to model snap through satisfactory. The ultimate strength prediction for the plate, see Section 5.2.3, is included to indicate the range of interest in the current work. From Figure 3.1 it is seen that the semi-analytical model will reach the ultimate strength prediction at a significantly lower load level than the load level where snapping is initiated. Up until the ultimate strength the deviation in load-shortening response between $\Delta\eta = 0.04$ and $\Delta\eta = 0.005$ are negligible. This indicates that $\Delta\eta = 0.04$ can be used to estimate the ultimate strength for the plate studied here.

Figure 3.2 shows that the deflection shape has changed from one half wave to three half waves in the x-direction. This was expected, and it was the reason for choosing $M_{wa} = 3$.

For the plate studied here the slenderness is approximately 3.5. Only plates with slenderness less than 4 will be studied in this report, to exclude plates of no practical interest. This limitation should also ensure that snapping behaviour does not influence the ultimate strength.

When computing the response of the plate with $\Delta\eta = 0.005$ the FORTRAN code became significantly slower. To ensure good results without increasing the computational time some criterion for selecting the arc length increment could be implemented. Such a criterion should reduce the arc length increment in regions with large variations of incremental stiffness. Such an approach will not be addressed further here.

Chapter 4

Finite element modelling

4.1 General overview

The finite element model is based on using suitable, simple, discrete displacement fields for elements. This discrete displacement field will consist of a suitable number of shape functions with nodal degrees of freedom as their weights. These degrees of freedom are then related to the neighbouring elements by continuity relations. Such an approach is also based on the Rayleigh-Ritz method, but the assumed displacements are per element and a complete stiffness matrix will be constructed based on continuity of nodes. This approach is very robust and suitable for modelling general cases. There will typically be a number of predefined element types with certain properties in finite element programs. Typical element categories are trusses, beams, membrane plates, shells and solids. Shell elements will be used in the current modelling since plates with out-of-plane deformations are studied.

The finite element modelling is performed in ABAQUS [18]. Some principle properties and solution techniques will be presented in this chapter. The element modelling will mainly be used to verify the proposed strength criteria for the semi-analytical model. In that respect the modelling procedures, material properties and element types should be in accordance with the theory presented in the previous chapters. The boundary conditions in the element models will correspond to the definitions in Section 3.4, unless anything else is specified.

4.2 Fully non-linear analysis

A fully non-linear analysis, as defined here, contains both material and geometric non-linearity. Including these non-linear effects will be necessary when estimating the ultimate capacity. Performing a fully non-linear analysis makes the finite element model capable of capturing the interaction between yielding and geometrical non-linearities. Using finite elements is therefore a convenient way of estimating the ultimate capacity for a system.

4.3 Analysis procedures

4.3.1 Linear elastic buckling mode calculations

The first linear elastic buckling mode will, as for the semi-analytical model, mainly be used as imperfection in the fully non-linear finite element analyses. This linear elastic buckling mode is estimated by solving an eigenvalue problem for a perfect plate without considering yielding. This eigenvalue problem is based on the element method formulation of the Rayleigh-Ritz approach for stationary potential energy. The linear elastic buckling mode will correspond to the bifurcation point, see Section 2.5, defined earlier. ABAQUS estimates both the linear elastic buckling load, the eigenvalue, and the linear elastic buckling shape, the eigenvector.

4.3.2 The modified Riks method

ABAQUS includes a suitable method for tracing load-responses based on the modified Riks method. This solution method, as in the semi-analytical model, uses an arc length incrementation with the advantages described earlier. The modified Riks approach is capable of performing a fully non-linear analysis making it possible to estimate the ultimate capacity of the plate. Such analyses are used for the ultimate strength limit estimates of ABAQUS presented in Chapter 5. ABAQUS uses equilibrium correction in the modified Riks method to secure accurate estimates. Such an equilibrium correction is not included in the semi-analytical model implying that larger steps can be used in ABAQUS. The modified Riks method can include several different loads but all loads will have the same load factor. This is not important for the current case, since only in-plane membrane loading in the x-direction is considered, but it might be an important limitation if a combination of several loads should be applied. The modified Riks method also includes an automatic procedure for determining the necessary arc length increment at each step. This makes the method more robust and quite efficient. Further information on the modified Riks method can be found in the ABAQUS documentation [18].

Using displacement or load control is an alternative to using the modified Riks method. Such approaches will not be able to trace all types of complex behaviours as snap-through and snap-back. Displacement control will be used in Section 8.2.4 and Section 8.3.2 when unloading behaviour is studied. This is necessary since the modified Riks method only is suitable for tracing the behaviour during loading.

4.4 Principle differences relative to the semi-analytical model

4.4.1 Material properties

The material properties presented in Section 2.2.3 will be used in the models, but strain hardening will be included to ensure satisfactory results. This applied strain hardening is linear with a Young's Modulus of $E_T = 1000$ MPa. Strain hardening is observed when studying the real behaviour of steel, but it is mainly introduced here to avoid numerical problems in the solution procedures.

4.4.2 Stiffener modelling

The stiffeners are modelled as beams in the semi-analytical model, while they are modelled as shells in the finite element models. The difference should be small as long as in-plane bending is correctly modelled in ABAQUS and shear deformations are negligible. The S4 shell elements used to model the stiffeners, see Section 4.5, will not suffer from problems with in-plane bending. Shear deformation of the stiffener is not included in the semi-analytical model, but will be present in the shell elements. The relative effect of shear deformation, in the stiffeners, is expected to be small for all cases presented in the current work.

4.5 Relevant element types

4.5.1 S4

The S4 element, see the ABAQUS documentation [18], is a 4 node general-purpose fully integrated shell element based on finite strain theory. Finite strain theory, also known as large deformation theory, includes large in-plane strains and rotations of the plate. In the semi-analytical, on the other hand, only large deflection theory (small in-plane strains and large rotations) is included. The theory of the S4 element is therefore more general then the theory in the semi-analytical model implying that S4 should be suitable for modelling the response.

Fully integrated elements are computationally costly, because of the number of integration points used. They are also known to have problems with shear locking for 4 node elements under in-plane bending, see Cook, Malkus, Plesha and Witt [15]. The S4 element, on the other hand, is formulated in a way that excludes the possibility of shear locking and makes it suitable for modelling in-plane bending. This is done by imposing a correction factor to the rate of deformations that accounts for shear locking and in-plane bending. A further discussion can be found in the ABAQUS documentation [18].

4.5.2 S4R

The S4R element, see the ABAQUS documentation [18], is based on the same basic theory as the S4 element, but with reduced integration. Shear locking will not be present for 4 node elements with reduced integration. A fine mesh of S4R elements will be needed when in-plane bending dominated problems are studied, since no correction factor for in-plane bending is introduced. A reduced element will be more flexible than a fully-integrated one causing a more conservative approach to the solution. In addition, such an element is computationally faster than a fully integrated element, since integration is carried out for one point in stead of four. The lack of correction for in-plane bending makes S4R less suitable when modelling problems with significant in-plane bending.

4.5.3 Selection of element type

For unstiffened plates the effect of in-plane bending will be limited, because of the imposed boundary conditions, and S4R will then be used to increase computational efficiency.

In stiffened plates the S4 element will be used since significant in-plane bending will be present in the stiffeners. This in-plane bending is a result of global plate deflection, which is resisted by the in-plane bending stiffness of the stiffeners.

4.6 Convergens testing

Convergence is tested for the linear elastic buckling estimates. These tests are performed by reducing the element size and comparing the estimates. If a significant change in element size results in a virtually negligible difference in the linear elastic buckling estimate, then the system has converged. This is a common approach for assuring that the results of numerical calculations are reliable.

The mesh used in most of the models will be quite fine, and a coarser mesh could probably give reasonable results. This is not pursued further here, since the computational time in ABAQUS already was satisfactory.

Chapter 5

Improved ultimate strength criteria

5.1 Investigations of the problem

Some basic considerations will be given before possible ultimate strength (collapse) criteria, for both unstiffened and stiffened plates, is presented. In the element models both geometrical non-linearity (finite strain theory) and material non-linearity are included when the ultimate strength limit (USL) of the plates are calculated. The semi-analytical model, on the other hand, only includes large deflections, and yielding of the material must be accounted for by selecting a suitable USL criterion. Such yielding of the material will result in plastic redistribution of stresses. Yielding in the flexible parts will reduce the carrying capacity in these regions implying increased membrane stresses along the stiff edges and, if present, along the stiffeners. In the original model, see Brubak [2], the USL criterion only accounted for first von Mises membrane yield found with a large deflection analysis. Considerable non-conservative deviations, for unstiffened plates, were observed for a large span of thicknesses when comparing to finite element results. The criterion should therefore be modified to account for significant yielding in the flexible parts of the plate. This is the motivation for finding a new suitable limit strength criterion.

The large deflection theory included in the semi-analytical model accounts for redistribution of membrane stresses from the flexible parts, with large deflections, to the stiffer parts with smaller deflections. This effect is also included in the finite strain theory used in the finite element analyses. The effect of geometrical redistribution of stresses will be significant for plate cases with low slenderness where the deflections are large.

5.2 Unstiffened plates

5.2.1 Plate criteria

Several different criteria for simply supported unstiffened plates with a free edge will be presented in this section. For simplicity the following definition is introduced:

$$(\sigma_e^{pm})_{max} = \sigma_e^{pm}\left(x = \frac{L}{2}, y = 0\right) \tag{5.1}$$

where σ_e^{pm} denotes the von Mises membrane stress (see Equation 2.15) and $(\sigma_e^{pm})_{max}$ is the maximum von Mises membrane stress. It is natural that the maximum von Mises membrane stress will be found along the stiffest edge, at $y = 0$. The critical point along this edge will be the point with the largest redistribution from the flexible parts. This point will present on the line, normal to the edge, with the largest deflection. The largest deflection will, for unstiffened plates, be present along the midline, at $x = L/2$. These observations explains the definition in Equation 5.1. This location of the maximum von Mises membrane stress has been verified by studying stress plots from the semi-analytical model and ABAQUS results.

Von Mises membrane stress criterion (UP1)

The von Mises membrane stress criterion states that the ultimate strength of the plate is reached when membrane yielding occurs along the supported edges. This criterion was used by Brubak [2] and it is restated here for simplicity:

$$(\sigma_e^{pm})_{max} = f_y \tag{5.2}$$

The motivation for this criterion is that the external loads are carried as membrane stresses. This can be seen by integrating the bending stress over the cross section. Such an integral will be zero, because of the linear variation of bending stress over the cross section. This indicates that the resultant load carried by the cross section is equal to the integrated membrane stress. It is therefore evident that the external loads will be carried as membrane stresses in the plate. When membrane yielding then occurs this imply that the maximum external load is reached. Large deflections in the plate will be expected, for unstiffened plates with a free edge, causing yielding due to bending in flexible regions. This yielding gives plastic redistribution of stresses in the plate, as discussed earlier, and this effect is not accounted for in this criterion.

Stress combination criterion (UP2)

In the stress combination criterion the following condition is used to estimate the ultimate strength:

$$(\sigma_e^{pm})_{max} + \beta \cdot \bar{\sigma}_e^{pb} = f_y \tag{5.3}$$

where $\bar{\sigma}_e^{pb}$ is the weighted average of the von Mises bending stress over the mid strip at $x = \frac{L}{2}$. The function β is defined as follows:

$$\beta = \beta(\bar{\sigma}_e) = \begin{cases} B \cdot \left(\frac{\bar{\sigma_e} - f_y}{f_y}\right), & \bar{\sigma}_e > f_y \\ 0, & \bar{\sigma}_e \leq f_y \end{cases} \tag{5.4}$$

where $\bar{\sigma}_e$ denotes the weighted average, over the mid strip at $x = \frac{L}{2}$, of total von Mises stress at the outer fibres and B is a constant to be determined.

The constant B, in Equation 5.4, will be found by tuning results from the semi-analytical model with finite element analyses. This tuning will be carried out for plates with typical slenderness values encountered in ship structures. $B = 2$, see Section 5.2.2, will be used in the current work.

The motivation for this criterion is to account for plastic redistribution of stresses from the flexible region to the stiffer region along the supported edges. In the flexible regions the plastic redistribution is a result of large bending stresses. These plastic redistributions are only present if the maximum total von Mises stresses exceed the yielding stress of the material. The redistribution will increase as the maximum value of the total von Mises stresses increases. Based on these observations the formula for $\beta(\bar{\sigma}_e)$ in Equation 5.4 is chosen. Any $\beta(\bar{\sigma}_e)$ satisfying $\beta(f_y) = 0$ could be used, but the linear variation presented here is chosen for simplicity.

The average value of the von Mises bending stresses is used in the criterion to reduce the effect of locally large bending stresses. If large bending stresses are present in very small areas of the plate this will not result in considerable amounts of plastic redistribution. It is therefore more appropriate to use an average value of the von Mises bending stresses when accounting for plastic redistribution in the plate. In a similar manner the average value of the von Mises total stress is used in the definition of β to reduce the influence of local stress concentration.

Average stress values are found by a weighted average computation, which accounts for the actual line segment related to each point. This method is illustrated in Figure 5.1 and the average stress value, $\bar{\sigma}$, will given by:

$$\bar{\sigma} = \frac{\sigma_1 \frac{a}{2} + \sigma_2 a + ... + \sigma_{n-1} a + \sigma_n \frac{a}{2}}{(n-1)a} = \frac{\frac{\sigma_1}{2} + \sigma_2 + ... + \sigma_{n-1} + \frac{\sigma_n}{2}}{(n-1)}$$

where σ_1, σ_2, ... denotes the stresses at the selected points, a is the length defined in Figure 5.1 and n is the total number of points. In the current studies 11, equally spaced, points along this midline will be used.

The von Mises bending stresses can be computed in two different ways. The first possibility is to calculate the von Mises bending stress as the difference between the von Mises total stress and the von Mises membrane stress. The other approach is to use the bending stresses components directly into the von Mises formula for stresses. These to approaches will give slightly different values due to the mathematical form of the von Mises yield criterion, see Equation 2.14. Testing of both possibilities showed that the difference

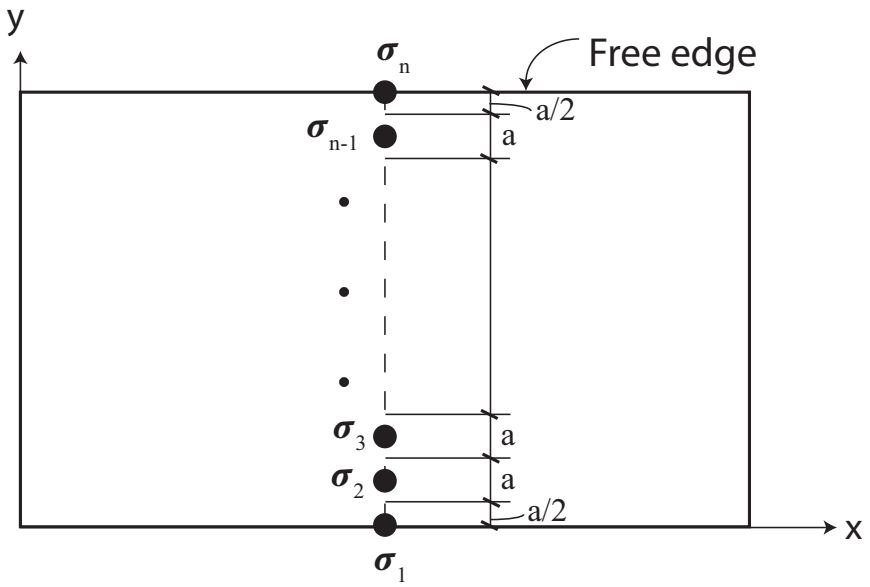

Figure 5.1: The relevant length for each point used in the weighted average calculation for stresses along a line parallel to the free edge.

was relatively small. The direct computation, using the bending stress components directly in the von Mises criterion, was selected because of the simple formulation and slightly better results.

Dual stress criterion (UP3)

Another approach to include the effect of plastic redistribution of stresses is the following criterion:

$$\max\left\{(\sigma_e^{pm})_{max},\ \bar{\sigma}_e(z=\pm c\cdot t)\right\} = f_Y \tag{5.5}$$

where c is constant and $\bar{\sigma}_e(z=\pm c\cdot t)$ gives the weighted average value over the mid strip at $x=\frac{L}{2}$, of total von Mises stress at a distance $c\cdot t$ from the mid surface of the plate.

The value of the constant c will be determined through tuning of the semi-analytical model with respect to finite element analyses. Only values of c $\in [0,\frac{1}{2}]$ will be considered since $z\in[-\frac{t}{2},\frac{t}{2}]$. The tuning performed here, see Section 5.2.2, gave $c=1/4$.

This criterion is based on the assumption that large average values of total von Mises stress over the mid strip results in considerable amounts of plastic redistribution. It is natural to assume that the external load is close to the ultimate load when such large plastic redistributions are present.

For this criterion, as for the stress combination criterion above, the weighted average (using 11 points) of total von Mises stress along the mid-strip, $x=\frac{L}{2}$, is used to reduce the effect of local stress concentrations. Local stress concentrations will, as mentioned above, not result in significant plastic redistribution of stresses in the entire plate and it is suitable to use the average value.

Reduced thickness

A criterion for reducing the plate thickness was implemented to account for plasticity due to bending stresses. The average von Mises total stress, both bending and membrane stress, along $x = \frac{L}{2}$ was computed and checked for yielding. If this average von Mises total stress exceeded yielding, the thickness of the entire plate was reduced so that the average von Mises total stress would be below the yield stress for the current load step. This new thickness was then used to calculate the incremental stiffness. The non-conservative effect of reducing the thickness after the calculation of the current load step is assumed to be balanced out by reducing the thickness of the entire plate. Some tests with reduction of thickness in combination with the UP1 criterion were carried out. The scheme showed instabilities and problems for thicknesses from 40 mm to 60 mm for L = B = 1000 mm. When reducing the arc length increments from $\Delta\eta = 0.04$ to $\Delta\eta = 0.01$ the method showed improvements, but problems were still encountered for thicknesses approaching 60 mm. The problems might be caused by large changes in the incremental stiffness matrix due to large thickness reductions. A further reduction of the incremental arc length might fix the problems, but the method will then be quite inefficient and numerical problems might be introduced. In light of the problems encountered and the need for efficient calculations this scheme will not be studied further in the following work.

Interaction criterion

An interaction criterion as used for arbitrarily stiffened plates in Brubak and Hellesland [6] was also considered in an early phase. This kind of strength criteria is based on the capacity interaction formula for a cross section and the strength is reached when:

$$\left(\frac{\sigma_e^{pm}}{f_Y}\right)^2 + \frac{1}{\alpha}\frac{\sigma_e^{pb}}{f_Y} = 1$$

where $\alpha = 1.5$ for rectangular cross sections. This condition checks if full plasticity has developed in a given point. Development of full plasticity in a cross section for one or more points in the flexible part of the plate does not necessarily imply that the strength of the plate is reached. This is due to the possibility of plastic redistribution of stresses from the region around the point to the stiffer parts. Therefore it is difficult to motivate the use of such a criterion for unstiffened plates. In Brubak and Hellesland [6] this criterion was used for critical points with considerable amounts of both membrane stresses and bending stresses. Such points will for instance be present in the vicinity of irregular stiffeners. Such points are not encountered for unstiffened plates and regularly stiffned plates with a free edge.

Such a criterion might be applicable if clamped edges or edges with rotational constraints are studied. In these cases large bending moments can be present along the edges. The interaction criterion might then be applicable along the supported edges when estimating the ultimate strength.

Based on the observations and discussion above this criterion is not considered further in the current work.

5.2.2 Selection of plate dimensions and parameters

Plate definitions

Testing of the criteria will be carried out for the dimensions in table 5.1.

Plate	L (mm)	b (mm)	t (mm)
1000X1000	1000	1000	[10-60]
2000X1000	2000	1000	[12-60]
3000X1000	3000	1000	[14-60]
1000X2000	1000	2000	[10-60]

Table 5.1: The selected plate dimensions used to test the criteria for simply supported unstiffened plates with a free edge.

The thickness spans have been selected so that the slenderness of the plate is less than 4. This limit is set to exclude plates which are of no practical interest. The selected range of plate cases represents a large variety of plate parameters.

Parameter selection for the model

The results presented for unstiffened plates are based on the following number of terms in the displacement expressions:

$$M_{wa} = 3, \quad M_{wb} = N_{wb} = 6, \quad M_{ua} = M_{ub} = N_{ub} = M_{va} = M_{vb} = N_{vb} = 10$$

The number of terms selected above was all verified through testing of convergence of ultimate strength limit predictions. In Brubak [2] the same number of terms was selected for all the sums except from M_{wa}. Testing performed here indicated that the plates with $L = 3000$ mm and $b = 1000$ mm, not studied by Brubak [2], needed $M_{wa} = 3$. This value for M_{wa} includes the possibility of mode snapping from one half wave in the x-direction to a deflection with two or three half waves in the x-direction. An example of snap through behaviour using the semi-analytical model was presented in Section 3.6. The arc length increments used will be $\Delta\eta = 0.04$, which is the same as used in Brubak [2].

Selection of constants for the strength parameters

For the stress combination criterion (UP2) the constant B is found through tuning with fully non-linear analyses, using ABAQUS, as described earlier. Through such tests, see Appendix A.1, it was found that B = 2 gave the best results.

The constant c in the dual stress criterion (UP3) is also found by tuning results from the semi-analytical model with fully non-linear finite element analyses. This tuning, see Appendix A.2, indicated that $c = \frac{1}{4}$ gave the best correspondence.

5.2.3 Results

The ultimate strength limit (USL) estimates found with UP1, UP2, UP3 and ABAQUS are given in Figure 5.2 for all the selected dimensions. In addition the elastic buckling stress limits (ESL) are included to indicate the slenderness of the plate for different thicknesses.

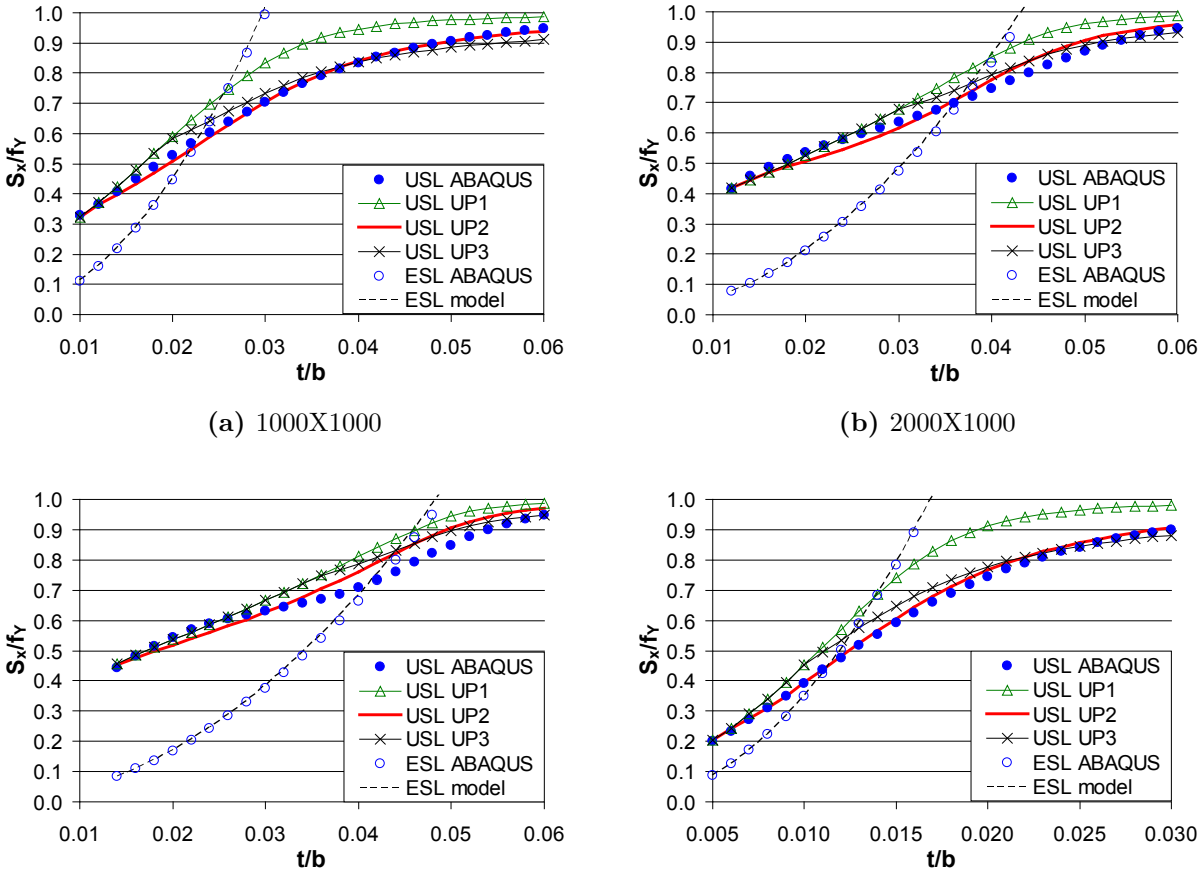

(a) 1000X1000 **(b)** 2000X1000

(c) 3000X1000 **(d)** 1000X2000

Figure 5.2: Ultimate strength limit (USL) estimates and elastic buckling strength limit (ESL) estimates are given in the subfigures for the plate dimensions in table 5.1. ABAQUS results are also included for comparison. The first linear elastic buckling mode, with an amplitude of 5 mm, is used as imperfection for all the USL calculations.

5.2.4 Discussion and conclusion

The von Mises membrane stress criterion (UP1) gives, as expected, considerable non-conservative deviations for the plates studied. For the cases in Figure 5.2a and Figure 5.2d it is observed that the stress combination criterion (UP2) has much better correspondence with ABAQUS, than the dual stress criterion (UP3).

Figure 5.2b and Figure 5.2c indicates that both UP2 and UP3 produce good estimates for these cases. UP3 estimates are somewhat better for the thinnest plates, but such cases with slenderness close to 4 will not be very common in practical ship applications. For the mid-range of thicknesses UP2 gives better estimates than UP3. For the thickest plates UP3 shows negligible better results than UP2.

UP2 is based on correcting the physically relevant UP1 criterion with a correction factor. This correction factor will give a continuous transition from cases with little plastic redistribution to cases with high plastic redistribution. UP3 will not have the same continuous behaviour since the criterion is a combination of two separate criteria. Another problem with UP3 is that high total von Mises stresses do not necessarily imply large bending stresses. This will for instance be the case for plates with low slenderness, where the deformation out-of-plane is almost linear and large membrane stresses are expected in the entire plate. These remarks make UP2 more suitable with respect to physical behaviour.

The displacement assumptions used in the semi-analytical model give bending stress concentration close to the corners of the simply supported edges. A finite element analysis was carried out to investigate these effects in more detail. This model includes large deformations and linear material. Stress predictions, at ultimate strength, from this analysis are presented in Figure 5.3. The dimensions of the plate is $L = 2000$ mm, $b = 1000$ mm and $t = 20$ mm. A rather fine mesh is used to investigate the effects of changes close to the corner. Contour plots in ABAQUS use the average nodal value as stress prediction for the elements. It is seen that stress concentrations are formed close to but not in the corner. This implies that large stress consentrations will be present close to the corners, due to in-plane shear bending stress concentrations. This effect is nevertheless assumed to be local and therefore negligible when the ultimate strength limit is estimated. All the criteria studied here neglect the effect of these bending stress concentrations in the corners.

The selected value of B, in UP2, is based on tuning the model for the cases in table 5.1. If for instance plates with a higher ratio between length and width should be included, it might be necessary to increase B somewhat to limit the non-conservative deviations. From Figure 5.2b and Figure 5.2c it is observed that the maximum non-conservative deviation increases somewhat when $\frac{L}{b}$ increases from 2:1 to 3:1. A higher value for B will have a significant effect on the strength estimates when large bending stresses are present. Such large bending stresses is expected for semi thick plates.

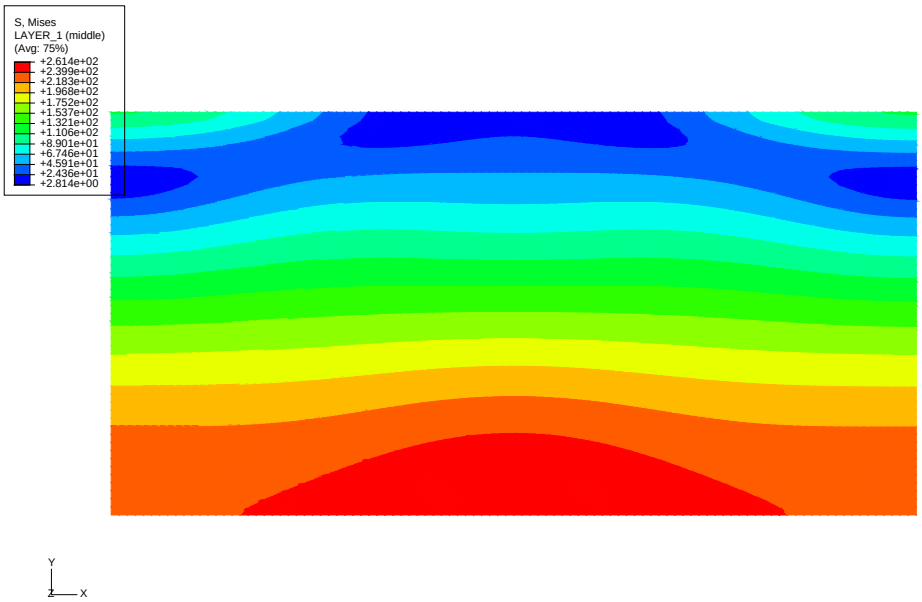

(a) Von Mises membrane stress

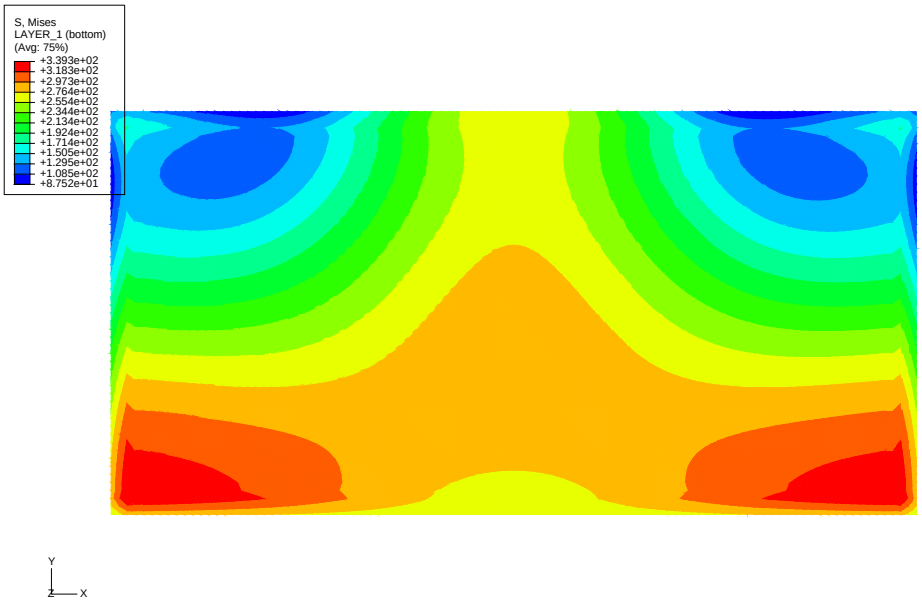

(b) Von Mises total stress at the most compressed side of the plate (surface stress)

Figure 5.3: (a) Von Mises membrane stresses (MPa) and (b) von Mises total stresses (MPa), at the most compressed side of the plate, for an unstiffened plate with $L = 2000$ mm and $b = 1000$ and $t = 20$ mm. Results are produced by ABAQUS with a linear elastic material model. A very fine mesh (5000 S4R elements) is used in order to get a detailed view at the corners. The external uniaxial in-plane load corresponds to the approximate ultimate strength of the plate. The upper edge in the plots is free while the other edges are simply supported.

For the results above $M_{wa} = 3$ was used instead of $M_{wa} = 1$. As explained earlier this is done to ensure convergence for the cases with $L = 3000$ mm and $b = 1000$ mm. If plates with a higher ratio between length and width should be studied, further increases in the value of M_{wa} might be appropriate. The difference encountered between $M_{wa} = 3$ and $M_{wa} = 1$ was significant for small thicknesses and decreasing as the thickness increases. For the lower thicknesses it will be expected that the plate will be somewhat flat in the middle and at the same time show tendencies towards mode snapping. The value of M_{wa} ,for thin plates with possibilities of snapping, should be increased, in accordance with the ratio between length and width, to ensure that the necessary modes are included. Snapping is not expected to occur before the ultimate strength limit is reached for the interesting cases, but tendencies towards it might be observed for slender cases.

5.3 Stiffened plates

5.3.1 Modified stress combination criterion (SP)

The original stress combination criterion (UP2), combined with the stiffener criteria in Section 5.3.2, was tested directly for stiffened plates. These tests showed significant conservative deviations for cases with high stiffeners and thin plates. The stiffened free edge will approaches a simply supported condition when the stiffener height, of the stiffened free edge, is increased. From earlier studies of simply supported plates, conducted by Brubak and Hellesland [5, 6], it was seen that first membrane yield of the plate combined with a suitable criterion for the stiffeners gave satisfactory results. To approximate the ultimate strength for all relevant cases the UP2 criterion was modified with a distribution factor. This distribution factor is dependent on the ratio between the maximum total deflection of the entire plate, $w_{t,max}$, and the maximum total deflection of the stiffened free edge, $w_{t,edge}$. The selected distribution factor is included in a modification of the constant B in UP2, B_{mod}, given by:

$$B_{mod}\left(\frac{w_{t,edge}}{w_{t,max}}\right) = \left[1 + \tanh\left(4\pi\frac{w_{t,edge}}{w_{t,max}} - 2\pi\right)\right] \tag{5.6}$$

where the absolute values of the deflections are used and $w_t(x, y) = w(x, y) + w_0(x, y)$.

B_{mod}, see Equation 5.6, gives the variation shown in Figure 5.4 for the relevant displacement ratios. The shape of B_{mod} was motivated by the relations between stiffener height and ultimate strength limit (USL), see the results in Section 5.3.4. These results indicate that cases with a low stiffener height have approximately the same USL as the corresponding unstiffened case. When the stiffener height becomes considerable the USL approaches the USL of an equivalent plate with all edges simply supported. These observations indicate an asymptotical behaviour, of the ultimate capacity, as the stiffener height approaches zero and infinity. A corresponding asymptotical behaviour is therefore included in B_{mod} to ensure good estimates for all the relevant cases. The selected B_{mod} should be approximately 2, the selected value of B, for cases where the stiffeners are insignificant. B_{mod} should in

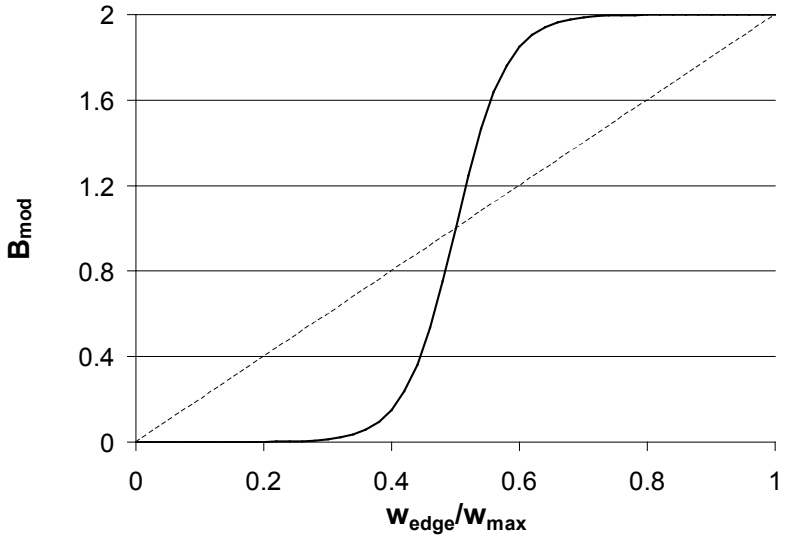

Figure 5.4: Shows the variation of the selected B_{mod} (solid line) and the alternative linear variation (dotted line) as a function of $w_{t,edge}/w_{t,max}$.

addition approach 0 as the stiffened free edge approaches simply supported. The case with insignificant stiffeners are given by $w_{t,edge}/w_{t,max}$ close or equal to 1, while $w_{t,edge}/w_{t,max}$ close to 0 indicates the approximate simply supported condition. B_{mod}, see Equation 5.6, will approaches the desired values ,$B_{mod}(1) = 2$ and $B_{mod}(0) = 0$, asymptotically.

A linear variation of B_{mod}, see the dotted line in Figure 5.4, was also tested. Such a linear variation of B_{mod} is compared to the selected variation and the original UP2 criterion in Appendix A.3. These results indicate that the selected variation of B_{mod} is the most reasonable.

When checking the von Mises membrane stress and selecting critical lines the stiffened case differs from the unstiffened case. The midline will no longer be the critical line for all cases. The von Mises membrane stress will in the stiffened cases be checked along the stiffest edge at $y = 0$. The maximum von Mises membrane stress will be present at the line(s), perpendicular to the edge, with the largest geometrical redistribution of stresses. Two critical lines will be used if the maximum von Mises membrane stress is not located at the center($x = L/2$). These two lines will then be placed symmetrically about the midline corresponding to the location of maximum von Mises membrane stress. The combination criterion will then be checked separately for each line, by combining the two critical von Mises membrane stresses with the bending contribution from the related critical lines. Only the part of the critical line prior to the first local maximum of deflection will be used to calculate the average stresses.

In the current procedure the maximum von Mises membrane stress is taken along the inner edge, at $y = 0$. Higher von Mises "membrane stresses" will be calculated under eccentric stiffeners, due to a change in the neutral axis. Some of the bending stresses

from the stiffeners will then be included in the plate membrane stress. These high von Mises membrane stresses are not critical when estimating the ultimate capacity, and the maximum von Mises membrane stress(es) along the inner edge will then be used in the criterion.

The modified plate criterion presented here, SP, will be combined with the stiffener criteria presented in Section 5.3.2. Results of the combined criteria will be given in Section 5.3.4.

5.3.2 Stiffener criteria

Reduced stiffener height (SS1)

This criterion was tested by Brubak and Hellesland in [6]. The stiffener reduction, illustrated in Figure 5.5, is preformed by removing the yielded part of the stiffener before calculating the incremental stiffness for the next step. This is done by finding the cross section with most yielding and then removing this yielded area, see Figure 5.5a, for all cross sections of the stiffener. This approach models the actual effect of yielding in a physical way by reducing the stiffness.

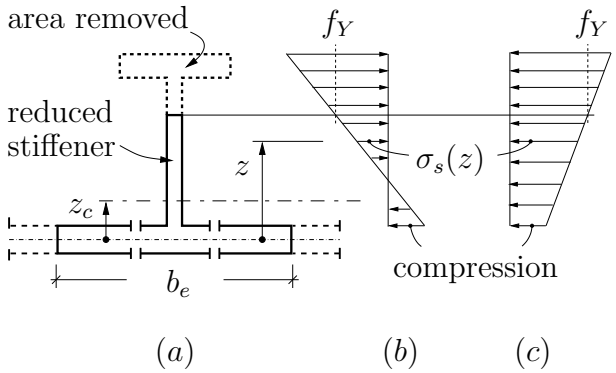

Figure 5.5: (a) the reduction of stiffener area due to yielding, (b) stiffener stress distribution due to bending in the positive z-direction and (c) due to bending in the negative z-direction. Only flat bar stiffeners will be studied here, implying $h_f = t_f = 0$.(figure from Brubak and Hellesland [6])

The reduction of stiffener height is done after the step where yielding actually occurs. Such an approach produces a non-conservative deviation, since the stiffness in the last step is overestimated. This effect is counteracted by reducing the stiffener height over the entire stiffener length, and not only the part of the stiffener with yielding.

The results presented later is computed with $\Delta\eta = 0.04$. This is a fairly small increment and it might be necessary to increase the arc length increment, to reduce the calculation time, when the final program is developed. Increasing the arc length increment might give problems in combination with this procedure due to large changes in the incremental

stiffness. Tests concerning the effect of increasing the step length will not be included in the following work.

In some cases the loading passed a significant limit point, a maximum load factor, before it was reduced. This is an effect of reducing the stiffener height, resulting in a negative incremental stiffness. Such limit points will then be used as an estimate for the ultimate strength limit (USL). For some cases the response became somewhat unstable after the limit point was passed. In these cases the load-shortening curves was studied to ensure that the top of the curve gave a reasonable estimate for the USL.

A problem with tracing the load-response were observed for two cases when using this stiffener criterion, in combination with the modified stress combination criterion (SP), for the combined imperfections in Section 7.2 . These two slender cases are discussed in detail in Appendix A.4. Reasonable solutions for the problem cases were found by selecting the solution giving an increase in the end shortening of the plate, instead of the using the condition in Equation 3.33. Equation 3.33 will still be used for all the cases where this problem is not present, to ensure that snapping and other similar physical behaviours can be modelled.

The stiffener reduction criterion will influence the solution for stiffened plates with globally dominated deformation shapes. In such cases the stiffeners will experience considerable curvatures and therefore large bending stresses resulting in stiffener yielding.

SS1 will be combined with the SP criterion presented above.

First yield criterion for stiffeners (SS2)

This criterion states that the ultimate capacity is reached when first yield occurs in the stiffeners. Mathematically this can be written as:

$$(\sigma_s)_{max} = fy$$

where $(\sigma_s)_{max}$ denotes the maximum stiffener stress, σ_s, present.

This stiffener criterion is expected to give very conservative estimates of the ultimate strength limit for cases with globally dominated deformation shapes, since the stiffeners then experiences large bending stresses at low load levels.

The criterion will be used in addition the SP criterion derived in Section 5.3.1.

Interaction criterion for stiffeners (SS3)

An interaction criterion for the stiffeners is also tested. This criterion is based on the interaction criterion for yield hinges in regular beam theory. Formation of yield hinges will not indicate collapse of the stiffener, since the stiffener is connected continuously to the plate. The criterion is still seen to be relevant since a local yield hinge, in the stiffener, will reduce the overall stiffness properties of the stiffener significantly. Mathematically this criterion can be written as:

$$\left(\frac{N}{N_p}\right)^2 + \frac{M}{M_p} \geq 1$$

where N is the normal force in the beam, N_p is the normal force corresponding to uniform yielding of the cross section, M gives the moment in the beam and M_p gives the plastic moment corresponding to fully plastic bending stresses. Mathematically $N = \sigma_{sm}A$, $M = \sigma_{sb}W$, $N_p = f_Y A$ and $M_p = f_Y Z$ where σ_{sm} is the stiffener membrane stress, σ_{sb} is the stiffener bending stress, A is the cross sectional area, W is the elastic section modulus and Z is the plastic section modulus. It is often common to define $\alpha = Z/W$. For a rectangular cross section the value of $\alpha = 1.5$. This value of α is used in the following study where only flat bar stiffeners are tested. Using these expressions the interaction criterion simplifies to:

$$\left(\frac{\sigma_{sm}}{f_Y}\right)^2 + \frac{1}{\alpha}\frac{\sigma_{sb}}{fy} = 1 \tag{5.7}$$

The criterion in Equation 5.7 will be used in addition to SP when estimating the ultimate strength limit. As for the other stiffener criteria, this criterion will only influence the estimate when the deformation is dominated by a global mode.

5.3.3 Selection of plate dimensions and parameter

Plate definitions

The criteria, for stiffened plates, presented above, are tested for the cases in table 5.2. Most of the dimensions selected are based on the cases studied by Brubak [2]. The cases with $L = 2400$ mm and $B = 2523$ mm, on the other hand, are based on a practical example, with three stiffeners, from a real ship structure. Plates with two stiffeners are not included in Brubak [2], but they are included here to test a wider range of cases. All stiffeners are equally spaced with one stiffener at the free edge. The plate cases studied will, as for the unstiffened cases, have slenderness below 4. Local stiffener buckling is neglected in the semi-analytical model, and ABAQUS results are studied to ensure that this effect is negligible in the test cases. A further discussion of local stiffener buckling can be found in Section 7.1.

Plate	N_{stiff}	**L (mm)**	**b (mm)**	**t (mm)**	t_w **(mm)**	h_w **(mm)**
$1000X1000_1$	1	1000	1000	12	10	[6-306]
$2000X1000_1$	1	2000	1000	30	10	[15-265]
$1000x1000_2$	2	1000	1000	12	10	[16-206]
$2400x2523_2$	2	2400	2523	11	12	[45.5-205.5]
$1000x1000_3$	3	1000	1000	12	10	[16-116]
$2000x1000_3$	3	2000	1000	30	10	[25-165]
$2400x2523_3$	3	2400	2523	11	12	[45.5-205.5]

Table 5.2: The selected plate dimensions used to test the criteria for simply supported stiffened plates with a stiffened free edge. Stiffeners are equally spaced and N_{stiff} gives the total number of stiffeners. The name convention used is $LXB_{N_{stiff}}$.

Parameter selection for the model

The results presented for stiffened plates are based on the following number of terms in the displacement expressions:

$$M_{wa} = M_{wb} = N_{wb} = 6, \quad M_{ua} = M_{ub} = N_{ub} = M_{va} = M_{vb} = N_{vb} = 10$$

These are the same values as used for unstiffened plates, see Section 5.3.3, except from M_{wa}. The value of M_{wa} is increased to ensure that more complex deformation shapes could be modelled satisfactory. Several tests have been conducted and the selected numbers of terms gives convergence of the ultimate strength limit estimates.

An arc length increment of $\Delta\eta = 0.04$ will also be used for the stiffened plates.

5.3.4 Results

Results for the reduced stiffener height criterion (SS1), in combination with the modified stress combination criterion (SP), are presented for the cases with one, two and three stiffener in Figure 5.7, Figure 5.8 and Figure 5.9 respectively. The other stiffener criteria, SS2 and SS3, are excluded due to too conservative results, as discussed in Appendix A.5.

5.3.5 Discussion and conclusion

Figure 5.7a shows that the modified stress combination criterion (SP) combined with reduced stiffener height criterion (SS1) gives good ultimate strength limit (USL) estimates for $1000\text{X}1000_1$. A small drop in the USL estimates, for small stiffeners, as the stiffener height increases is observed. This reduction is negligible and the estimates are reasonable. The USL estimates from the semi-analytical model are also good for $2000\text{X}1000_1$. As the USL reaches the plateau, representing an approximately simply supported edge, a small drop in the USL estimates are observed. This is a result of a change from a global imperfection shape to a local imperfection shape. This transition would be smoother if a combination of a local and global imperfection is used. Further considerations with respect to combined imperfection shapes will be given in Section 7.2.

In Figure 5.8a, $1000\text{X}1000_2$, the model gives a noticeable non-conservative deviation for $h_w = 76$ mm. This deviation is a result of different imperfections estimates in ABAQUS and the semi-analytical model. The first buckling shape of the semi-analytical model is local, resulting in a stiffer configuration than the global first buckling shape found with ABAQUS. Using the local buckling mode as imperfection in ABAQUS gave very good accordance between semi-analytical model and ABAQUS. This indicates that a combination of a global and local mode should be used when computing reasonable USL estimates. Such considerations, with respect to combined imperfections, will be performed in Section 7.2. When the same imperfection shape is used, for both ABAQUS and the semi-analytical model, it is seen that the USL estimates of the model is good for $1000\text{X}1000_2$.

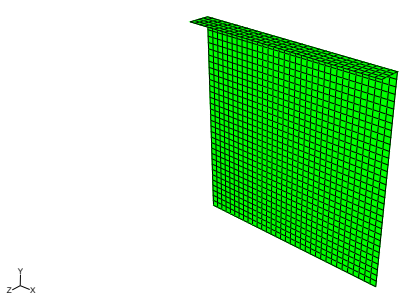

(a) 1000X1000$_1$

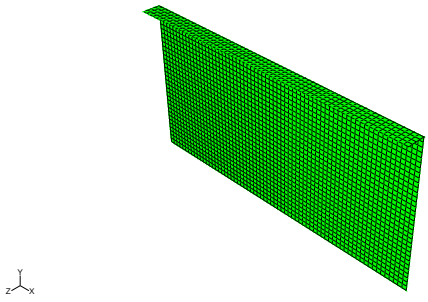

(b) 2000X1000$_1$

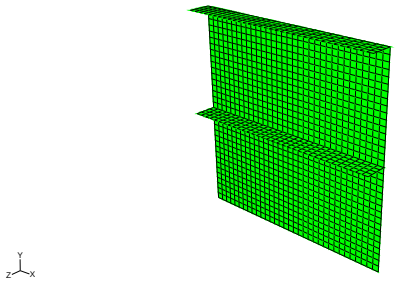

(c) 1000X1000$_2$

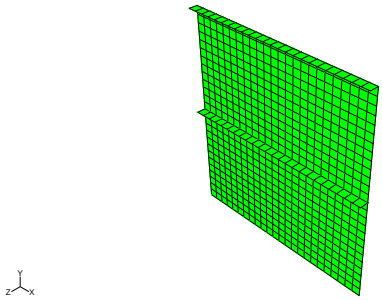

(d) 2400X2523$_2$

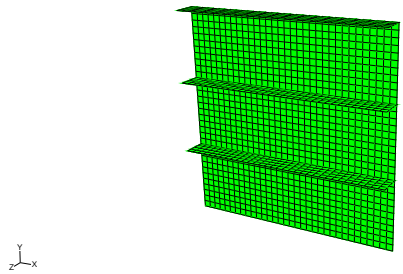

(e) 1000X1000$_3$

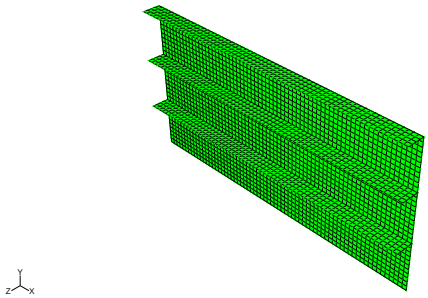

(f) 2000X1000$_3$

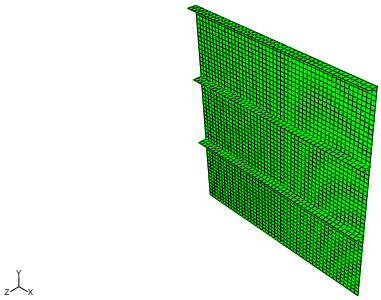

(g) 2400X2523$_3$

Figure 5.6: The plate cases in table 5.2 for a stiffener height of $h_s = 100$ mm (from ABAQUS).

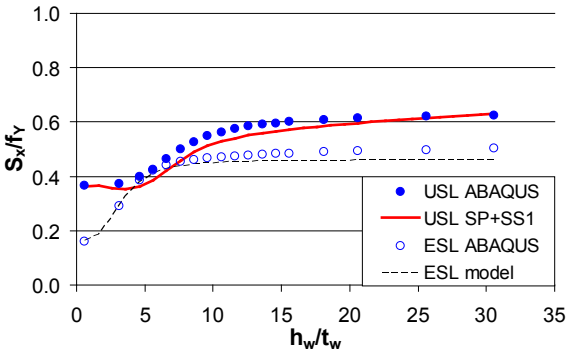

(a) 1000X1000$_1$

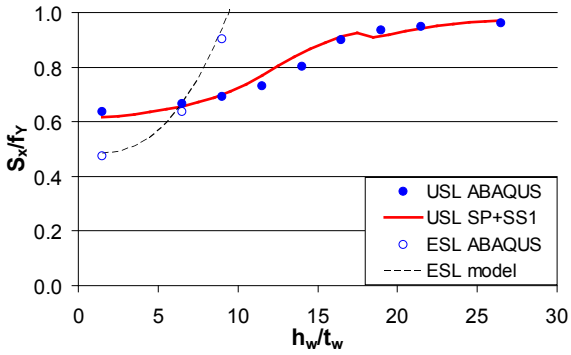

(b) 2000X1000$_1$

Figure 5.7: Ultimate strength limits (USL) and elastic buckling strength limits (ESL) for (a) 1000X1000$_1$ and (b) 2000x1000$_1$ with the selected criterion, SP + SS1 (plate definitions are given in table 5.2). ABAQUS results are included for comparison. The first linear elastic buckling mode, with an amplitude of 5 mm, is used as imperfection for all the USL calculations.

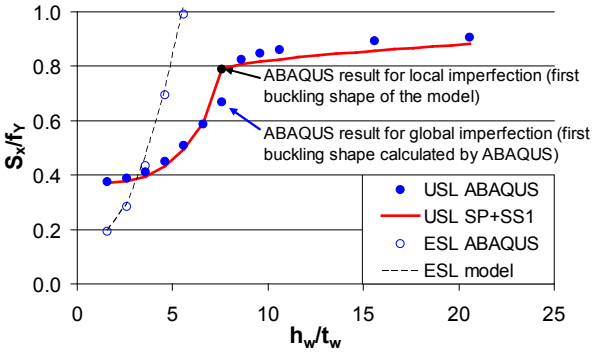

(a) 1000X1000$_2$

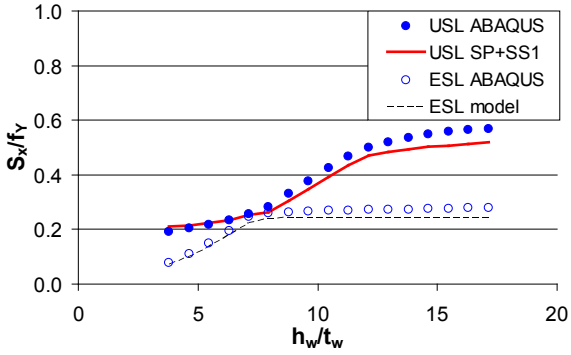

(b) 2400x2523$_2$

Figure 5.8: Ultimate strength limits (USL) and elastic buckling strength limits (ESL) for (a) 1000X1000$_2$ and (b) 2400x2523$_2$ with the selected criterion, SP + SS1 (plate definitions are given in table 5.2). ABAQUS results are included for comparison. The first linear elastic buckling mode, with an amplitude of 5 mm, is used as imperfection for all the USL calculations.

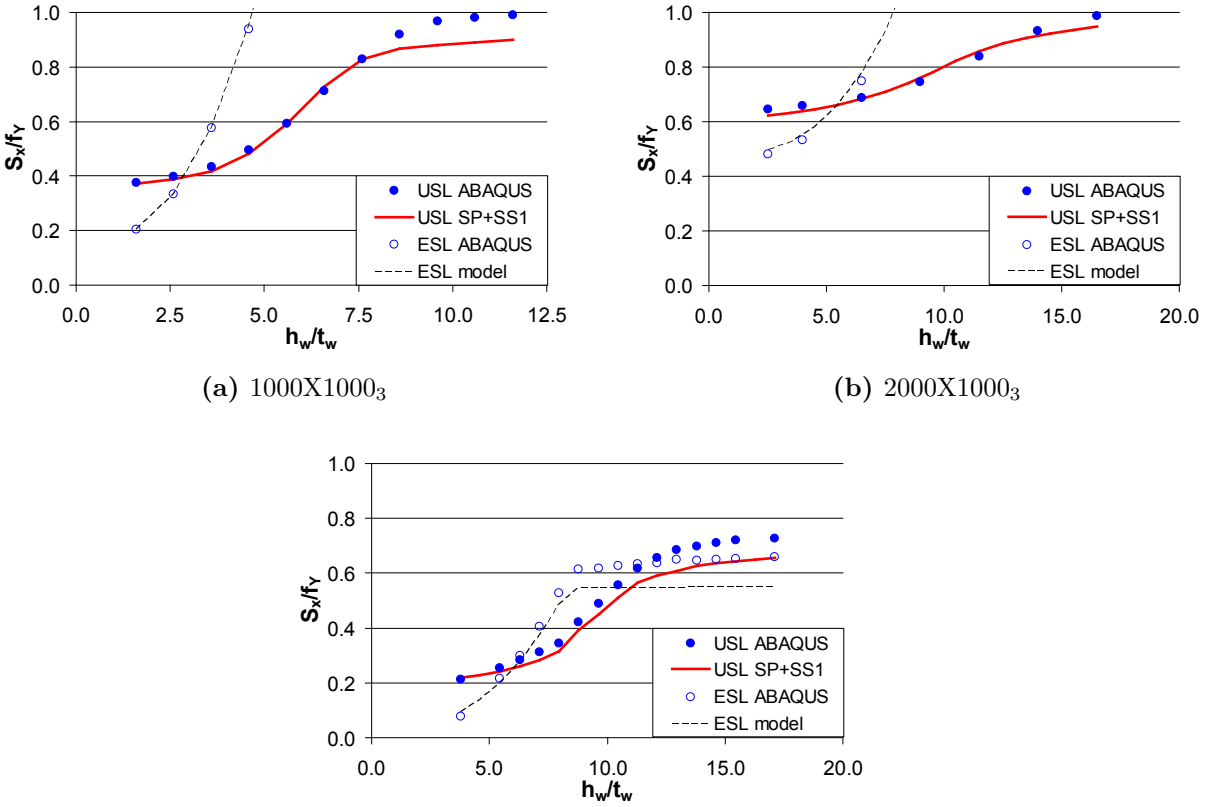

(a) $1000X1000_3$

(b) $2000X1000_3$

(c) $2400x2523_3$

Figure 5.9: Ultimate strength limits (USL) and elastic buckling strength limits (ESL) for (a) $1000X1000_3$, (b) $2000X1000_3$ and (c) $2400x2523_3$ with the selected criterion, SP + SS1 (plate definitions are given in table 5.2). ABAQUS results are included for comparison. The first linear elastic buckling mode, with an amplitude of 5 mm, is used as imperfection for all the USL calculations.

For 2400x2523$_2$, Figure 5.8b, the estimates from the semi-analytical model is good. Some conservative deviations are present as the stiffened free edge approaches simply supported. This is seen to be a common deviation and it will be addressed further below.

In Figure 5.9 it is generally observed that the estimates are reasonable for the cases with 3 stiffeners. Some conservative deviations are still present as the stiffened free edge approaches simply supported. This deviation is very small for 2000X1000$_3$, which represents rather thick plates ($t = 30$ mm). The other plate cases have a significantly smaller plate thickness, implying a larger influence by the stiffeners. This indicates that the deviation is a result of the simplifications made for the stiffeners, when using beam theory and neglecting the torsional stiffness, in the semi-analytical model.

A conservative deviation is observed, for cases with two and three stiffeners, as the stiffened free edge approaches simply supported. In such cases the stiffeners resits out-of-plane deformation of the plate, giving significant torsional components in the stiffeners due to twisting. The effect of including torsional stiffness of the stiffeners in the model will be discussed further in Chapter 6.

The USL estimates produced by combining SP and SS1, presented here, are satisfactory when compared to the ABAQUS results. The reduced stiffener height criterion, SS1, was also recommended by Brubak and Hellesland in [6] for the case of a simply supported plate with arbitrarily stiffeners. In that work the stiffener criterion was combined directly with first von Mises membrane yield of the simply supported edges. The present criterion will practically be equal to the criterion presented by Brubak and Hellesland [6] for strong edge stiffeners.

Chapter 6

Torsional stiffness of stiffeners in the semi-analytical model

6.1 Introduction

Stiffeners that resist out-of-plane deformation of the plate will experience twisting along the stiffener. Such twisting along the stiffeners is not resisted in the current model, but would be in a real structure. This effect is included in the finite element models, since shell elements are used for the stiffeners. The effect of torsional stiffness can be approximated by the potential energy due to St. Vernant torsion, see Equation 2.26, restated here for simplicity:

$$U^{sT,x} = \frac{GJ}{2} \int_0^L \left[w^2_{,xy} \right]_{y=y_s} dx \tag{6.1}$$

where G is the shear stiffness and J is the torsional constant. The torsional constant J for a flat bar stiffener is approximately given by (see Brush and Almroth [16]):

$$J = \frac{1}{3} \left(h_w - \frac{t}{2} \right) t_w^3 \tag{6.2}$$

Torsional rigidity of the stiffeners, due to St. Venant torsion, was not included in the original model developed by Brubak [2]. The corresponding stiffness contribution will therefore be developed and included in an expansion of the current model.

The effect of torsional stiffness will be considerable for cases with a local deformation shape. Such a deformation shape will be present when the stiffened free edge approaches simply supported. It was observed, in Section 5.3.4, that the current model, without torsion, gave conservative estimates for such cases.

Including the torsional stiffness will influence the ultimate limit strength (USL) estimates both with respect to imperfection and incremental stiffness. The imperfection, first buckling mode, will have reduced amplitude between stiffeners due to twisting resistance in the stiffeners. Smaller imperfection amplitudes in spans between stiffeners imply a stiffer configuration. The imperfection amplitude is the same for all spans if the torsional stiffness

is neglected. The increased incremental stiffness is a result of accounting for the torsional rigidity of the stiffeners when tracing the load-response.

Two semi-analytical models, model 1 and model 2, will be used in the current chapter. Model 1 will not include torsion, while model 2 includes torsion. The two models will both use the selected criterion in Section 5.3, where the plate criterion (SP) is combined with the reduced stiffener height criterion (SS1). Torsion will be included in both the buckling and large deflection calculations for model 2.

6.2 Incremental torsion matrix

The second variation of the potential energy due to St. Vernant torsion (Equation 6.1) must be found to include St. Vernant torsion in the current model. This second variation will then be include in the equation for stationary potential energy on rate form. The St. Vernant torsion matrix, for a longitudinal stiffener, will be denoted by $\mathbf{K^{sT,x}}$. A derivation of the St. Vernant torsion matrix is given in Appendix B.

The matrix derived in Appendix B includes all displacement components. This full matrix is then directly applicable in the load-displacement incrementation. Only the deflection components, corresponding to w_a and w_b, will be of interest when calculating the buckling load. The torsional matrix for the buckling calculations will be the sub matrix in the lower right corner of $\mathbf{K^{sT,x}}$ corresponding to the d_i entries related to w_a and w_b.

The derivation of the torsional stiffness for transverse stiffeners will be analogous to the derivation given in Appendix B. This contribution is not derived here, since transverse stiffeners are excluded from the current work.

6.3 Selection of plate dimensions and parameter

The cases in table 5.2 will be used to test the effect of torsional stiffness of the stiffeners.

Plate	N_{stiff}	**L (mm)**	**b (mm)**	**t (mm)**	t_w **(mm)**	h_w **(mm)**
$2400x2523_2$	2	2400	2523	11	12	[45.5-205.5]
$1000x1000_3$	3	1000	1000	12	10	[16-116]
$2000x1000_3$	3	2000	1000	30	10	[25-165]
$2400x2523_3$	3	2400	2523	11	12	[45.5-205.5]

Table 6.1: The selected plate dimensions used to test the effect of torsional stiffness of the stiffeners. Stiffeners are equally spaced and N_{stiff} gives the total number of stiffeners. The name convention used is $LXB_{N_{stiff}}$.

The same arc length increment and number of terms as for the stiffened case, Section 5.3.3, will be used.

6.4 Results

Results for the cases in table 6.3 is presented in Figure 6.1.

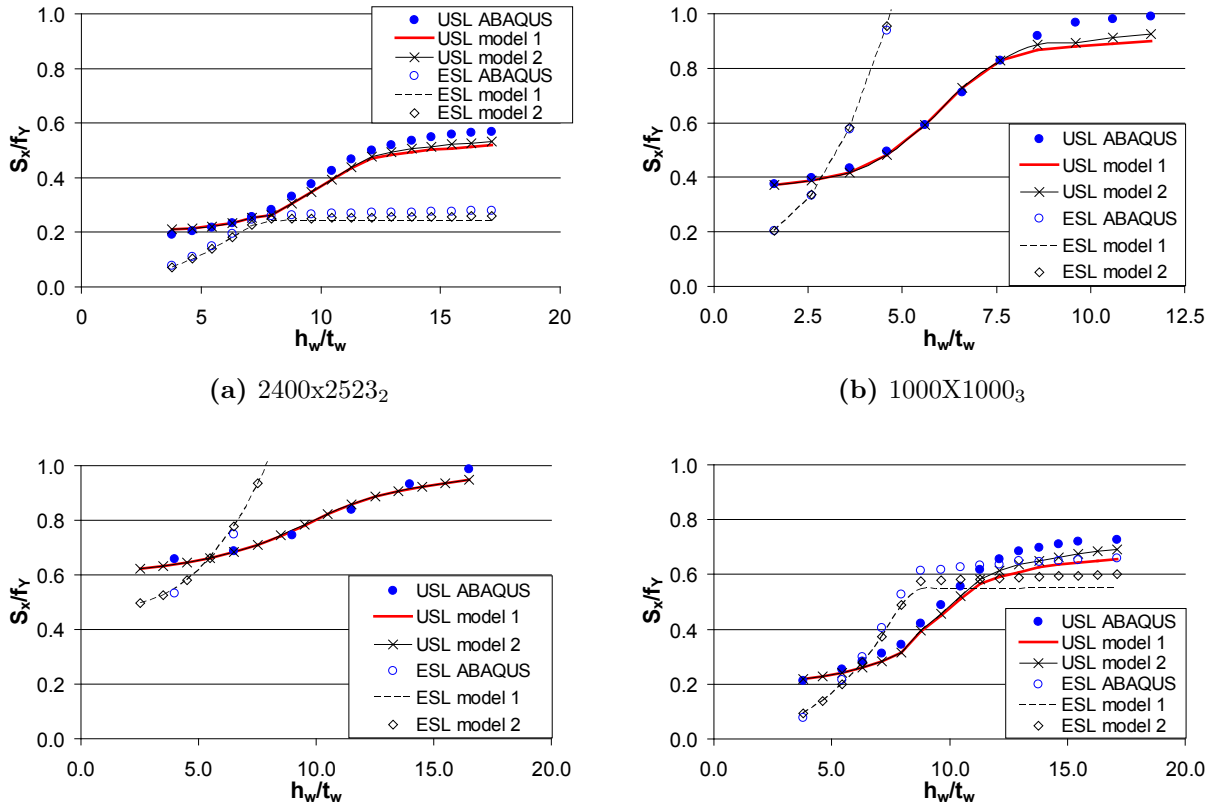

(a) 2400x2523$_2$ **(b)** 1000X1000$_3$

(c) 2000X1000$_3$ **(d)** 2400x2523$_3$

Figure 6.1: Ultimate strength limits (USL) and elastic buckling strength limits (ESL) estimates from model 1(without torsion) and model 2(with torsion) for (a) 2400x2523$_2$, (b) 1000X1000$_3$, (c) 2000X1000$_3$ and (d) 2400x2523$_3$. ABAQUS results are included for comparison. The first linear elastic buckling mode, with an amplitude of 5 mm, is used as imperfection for all the USL calculations.

6.5 Discussion and conclusion

Figure 6.1a, 2400x2523$_2$, shows that the effect of torsional stiffness of the stiffeners is moderate for this case. It is seen that the estimate becomes somewhat better, both for the elastic buckling limits (ESL) and the ultimate strength limits (USL). The deviation between the models increases as the stiffened free edge approaches simply supported condition.

For 1000X1000$_3$, Figure 6.1b, the estimates are also somewhat better when torsional stiffness of the stiffeners is included. The improvements in the results are still relatively small with respect to the actual deviation from the ABAQUS results.

The case 2000X1000$_3$ has a significantly higher plate thickness then the other plates. This high plate thickness gives globally dominated deformation shapes, implying limited twisting of the stiffeners, for all the considered stiffener heights. This explains the negligible difference between model 1 and model 2 in Figure 6.1c.

The deviation between the semi-analytical model and ABAQUS is significantly reduced when torsional stiffness of the stiffeners is included for 2400x2523$_3$, see Figure 6.1d. This improvement is observed for both the USL and ESL estimates.

Including torsional stiffness of the stiffeners improved the estimates for ESL and USL in all cases except from 2000X1000$_3$, where the solution is practically the same. The effect of including the torsional stiffness is largest for 2400x2523$_2$ and 2400x2523$_3$. These cases have a small slenderness and a higher web thickness, $t_w = 12$ mm, than the other plates, $t_w = 10$ mm. A higher web thickness gives a significant increase in the torsional constant J, see Equation 6.2. The small slenderness indicates that large deflections will be present in the plate. A local deformation shape is observed for most of the stiffener heights, since the plate thickness is small. This combination, of large deflections and a local deformation shape, implies considerable twisting of the stiffeners, which is resisted by the torsional rigidity of the stiffeners. These properties explains why the relative accordance with ABAQUS is better for 2400x2523$_2$ and 2400x2523$_3$.

Including torsional stiffness of the stiffeners does not fully explain the general deviation, between the semi-analytical model and the ABAQUS results, observed for cases with a small plate thickness and large stiffeners. The rest of the deviation might be a result of modelling the stiffeners as beams in the semi-analytical model. It is then possible that the potential energy is underestimated, due to limitations in beam theory. Such aspects will not be discussed further here.

The effect of neglecting torsional rigidity of the stiffeners is, as expected, seen to be conservative. Including this effect will increase the computational time, especially when stiffener reduction is included. The largest deviation found, when torsion is neglected, is about 11 percent. Such a conservative deviation is well within acceptable limits and the torsional stiffness of the stiffeners can be neglected. Selecting a conservative approach is a sound way of doing things and the torsional rigidity of the stiffeners will be neglected in the rest of this thesis. Similar conclusions for ESL estimates was drawn by Eiding in [1].

Chapter 7

Design codes and rules

7.1 Local stiffener buckling

Local buckling of stiffeners is discussed in DNV-RP-C201 [3]. The criterion for welded flange outstands, relevant for eccentric flat bar stiffeners, states that:

$$h_s \leq 14 t_w \sqrt{\frac{235}{f_Y}} \tag{7.1}$$

where h_s is the height of the flat bar stiffener and t_w is the thickness of the stiffener.

In the current study $f_Y = 235$ MPa giving the following criterion:

$$h_s \leq 14 t_w$$

For the stiffened cases studied in Section 5.3 the flat bar web thicknesses was either 10 mm or 12 mm. These values for h_w gives the following conditions:

$$h_s \ \leq \begin{cases} 140 \text{ mm}, & t_w = 10 \text{ mm} \\ 168 \text{ mm}, & t_w = 12 \text{ mm} \end{cases} \tag{7.2}$$

Table 7.1 gives the h_s-spans and t_w-values for the stiffened cases in table 5.2.

Plate	t_w **(mm)**	h_s **(mm)**
$1000X1000_1$	10	[10-300]
$2000X1000_1$	10	[10-270]
$1000x1000_2$	10	[10-200]
$2400x2523_2$	12	[40-200]
$1000x1000_3$	10	[10-110]
$2000x1000_3$	10	[10-150]
$2400x2523_3$	12	[40-200]

Table 7.1: The h_s-spans and t_w-values for the plate cases of table 5.2.

It is observed that the h_s-values, table 7.1, used in the current study exceeds the appropriate limits of Equation 7.2. Such design criteria are usually conservative, indicating that the model might give reasonable estimates for higher value of h_s. Results of the finite element models were then studied and severe local stiffener buckling was not observed.

The first linear elastic buckling mode will mainly be local when the stiffener web heights exceed the limit values. For such cases the stress in the stiffener are approximately the same as the plate membrane stress (in the x-direction) under the stiffeners, due to marginalised bending of the stiffeners out-of-plane. Some bending of the stiffeners will always be present since a global mode will be initiated, in the non-linear geometrical analysis, by the eccentric loading. This results in a tensional bending stress component in the stiffeners. The large stiffeners will then experience a compression stress close to the plate membrane stress (in the x-direction), but with some unloading over the height due to the bending deflections. The requirement in Equation 7.1 accounts for both elastic and plastic buckling of the stiffeners. Plastic buckling will not be a problem for the eccentric stiffeners present here, since stiffener yielding, if present, only will be in tension and not compression. The most conservative load case, uniform compression, is also assumed in the development of the requirement for flange outstands. Equation 7.1 will then be conservative for the current cases, since it includes plastic buckling and assumes a failure mode not relevant for the present analysed cases. More refined analysis might be carried out resulting in a more refined requirement for the stiffener height of the eccentric flat bar stiffeners considered here. This will not be done in the current work.

The ultimate strength limit estimates of the semi-analytical model should then, in lieu of the observations above, be reasonable for all the included stiffener web heights.

7.2 PULS imperfections - Combined local and global mode

7.2.1 Imperfection definition

The first buckling mode was used as imperfection when testing the criteria in Chapter 5. For unstiffened plates the first buckling mode will typically be critical, since the free edge implies a global imperfection. The critical imperfection for stiffened plates will, on the other hand, be either local or global, depending on the stiffeners. It is therefore common to combine a local and global initial deformation shape, for stiffened cases, to ensure that the critical mode is included. The global imperfection, see Figure 7.2a, corresponds to the imperfection shape of an unstiffened plate and is defined by:

$$w_{imp,gloabal} = \frac{L}{1000} \sin\left(\frac{\pi x}{L}\right) \frac{y}{b} \tag{7.3}$$

The local imperfection, see Figure 7.2 (b), is defined by deflections between the stiffeners:

$$w_{imp,local} = \frac{s}{200} \sin\left(\frac{\pi n_x x}{L}\right) \sin\left(\frac{\pi n_y y}{b}\right) \tag{7.4}$$

where n_x gives the number of half-waves in the x-direction, n_y gives the number of half-waves in the y-direction and s gives the stiffener spacing.

The n_x and n_y value are found by studying the analytical solution for buckling of an unstiffened plate with simply supported edges, subjected to a uniform uniaxial in-plane compression. This unstiffened plate, will correspond to the unstiffened plate parts between stiffeners, or between the inner stiffener and the inner edge, at $y = 0$. Figure 7.1 shows a typical geometry for a stiffened plate and the equivalent unstiffened plate, used to calculate the local buckling shape between stiffeners. The analytical solution for such an unstiffened case, under uniform uniaxial in-plane compression, can be found in Bush and Almroth [16]. Bush and Almroth [16] uses the linear partial equation to find the linear elastic buckling mode. The elastic buckling shape, of the equivalent unstiffened plate, will be given by:

$$w = \sin\left(\frac{m\pi x}{L}\right)\sin\left(\frac{n\pi y}{s}\right) \tag{7.5}$$

where m and n will be found by minimizing the corresponding buckling load, P_x.

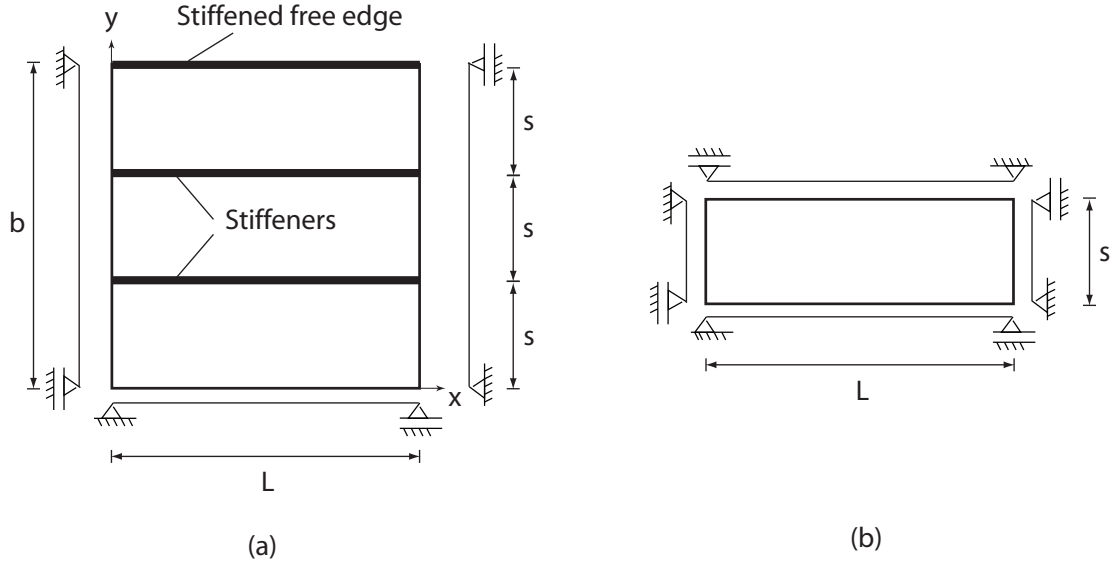

Figure 7.1: (a) the plate geometry and (b) the equivalent unstiffened plate for local buckling between stiffeners. Three stiffeners are included in this principle figure.

The corresponding buckling load is:

$$P_x = sD\left(\frac{\pi L}{m}\right)^2\left[\left(\frac{m^2}{L} + \frac{n^2}{s}\right)\right]$$

It is evident that the lowest buckling load is given by $n = 1$ and the expression simplifies to:

$$P_x = k_c\frac{\pi^2 D}{s}$$

where $D = Et^3/[12(1-\nu^2)]$ is the bending stiffness of the plate and k_c is defined as follows:

$$k_c = \left(\frac{ms}{L} + \frac{L}{ms}\right)^2 \tag{7.6}$$

The value of m giving the lowest buckling load will then be selected. This value will correspond to the value of m giving the lowest k_c value. It will be sufficient to check the two m values closest to the ratio between length, L, and stiffener spacing, s. The value of n_x will then be the m value corresponding to the lowest buckling load of the equivalent unstiffened plate. Matching the imperfection shape in Equation 7.4 with the buckling shape in Equation 7.5 (for $n = 1$), it is evident that n_y will be equal to the number of stiffeners, N_{stiff}.

Combining the local and global imperfection for $n_y = 3$ gives the total imperfection shown in Figure 7.2c. The imperfection amplitudes used for local and global imperfections, see Figure 7.2a and Figure 7.2b, are consistent with those used for simply supported stiffened plates in PULS [7].

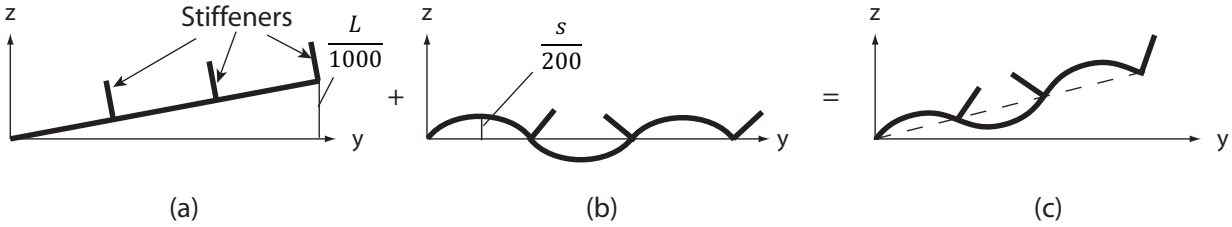

Figure 7.2: The imperfection, at the midline (x = L/2), for (a) the global mode, (b) the local mode and (c) the combined imperfection, when $n_y = 3$ and n_x is an odd number.

7.2.2 Plate dimensions and model parameters

Ultimate strength limit (USL) estimates will be presented for the plate cases in table 7.2. The model parameters, number of terms etc., will be the same as given in Section 5.3.3.

7.2.3 Results

Exactly the same imperfection is used in both ABAQUS and the semi-analytical model. The results should then be directly comparable. Ultimate strength limit (USL) predictions for the plate cases with one, two and three stiffeners are given in Figure 7.3, 7.4 and 7.5 respectively. Elastic buckling strength limits (ESL) is also included to indicate the slenderness of the plates. The selected criterion (SP + SS1) will be used in the semi-analytical model.

Plate	N_{stiff}	L (mm)	b (mm)	t (mm)	t_w (mm)	h_w (mm)
$1000X1000_1$	1	1000	1000	12	10	[6-306]
$2000X1000_1$	1	2000	1000	30	10	[15-265]
$1000x1000_2$	2	1000	1000	12	10	[16-206]
$2400x2523_2$	2	2400	2523	11	12	[45.5-205.5]
$1000x1000_3$	3	1000	1000	12	10	[16-116]
$2000x1000_3$	3	2000	1000	30	10	[25-215]
$2400x2523_3$	3	2400	2523	11	12	[45.5-205.5]

Table 7.2: The selected plate dimensions used to test the selected criterion (SP + SS1) for the combined imperfections shown in Figure 7.2. Stiffeners are equally spaced and N_{stiff} gives the total number of stiffeners. The name convention used is $LXB_{N_{stiff}}$.

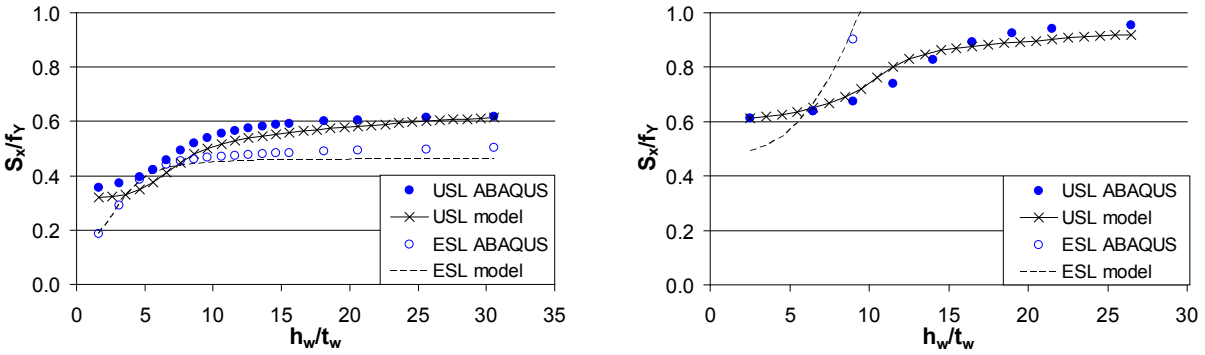

(a) $1000X1000_1$ **(b)** $2000X1000_1$

Figure 7.3: Ultimate strength limits (USL) for (a) $1000X1000_1$ and (b) $2000X1000_1$, see table 7.2, with combined imperfections. Elastic buckling strength limits (ESL) is also included to indicate the slenderness of the plate cases.

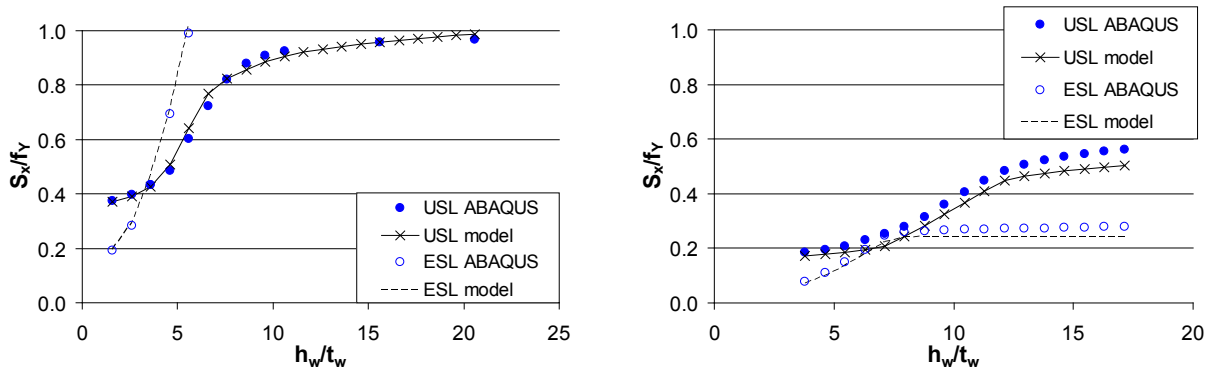

(a) $1000X1000_2$ **(b)** $2400x2523_2$

Figure 7.4: Ultimate strength limits (USL) for (a) $1000X1000_2$ and (b) $2400x2523_2$, see table 7.2, with combined imperfections. Elastic buckling strength limits (ESL) is also included to indicate the slenderness of the plate cases.

7.2.4 Discussion and conclusion

The model estimates for the cases with one stiffener, see Figure 7.3, are quite good. They are similar to the results obtained when testing the criterion in Section 5.3.4. Estimates for the case $1000X1000_1$ is very satisfactory. For $2000X1000_1$ a non-conservative deviation of approximately 8 percent is observed, which is within acceptable limits. In Figure 5.7b a small drop was observed when the threshold value was approached. This small drop is not present in Figure 7.3a since combined imperfections are used.

Figure 7.4a shows good accordance between the semi-analytical model and ABAQUS for $1000X1000_2$. For $2400x2523_2$, see Figure 7.4b, the estimates of the semi-analytical model are conservative for all cases, but within acceptable limits.

Accordance between the model and ABAQUS for $1000X1000_3$, see Figure 7.5a, is good for the first half of the stiffener height range. The deviation increases when the stiffened free edge approaches a simply supported condition. The maximum conservative deviation is approximately 8 percent, which is within tolerance. USL estimates for $2000X1000_3$ in Figure 7.5b are very good.

Moderate relative deviations for low stiffener heights are observed, in Figure 7.5c, for $2400X2523_3$. One possible explanation is that ABAQUS results are based on finite strain formulations, while the semi-analytical model uses large deflection theory. For such cases with low slenderness, the large deflection theory might be somewhat insufficient. The USL estimates of the semi-analytical model are conservative and this is desirable for low slenderness cases, due to large insecurities with respect to imperfections etc. These deviations will not be discussed further here, since such plate cases are not expected in real structures. For the rest of the stiffener heights studied the results for $2400X2523_3$ are conservative and reasonable. The estimates for $2400X2523_3$ are, based on the observations above, reasonable

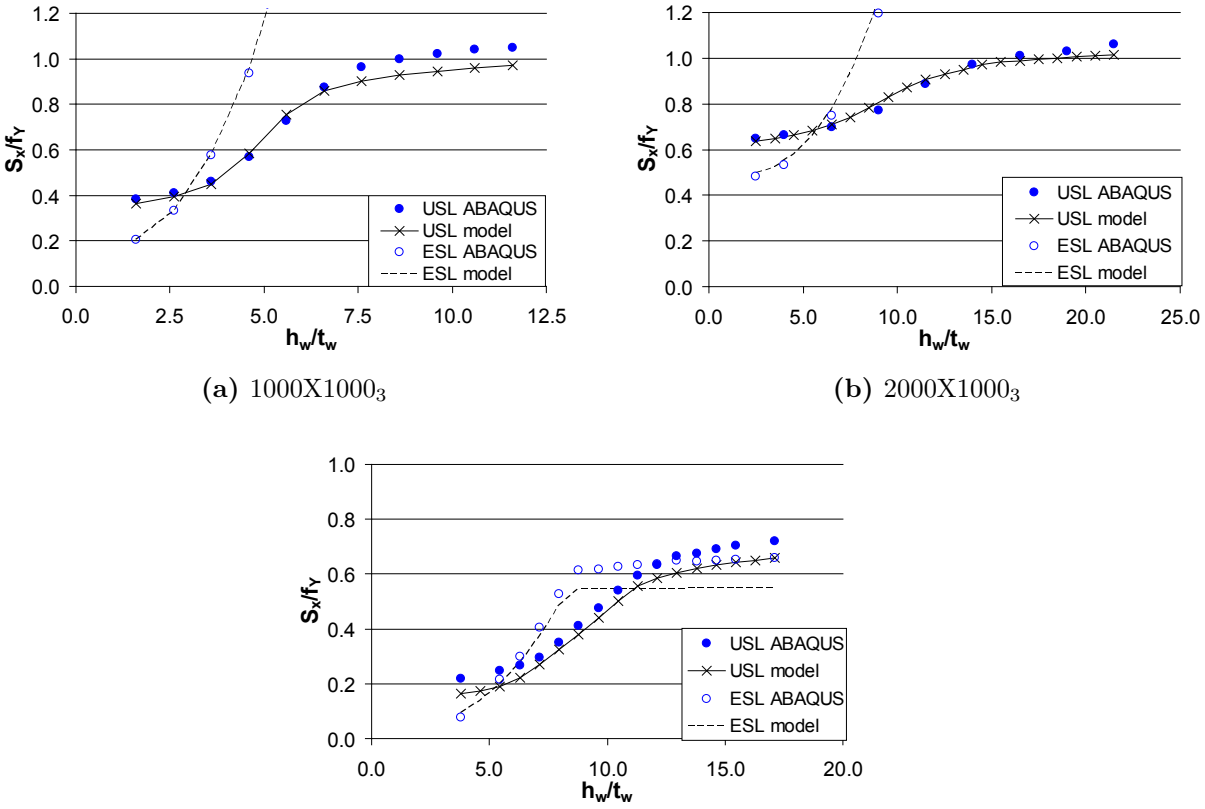

(a) 1000X1000$_3$

(b) 2000X1000$_3$

(c) 2400x2523$_3$

Figure 7.5: Ultimate strength limits (USL) for (a) 1000X1000$_3$, (b) 2000X1000$_3$ and (c) 2400x2523$_3$, see table 7.2, with combined imperfections. Elastic buckling strength limits (ESL) is also included to indicate the slenderness of the plate cases.

for the practical range of stiffener heights.

For 1000X1000$_3$ and 2000X1000$_3$ the USL estimates are observed to exceed the yield stress, f_Y. For 1000X1000$_3$ this is only observed in the ABAQUS results, while it for 2000X1000$_3$ is present in both ABAQUS and the model. Such USL estimates exceeding the yield stress is a result of stiffeners absorbing significant amounts of loads. In a fully non-linear finite element analysis membrane yielding of the plate will be present close to the loaded edge. The stress level in the yielded parts will in addition be able to increase somewhat due to strain hardening in the finite element models. Stresses will then be redistributed to the large stiffeners over a short region close to the end. These stiffeners are strong enough to avoid global collapse of the plate, and the USL estimates will then exceed the yield stress of the material. The ULS estimates are able to exceed the yield stress due to the definition of externally applied stress, S_x. This externally applied stress is related to the cross sectional area of the plate, and not the total cross sectional area of the plate and stiffener. The externally applied load is, as explained above, in practice carried by both the stiffeners and the plate. The USL predictions will then be able to exceed the yield stress, since the applied load only is distributed over the cross section of the plate. USL estimates exceeding the yield stress in the semi-analytical model will be a result of high potential strain energy contributions from the stiffeners, which contributes to the overall load carrying capacity of the plate.

The estimates of the semi-analytical model are generally seen to be good for combined imperfections. This indicates that the current criterion is quite independent of imperfection shapes and amplitudes.

Chapter 8

Investigation of model assumptions

8.1 Introduction

Several aspects with respect to the assumptions made in the semi-analytical model will be discussed here. Possible deviations with respect to imperfections and boundary conditions will be discussed. Some considerations regarding the effect of permanent plastic deformations, when unloading from the ultimate strength limit etc., are also included. Two unstiffened plate cases, see Section 8.2, and two stiffened plate cases, see Section 8.3, are studied. This is a rather limited number of cases but they are selected to illustrate some important aspects. The studies conducted here is also included to give a better understanding of the the general principle of ultimate capacity (collapse).

8.2 Unstiffened

8.2.1 Plate definitions

The results in this section will be based on finite element analysis of unstiffened plates with a free edge and the dimensions are given in table 8.1. The slenderness values corresponding to the chosen dimensions are believed to be quite typical for unstiffened plates with a free edge used in ship applications.

Plate	L (mm)	b (mm)	t (mm)
Plate 1	2000	1000	20
Plate 2	2000	1000	44

Table 8.1: The plate dimensions considered in this section.

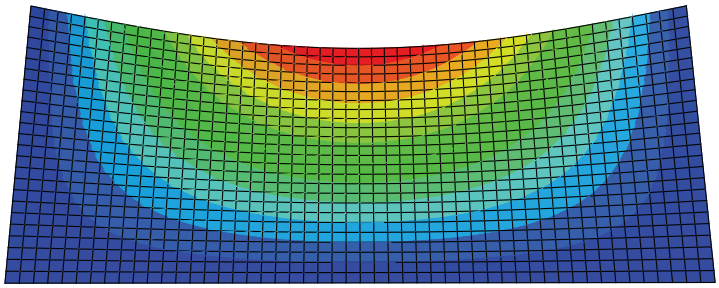

Figure 8.1: First buckling mode of a simply supported unstiffened plate with a free edge computed by ABAQUS. The current dimensions are L = 2000 mm, b = 1000 mm and t = 20 mm.

8.2.2 Effect of changes in imperfection amplitude

In this section, the effect of uncertainties in the imperfection is investigated using finite element models. A simply supported unstiffened plate with a free edge will be studied. For such unstiffened plates the first buckling mode, see Figure 8.1, will be quite similar to the expected imperfection shapes in ship applications. This implies that the effect of changes in the imperfection can be modelled by varying the imperfection amplitude, while using the same imperfection shape. The imperfection amplitudes studied here will be 0.1 mm, 1 mm and 5 mm.

Elastic buckling stress and slenderness

The elastic buckling stress is about 21 percent of the yield stress for plate 1 and approximately equal to the yield stress for plate 2. Plate 1 will then have a slenderness of approximately 2.2, while plate 2 will have a slenderness of approximately 1.

Finite element model

A fully non-linear analysis using the modified Riks method (see Section 4.3.2), considering both material and geometrical non-linearity, is carried out for these cases. The model contains 1250 S4R elements and the mesh is shown in Figure 8.1.

Results

The load-shortening curves for the different imperfection amplitudes are shown in Figure 8.2 for plate 1 and Figure 8.3 for plate 2.

Discussion and conclusion

Plates with a small imperfection will experience elastic buckling behaviour for applied stress close to the elastic buckling stress. The response of perfect plates with linear material properties will be addressed before imperfect plates are studied further. For perfect plates

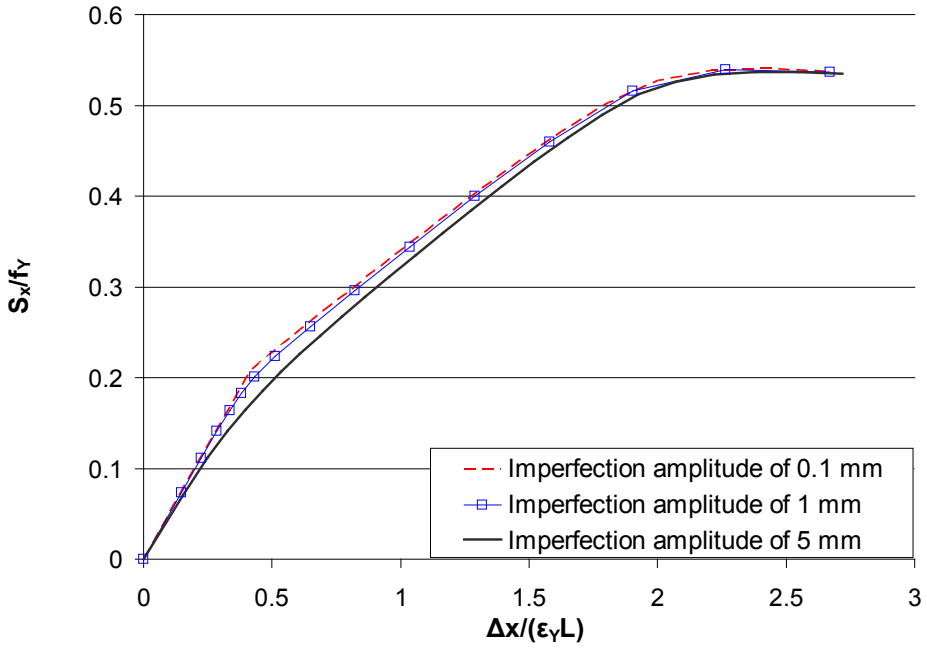

Figure 8.2: Load-shortening curves for plate 1 with different imperfection amplitudes.

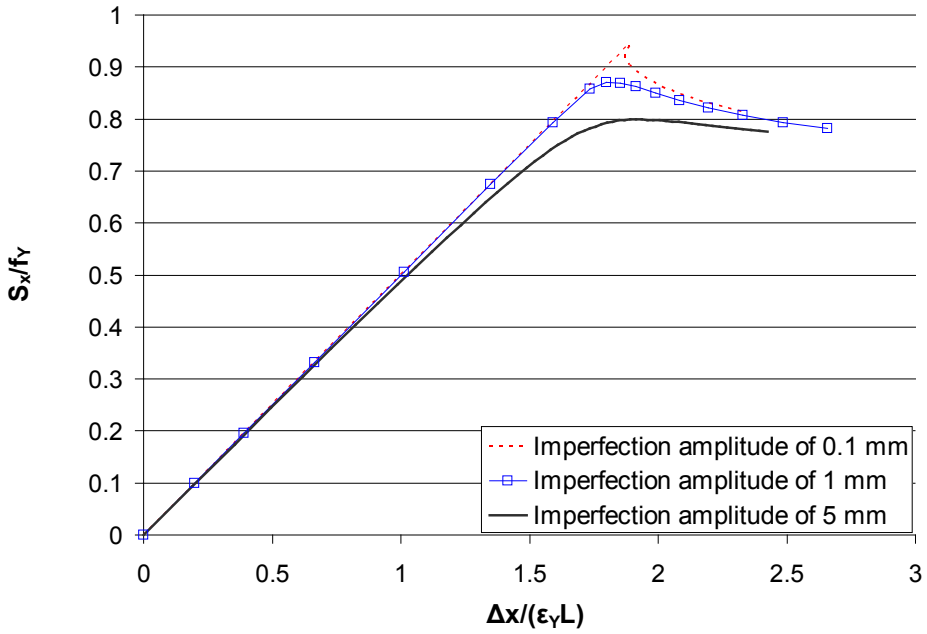

Figure 8.3: Load-shortening curves for plate 2 with different imperfection amplitudes.

there is no out-of-plane displacement present before the elastic buckling stress is reached. The out-of-plane displacement will develop when the applied stress exceeds the linear elastic buckling stress and a small disturbance is introduced. Such an out-of-plane displacement implies a reduction of the overall stiffness for the plate since the flexibility of the plate increases. For an imperfection amplitude of 0.1 mm, the plates are practically perfect and the load-shortening response for this imperfection amplitude can be regarded as the response of the perfect plate.

For plate 1 it is observed that the inclination of the load-shortening curve is significantly reduced when the external stress approaches the linear elastic buckling stress. The load-shortening curve becomes smoother as the initial imperfection increases. This is an effect of increased flexibility due to a relatively large initial imperfection, causing a continuous variation of stiffness. The load-shortening curves for plate 1 will asymptotically approach the same curve for all imperfections when the external load is increased above the linear elastic buckling load. This behaviour is natural since the size of the imperfection only affects the response close to the elastic buckling limit (ESL). As the external stress is increased above the ESL, the deformations will approach each other for the different imperfections amplitudes. This effect explains the asymptotic behaviour observed for plate 1

For plate 1 there will be no yielding in the region with elastic buckling behaviour. The yielding becomes important when the applied stress approaches the ultimate strength of the plate. Since there is little interaction between yielding and the buckling behaviour for plate 1, the ultimate strength is practically independent of the imperfection.

The elastic buckling stress for plate 2 is approximately the same as the yield stress, which implies that yielding of the plate will occur close to the elastic buckling stress. This is the reason for the large variation of ultimate strength predictions for plate 2. The maximum difference in ultimate strength for plate 2 is about 18 percent for the current imperfection amplitudes.

The ratio between thickness, t, and width, b, of plate 2 is more common for typical unstiffened plates with a free edge in ships than the equivalent ratio for plate 1. This implies that load-shortening responses as that of plate 2 will be expected in practical applications. The results above then indicate that the imperfection amplitude is important when computing the ultimate strength of real plates.

8.2.3 Effect of changes in boundary conditions

For plates encountered in real ship structures there will always be some rotational stiffness provided by neighbouring plates or girders. This effect is neglected in the current study since simply supported boundary conditions are used. In this section the consequences of such a simplification are investigated and discussed.

Several combinations of simply supported and clamped edges are tested and the cases considered are given in table 8.2. These analysis are carried out for plate 1 with an imperfection amplitude of 5 mm. The imperfection shape used for all cases is the first buckling mode of plate 1 with three simply supported edges, see Figure 8.1. This imperfection shape

is used for all cases since some initial rotations along the edges, due to welding etc., are expected for all types of boundary conditions in practical applications.

Case	x = 0	y = 0	x = L
$[ss/ss/ss]$	simply	simply	simply
$[ss/cc/ss]$	simply	clamped	simply
$[cc/ss/cc]$	clamped	simply	clamped
$[cc/cc/cc]$	clamped	clamped	clamped

Table 8.2: The combinations of support conditions used to investigate the effect of changes in boundary conditions.

Finite element model

The same finite element model as in Section 8.2.2 is used. The only difference is that the boundary conditions are varied instead of the imperfection amplitudes. Clamped end conditions will, when present, be applied relative to the initial rotations of the edges.

Results

The results for different combinations of boundary conditions are presented in Figure 8.4.

Discussion and conclusion

The plate studied here is rather slender. Figure 8.4 shows that deviations in the boundary conditions can give rather large changes in the ultimate strength. The relative difference between the case with only clamped ends and the case with only simply supported edges is approximately 25 percent. It is also evident that the ultimate strength when all edges are simply supported will give a conservative estimate for all practical plates. This is also expected since rotational constraints imply a stiffer configuration. The differences between the cases are mainly an effect of changes in the elastic buckling stress (eigenvalue) as boundary conditions are changed. A stiffer configuration, gives a higher elastic buckling stress, resulting in a less non-linear response. This is then an important effect when the ultimate strength is estimated.

The variation in ultimate strength, due to boundary conditions, will decrease as the slenderness decreases. When the slenderness is sufficiently small, the non-linear geometrical effects, due to elastic buckling behaviour, will be significant at external stresses much higher than the yield stress. When yielding is included, such external stress levels above the yield stress will not be possible since collapse due to yielding will occur. Therefore, the geometrical non-linearity is negligible for sufficiently thick plates and the deflection of the plate will be small. When the deflection is small, it is known from linear theory that the membrane stresses will be dominated by in-plane strains. Imposing rotational constraints along supported edges will mainly effect the deflection of the plate. The ultimate strength

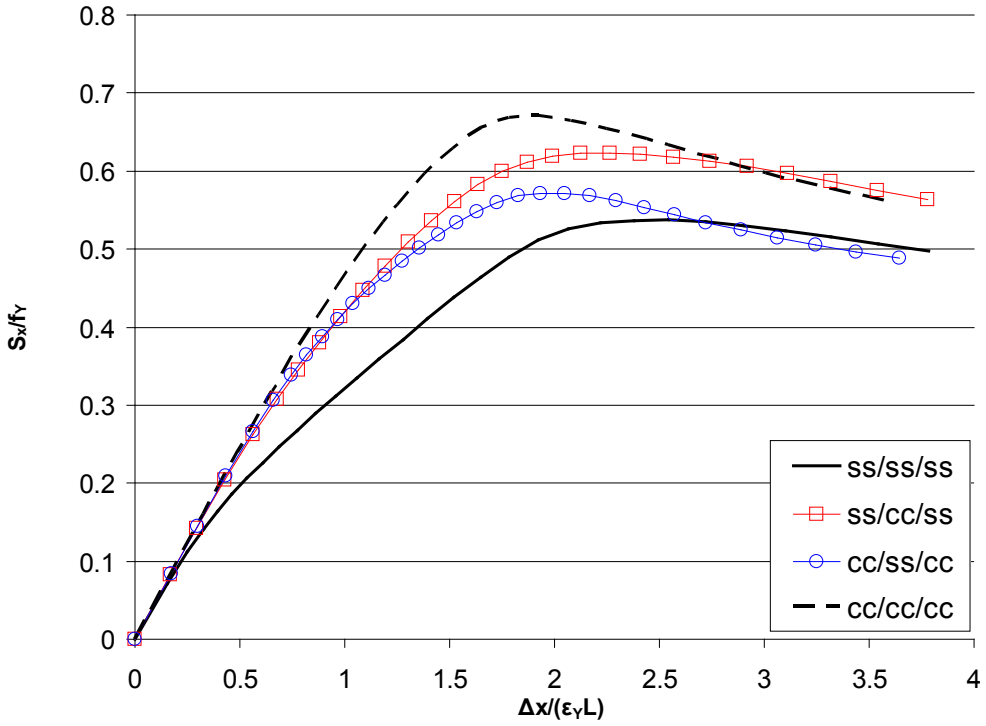

Figure 8.4: The load-shortening response of plate 1 when the boundary conditions are varied. An imperfection amplitude of 5 mm is used in the calculations.

of the plate is dependent on the membrane stresses in the plate. For plates with low slenderness, these membrane stresses are independent of the deflection. This implies that the effect of rotational constraints along the boundaries will decrease as the thickness increases.

The results found above imply that the use of simply supported boundary conditions can give quite conservative results for thin plates. As mentioned earlier, it is common that the ratio between thickness and length/width is higher than for plate 1. Therefore, it is expected that the effect of variations in boundary conditions usually is somewhat smaller than what encountered for the current case. This motivates the possibility of using simply supported edge conditions as a conservative approach.

8.2.4 Permanent plastic deformation

The practical strength of a plate is assumed to be given by the ultimate strength. Yielding of the material will be present before the ultimate strength of the plate is reached. If yielding is present for large areas of the plate, it will cause considerable amounts of permanent plastic deformations. Such large permanent plastic deformations will not be allowed when dimensioning a real plate. The scope of the following section is to investigate the possibilty

of considerable permanent plastic deflections for the plate cases in table 8.1. As earlier, the first buckling mode is used as imperfection shape with an amplitude of 5 mm.

It will be necessary to calculate the loading-unloading response to find the permanent plastic deformation. Unloading from several deformation states will be performed.

Finite element model

The finite element model used in these analyses includes both non-linear material properties and large deflections. To be able to include unloading after the maximum load is reached, it is necessary to use displacement control. The displacements at interesting load levels are selected by studying solutions found with the modified Riks method, see 4.3.2. The same mesh and element type as in Section 8.2.2 will be used.

Results

Load-shortening curves are given in Figure 8.5 for plate 1 and Figure 8.8 for plate 2. In addition, the load-deflection response is shown in Figure 8.6 for plate 1 and in Figure 8.9 for plate 2. First Von Mises surface and membrane yield are indicated in the figures. Plot of the Von Mises membrane stress with deflection at point (1) and (2), defined in Figure 8.5 and Figure 8.6, are given in Figure 8.7a and Figure 8.7b respectively.

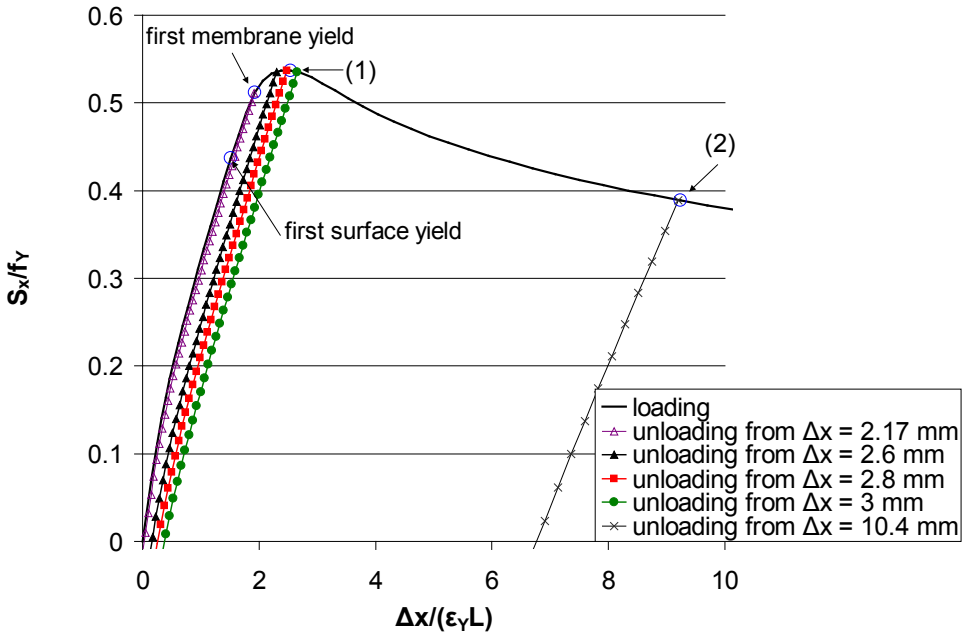

Figure 8.5: The load-shortening response for unloading of plate 1, with imperfection amplitude of 5 mm, for different end shortenings Δx.

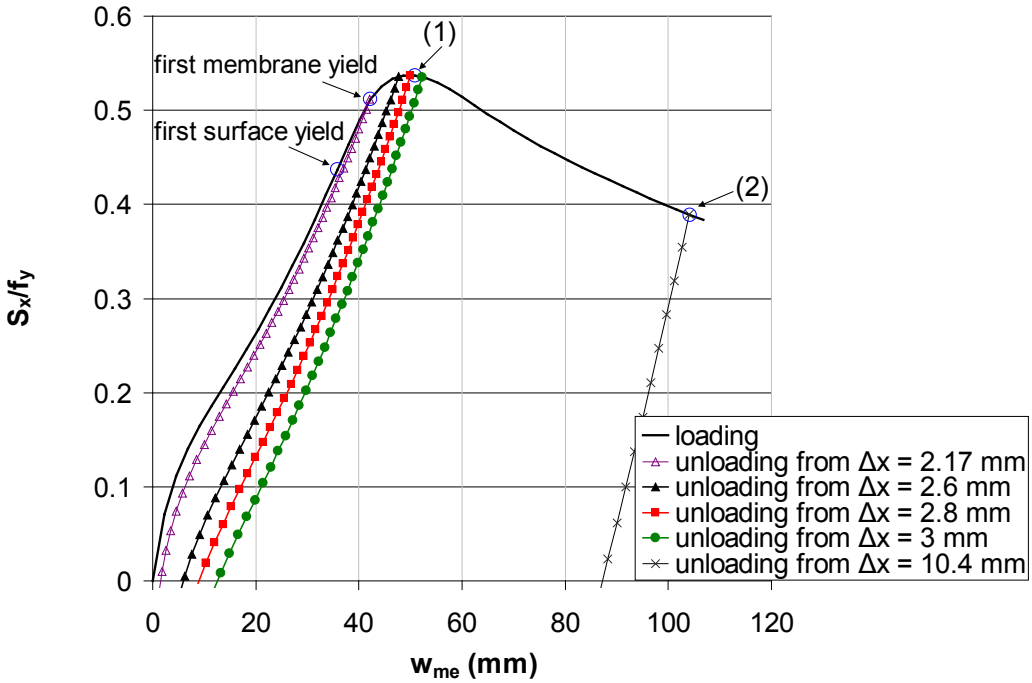

Figure 8.6: The load-deflection response for unloading of plate 1, with imperfection amplitude of 5 mm, for different end shortenings Δx. w_{me} denotes the deflection of the midpoint of the free edge.

Discussion and conclusion

To investigate the importance of unloading from different end-shortenings, Δ_x, several values in the vicinity of the ultimate strength were checked. It was also included a case for unloading in the region of post collapse for plate 1, see point (2) in Figure 8.5 and Figure 8.6.

The permanent plastic deflections are calculated relative to the initial imperfection. When unloading from the ultimate strength it is observed that the permanent plastic deflection amplitude is about 10 mm for plate 1 and 5 mm for plate 2. The permanent plastic deflection is about twice the initial imperfection for plate 1 and approximately equal to the initial imperfection for plate 2. These permanent plastic deflections will serve as extra imperfections for the plates after unloading. For plate 1 the value of permanent plastic deformation is considerable, while it for plate 2 is within acceptable limits.

If the deflection at ultimate strength, shown in Figure 8.7a, is compared to the initial imperfection, shown in Figure 8.1, it is observed that the deflection shape is basically the same, and harmonic in shape. The deflection in the post collapse region, given in Figure 8.7b, shows a large extra deflection along the mid strip. These locally large deflections along $x = \frac{L}{2}$ is typical for collapse of such plates when compressed in the x-direction. The

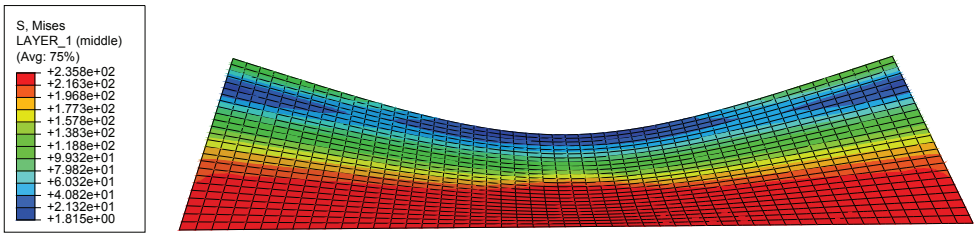

(a) Point (1)

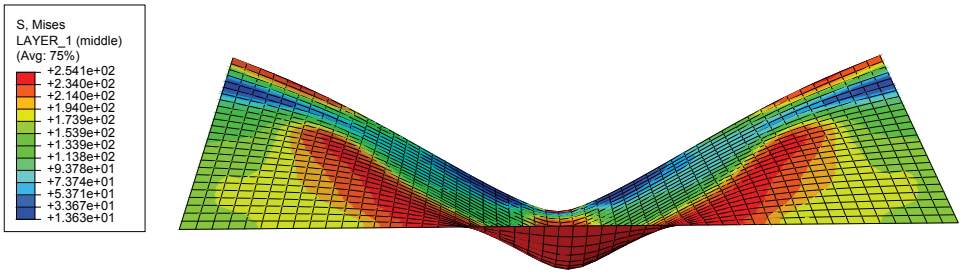

(b) Point (2)

Figure 8.7: Plot of Von Mises membrane stress (MPa) with deformed shape corresponding to (a) point (1) and (b) point (2) in Figure 8.5 and Figure 8.6. The deformation is scaled with a factor of 5.

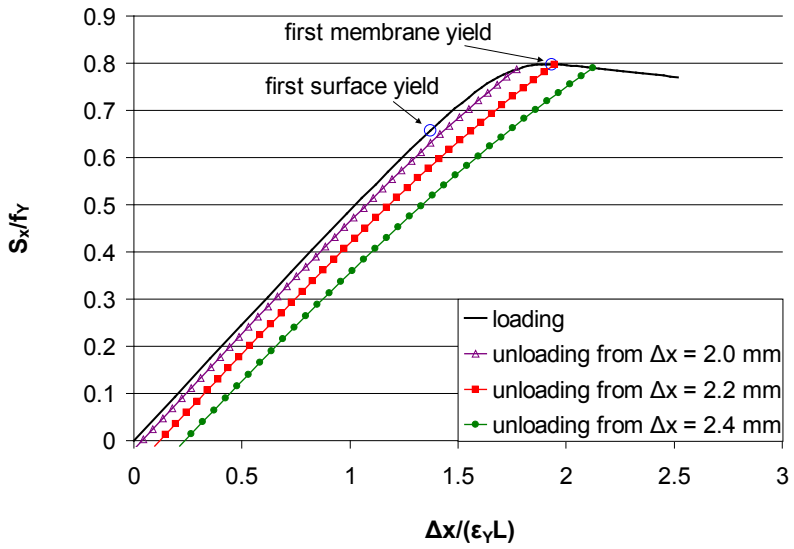

Figure 8.8: The load-shortening response for unloading of plate 2, with imperfection amplitude of 5 mm, for different end shortenings Δx.

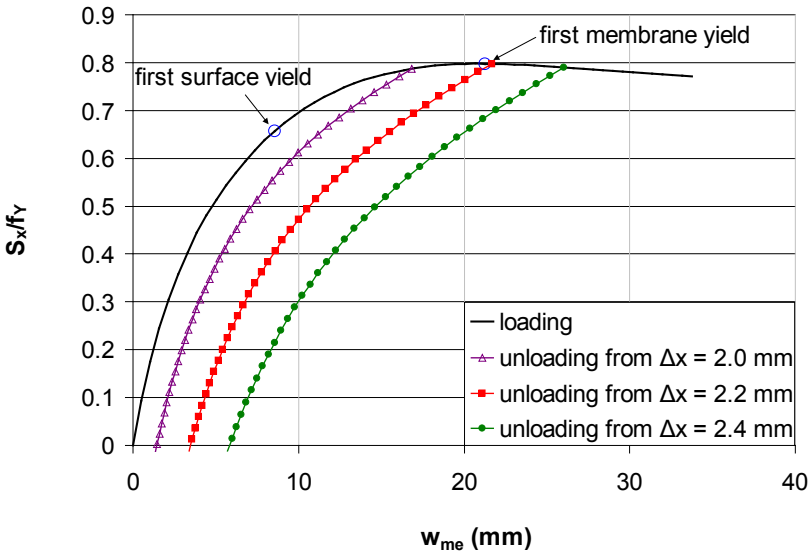

Figure 8.9: The load-deflection response for unloading of plate 2, with imperfection amplitude of 5 mm, for different end shortenings Δx. w_{me} denotes the midpoint deflection of the free edge.

Von Mises membrane stress distribution changes significantly from the ultimate strength region to the post collapse region. Such redistributions will be natural since large local deflections and significant material yielding are present at these states.

Based on the observations above, some extra considerations of the practical strength for plate 1 are conducted. In Section 5.2.3, the ultimate strength predicted with ABAQUS is compared to the semi-analytical model. These results imply that the semi-analytical model gives a conservative estimate for the ultimate strength of plate 1 for all the tested strength criteria. From Figure 8.6 it can be observed that first membrane yield is present before the ultimate strength is reached. The selected strength criterion used in the semi-analytical guarantees that the strength is reached at, or, before first Von Mises membrane yield. This can explain why the semi-analytical model gives a somewhat conservative ultimate strength estimate for plate 1. The ultimate strength found for plate 1 with the semi-analytical model is approximately the same as the load factor corresponding to first membrane yield in Figure 8.6. Figure 8.6 shows that unloading from the state of first membrane yield produces a permanent plastic deflection with amplitude of approximately 1.5 mm. Such a value for the plastic deflection will be negligible. Unloading from the ultimate strength limit estimate of the semi-analytical model will then result in negligible permanent plastic deformations for plate 1.

A negligible non-conservative difference is observed when comparing the semi-analytical model with the finite element analysis for plate 2, see Section 5.2.3. This small deviation will not affect the conclusion drawn above with regard to permanent plastic deflections for plate 2.

The observations above imply that the results of the semi-analytical model give good estimates for the practical strength of the plates considered in this chapter.

8.3 Stiffened

8.3.1 Plate definitions

The investigations for stiffened plates will be based on finite element analyses of plates with three eccentric flat bar stiffeners and the dimensions given in table 8.3. Figure 8.10 shows the plate geometry of the stiffened cases considered. A uniform compression load will, as before, be applied in the x-direction of the plate. The boundary conditions will be as specified in Section 3.4. An initial imperfection, equal to the first linear elastic buckling mode, with amplitude of 5 mm will be used in all the subsequent analyses.

Plate	**L (mm)**	**b (mm)**	**t (mm)**	h_w **(mm)**	t_w **(mm)**
Plate 3	2400	2523	11	155.5	12
Plate 4	2400	2523	8	154	12

Table 8.3: The plate dimensions considered in this section. Figure 8.10 shows the geometry of the cases.

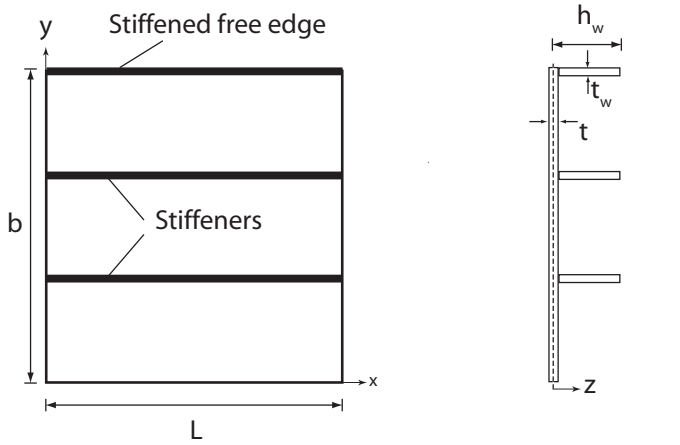

Figure 8.10: (a) the plate geometry and (b) the cross section, perpendicular to the free edge, of the stiffened plates considered here

Plate 3 is based on a real example from a ship's hull, while plate 4 is selected to illustrate the behaviour of a more slender case. The first linear elastic buckling stress of plate 3 and plate 4 is $0.65f_Y$ and $0.38f_Y$ respectively. Both plates have a local first buckling shape which is the common case for plates in real structures.

8.3.2 Permanent plastic deformation

The degree of permanent plastic deformation for the cases in table 8.3 will be studied here. An equivalent analysis for unstiffened plates was conducted in Section 8.2.4.

Finite element model

The analysis procedure will be the same as described in Section 8.2.4 and the stiffeners will be modelled using shell elements as discussed in Section 4.4.2.

Results

load-response curves for the plates in table 8.3 will be presented. load-shortening curves, with unloading, are given in Figure 8.11 and Figure 8.14. Similar the load-deflection curves are given in Figure 8.12 and Figure 8.15. Deformation plots for some interesting locations along the load-response curves of plate 3 is given in Figure 8.13.

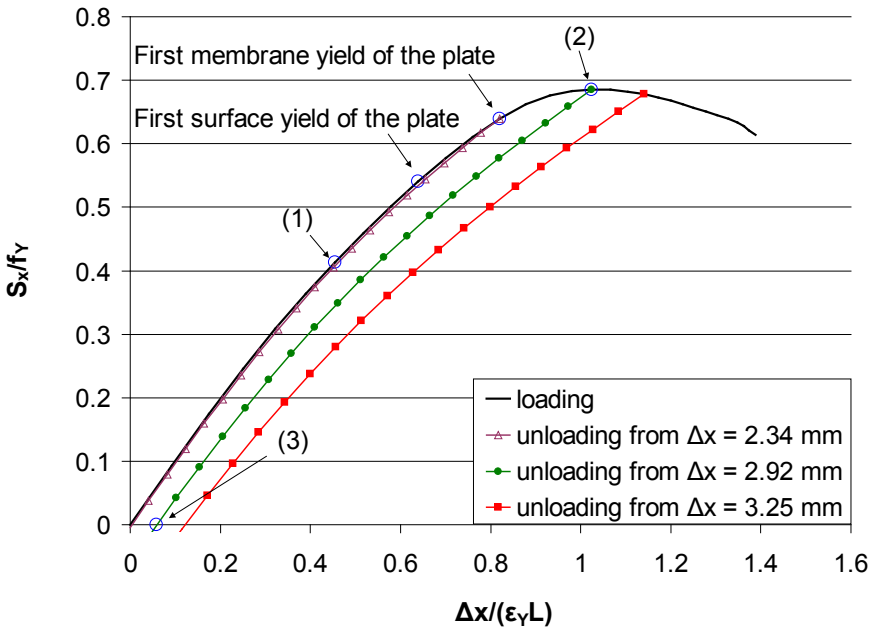

Figure 8.11: The load-shortening response for unloading of plate 3, with imperfection amplitude of 5 mm, for different end shortenings Δx.

Discussion and conclusion

Figure 8.12a and Figure 8.15a show that the end deflection increases to a significant value before decreasing to a small value. The permanent plastic deformation along the stiffened free edge is observed to be neglectable when unloading from the ultimate strength limit

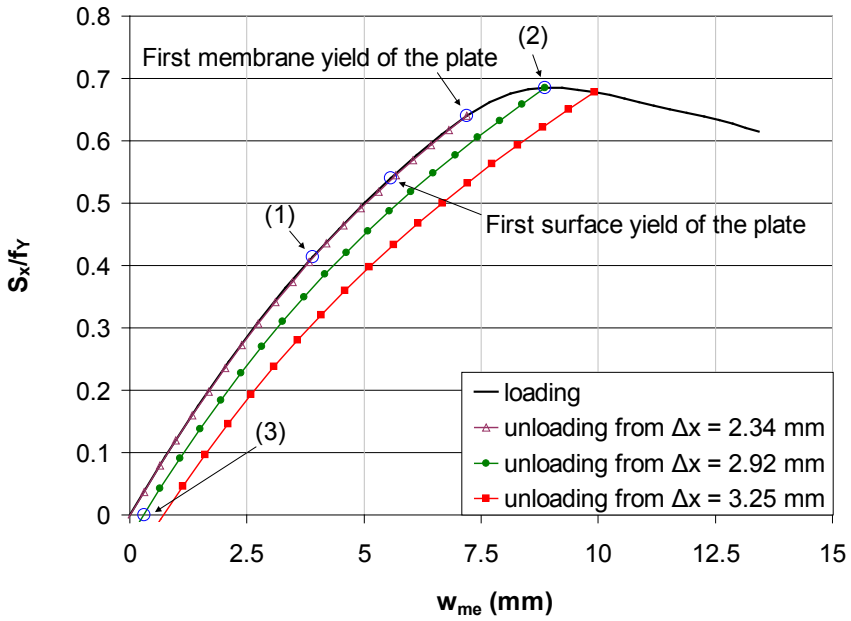

(a) Deflection of free edge midpoint

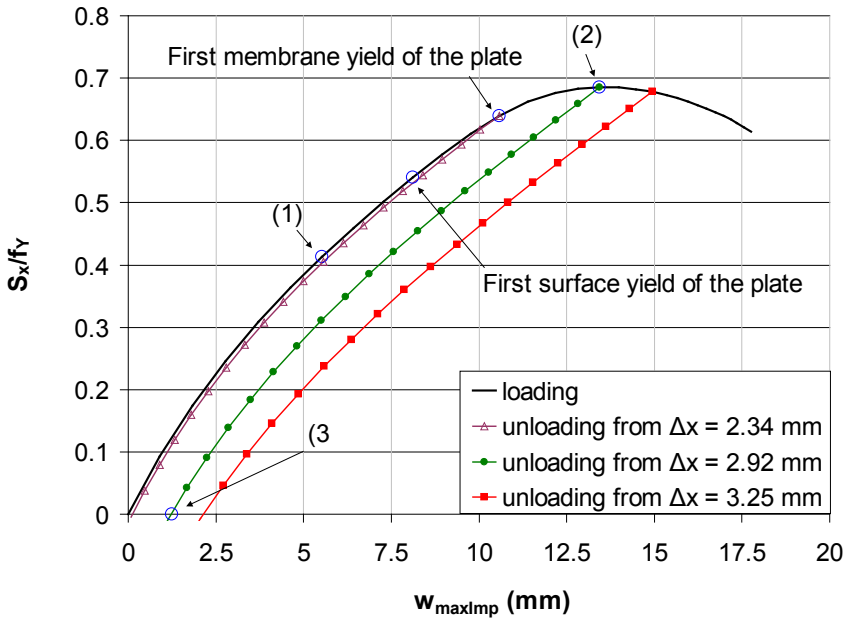

(b) Deflection of point at max imperfection

Figure 8.12: The load-deflection response for unloading of plate 3, with imperfection amplitude of 5 mm, for different end shortenings Δx. (a) shows the midpoint deflection of the free edge, w_{me}, and (b) shows the deflection of the point with maximum imperfection, w_{maxImp}. The imperfection amplitude used is 5 mm.

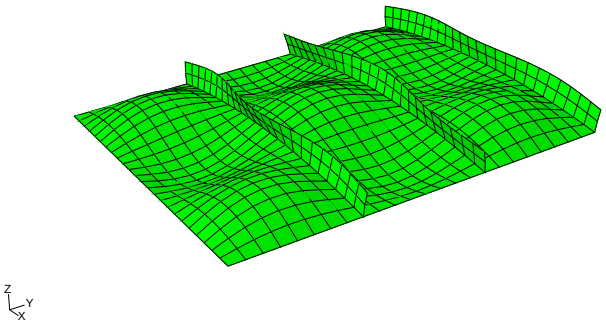

(a) Point (1)

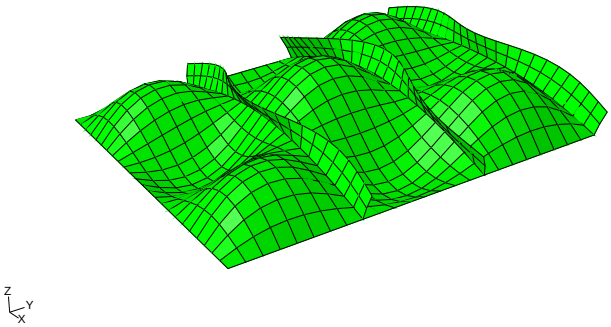

(b) Point (2)

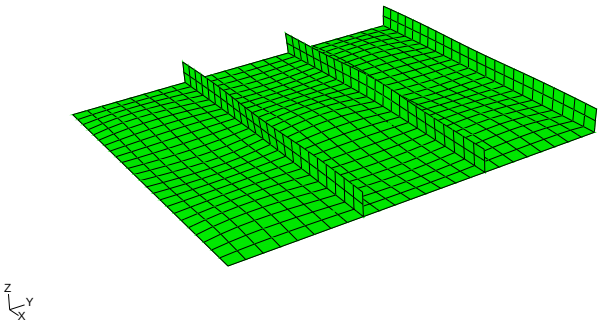

(c) Point (3)

Figure 8.13: Plot of deformed shape for plate 3 corresponding to respective points in Figure 8.11 and Figure 8.12. All the deformations are scaled with a factor of 20.

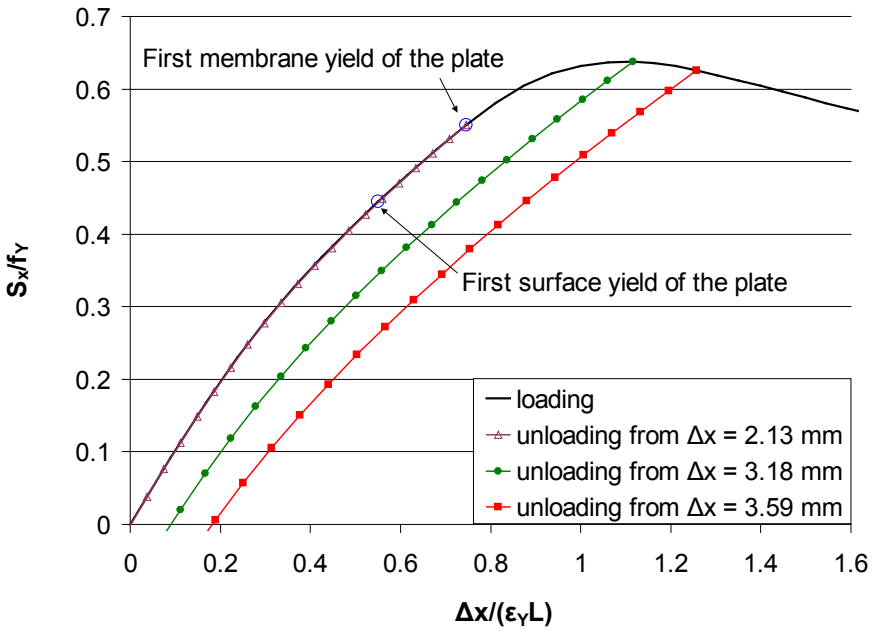

Figure 8.14: The load-shortening response for unloading of plate 4, with imperfection amplitude of 5 mm, for different end shortenings Δx.

(USL). When the point with maximum imperfection is studied, Figure 8.12b and Figure 8.15b, it is observed that the permanent plastic deformation is considerable. The deflection with respect to the initial imperfection is about 25 percent of the initial imperfection for plate 3 and about 40 percent for plate 4. The end shortening of the plates, Figure 8.11 and Figure 8.14, are included to indicate the degree of in-plane plastic deformation.

First membrane and surface yield of the plates are indicated in the figures, see for instance Figure 8.12 and Figure 8.15. It is observed that first membrane yield of the plates are reached somewhat before the USL of the plate. The difference between the loading at first membrane yield and USL is seen to be approximately 7 percent for plate 3 and 10 percent for plate 4. First surface yield of the plate occurs at a significantly lower load level than first membrane yield. It is observed, by unloading from first membrane yield, that the effect of surface yielding for such thin plates is small. This is also expected since the plates considered are thin indicating that the plastic distribution of stresses will be limited.

The plots in Figure 8.13 is included to graphically illustrate the effect of loading and unloading of a plate. The total deformation at half the USL load, at the USL load and after unloading is shown to indicate the effect of permanent plastic deformations.

Both the plate cases studied here have a local first linear elastic buckling mode as shown in Figure 2.6b. Such a local first elastic buckling mode is expected for stiffened panels with a free edge in real ship structures due to desired deformation and stiffness properties. As for unstiffened plates, see Section 8.2.4, it was observed that permanent plastic deformation is considerable in some cases. Unloading from first membrane yield of the plate, results in

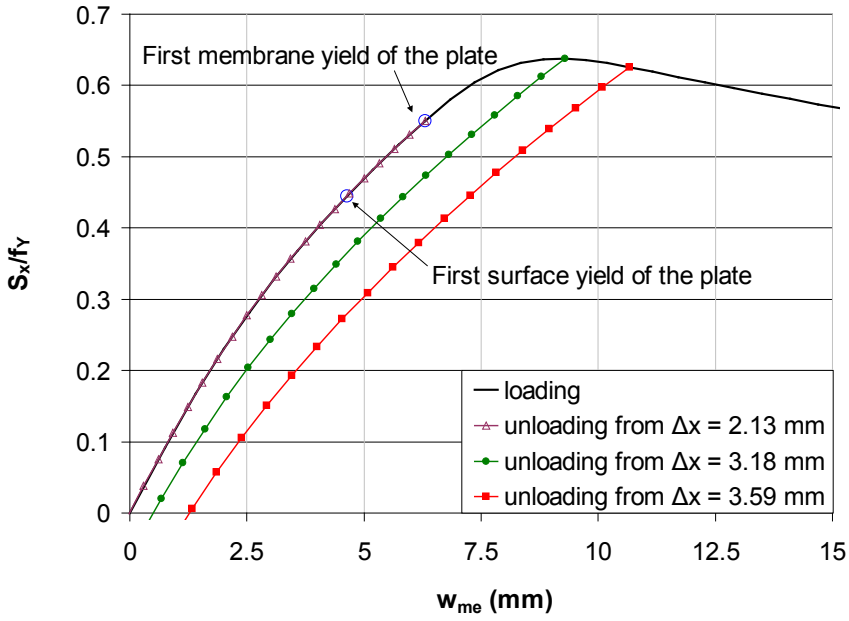

(a) Deflection of free edge midpoint

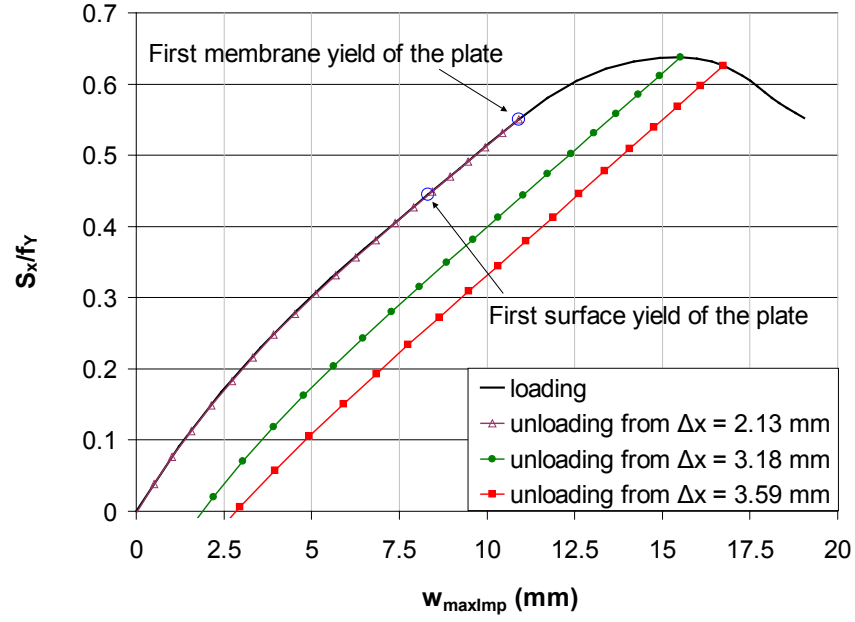

(b) Deflection of point at max imperfection

Figure 8.15: The load-deflection response for unloading of plate 4, with imperfection amplitude of 5 mm, for different end shortenings Δx. (a) shows the midpoint deflection of the free edge, w_{me}, and (b) shows the deflection of the point with maximum imperfection(5 mm), w_{maxImp}.

negligible permanent deformation for all the cases studied. This indicates that the plate criterion used in Section 5.3, which is based on first von Mises membrane yield, should give reasonable pratical estimates of the USL (with negligble permanent plastic defomration). Further studies must be conducted to draw general conclusions with regards to permanent plastic deformations of stiffened plates. The ultimate capacity of the plate should only be utilised when dimensioning an extreme condition, where the objective is to avoid collapse. For such cases the degree of permanent deformation found above will be within acceptable limits.

8.3.3 Straight edge assumptions at $y = 0$

In the general boundary conditions presented in Section 3.4 it is assumed that $v(x, 0) = 0$, which implies that the edge at $x = 0$ is straight. When studying a typical stiffened plate with a free edge in ships, see Figure 8.16, it is natural to assume that the bottom of the ship provides small resistance towards bending of the corresponding edge. The same applies to the stiffened free edge of the plate, where the stiffener provides little resistance towards bending along the edge. The boundary conditions assumed in the semi-analytical model makes the stiffened free edge, at $y = b$, free to bend along the edge while the inner edge, at $y = 0$, is kept straight. This makes the semi-analytical model stiffer than the real case for the example in Figure 8.16. The possibilty of using the current semi-analytical model to approximate the ulitmate strength limit (USL) of such plates will be adressed in the following section.

Plate 3 above will be used to study the possibilty of such an approxiamtion. USL predictions for varying plate thickness, of plate 3, will also be included to investigate the effect of varying the slenderness.

Finite element model

Solutions are found by using the modified Riks method, see Section 4.3.2. The model for the two cases will be equal except from the boundary condition at $y = 0$.

Results

Figure 8.17 shows the load-shortening response of plate 3 for the two cases, while Figure 8.18 shows the USL prediction for different plate thicknesses.

Discussion and conclusion

Figure 8.17 shows that the initial stiffness of the two cases are equal. This is natural since the initial imperfection is based on a standard linear elastic buckling computation, which only includes deflection of the plate. The difference between the two load-shortening paths increases as the load increases. Free in-plane bending along the edge at $y = 0$ gives, as expected, a more flexible confguration. This is natural since the straight edge assumption

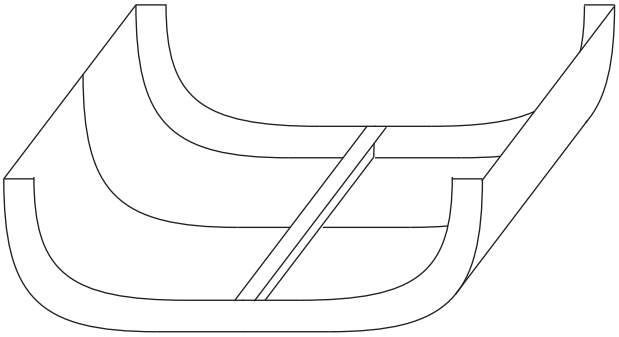

Figure 8.16: A ship's hull including a typical plate with a stiffened free edge.

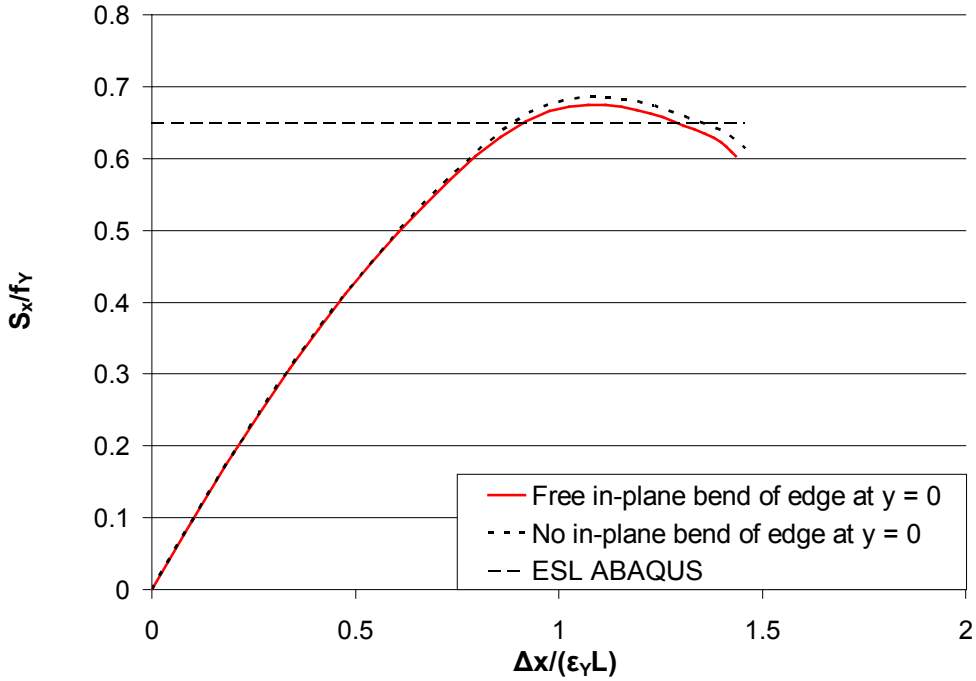

Figure 8.17: Load-shortening curves for plate 3 with the edge at $y = 0$ straight or free to bend in plane. The ESL prediction is also included to indicate the slenderness of the plate.

increases the stiffness of the system. The relative difference in the USL prediction is less than 2 percent and the approximation is good.

When varying the thickness, as done in Figure 8.18, it is observed that the difference decreases as the thickness increases. An increased thickness of the plate results in reduced deflections, implying that the load is carried directly as membrane stresses in the plate. The difference between the USL estimates is negligible for all the plate thicknesses studied here. More tests should still be performed to ensure that the USL estimate, from the current semi-analytical model, can be used for cases as in Figure 8.16.

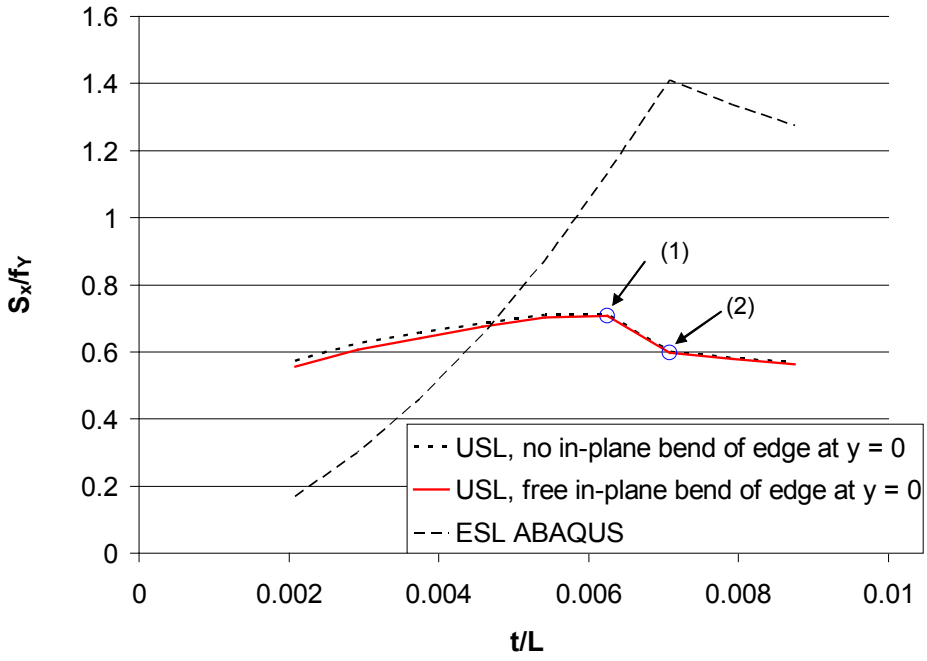

Figure 8.18: The USL and ESL prediction for plate 3 as the plate thickness is varied. The stiffener height, h_s, will be 150 mm for all cases. Point (1) and point (2) refers to Figure 8.19 and will be discussed further in Section 8.3.4.

8.3.4 Assumed imperfection shape

Figure 8.18 shows a decrease in the ultimate strength limit (USL) when the thickness, t, exceeds approximately 15 mm. The curve changes quite drastic between point (1), corresponding to $t = 15$ mm, and point (2), corresponding to $t = 17$ mm. Plots of the first linear elastic buckling shape corresponding to point (1) and point (2) are given in Figure 8.19. Figure 8.19a shows that the first buckling shape is local for point (1), while Figure 8.19b indicates a more global first buckling shape for point (2). The change in first buckling mode is also indicated by the change in the ESL curve in Figure 8.19. When studying the load-response of the plate case corresponding to point (1), it is observed that the initial local imperfection is dominated by a global deflection as the load increases. This significant change in deflection shape indicates that a global buckling shape should be used when estimating the USL. When testing a more global mode for a plate with thickness $t = 15$ mm it is observed that the USL prediction is reduced by approximately 14 percent. This indicates that a combination of a local and a global mode, as done in Section 7.2, should be used when estimating the USL.

If a combined local and global mode is used as imperfection the curve in Figure 8.18 is expected to smoothen, but the USL stress prediction is still expected to reduce as the thickness becomes sufficiently large. This can be motivated by studying the Euler buckling

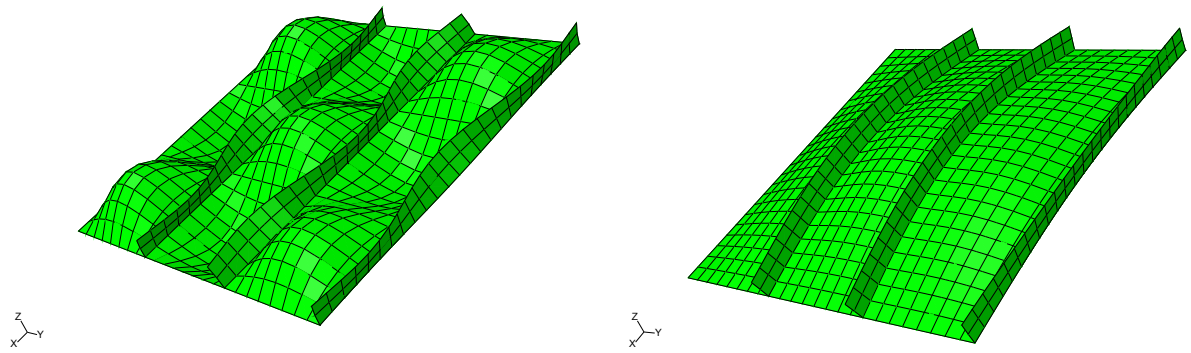

(a) Point (1) **(b)** Point (2)

Figure 8.19: The first linear elastic buckling mode corresponding to plate cases at point (1) and point (2) in Figure 8.18

stress of a simply supported column:

$$\sigma_{cr} = \frac{\pi^2 EI}{A_p L_s^2} \tag{8.1}$$

where σ_{cr} denotes the critical axial stress of the column, EI denotes the bending stiffness, A_p denotes the cross sectional area of the plate part included in the column section and L_s gives the length of the column. The plate area of the column cross section, A_p, is used to calculate the elastic buckling stress σ_{cr}, since the external stress, S_x, on the plate is defined by $S_x = P_x/A_{plate}$.

From Figure 8.18 it is observed that the reduction in linear elastic buckling stress is present for the cases dominated by global buckling. The global buckling behaviour of the characteristic plate section for one of the inner stiffeners, see Figure 8.20, should be similar to the one of a column with the same characteristic cross section and simply supported ends. The breadth of the column, b_s, should be equal to the stiffener spacing and $L_s = L$.

The second moment of inertia, for bending along a beam, about the neutral axis, I, with the cross section in Figure 8.20 is:

$$I = \frac{t_w(h_w - \frac{t}{2})^3}{12} + \frac{b_s t^3}{12} + t_w \left(h_w - \frac{t}{2}\right)\left(\frac{h_w}{2} + \frac{t}{4} - z_{NA}\right)^2 + b_s t z_{NA}^2 \tag{8.2}$$

where

$$z_{NA} = \frac{\frac{1}{2}\left(h_w + \frac{t}{2}\right) h_w t_w}{b_s t + \left(h_w - \frac{t}{2}\right) t_w}$$

The cross sectional area, A, and the second moment of inertia, I, are the only parameters in Equation 8.1 that changes as the plate thickness varies. The effect of changing the thickness of the plate will then be governed by the ratio $\frac{I}{A}$. If $\frac{I}{A}$ decreases as the plate thickness, t, increases then the buckling load will be reduced. The linear elastic buckling stress from the column approach is compared to the first linear elastic buckling stress from

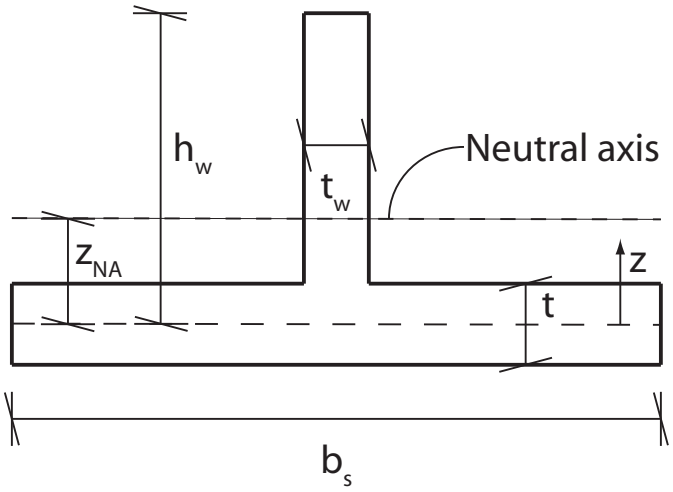

Figure 8.20: The equivalent beam cross section used in the column approach presented in this section.

ABAQUS in Figure 8.21. The column approach gives very good estimates for the range of plate thicknesses (t) corresponding to globally dominated first buckling shapes. Including the column approach was done to explain the behaviour observed in Figure 8.18.

The reduction of USL stress in Figure 8.18 relates to the reduction of the linear elastic buckling stress. A reduction in buckling stress implies a more non-linear deflection response causing larger plastic and geometrical redistribution of stresses and a lower USL stress. A reduction of the USL stress as the plate thickness is increased implies a less efficient design and such plates should not be used in real structures.

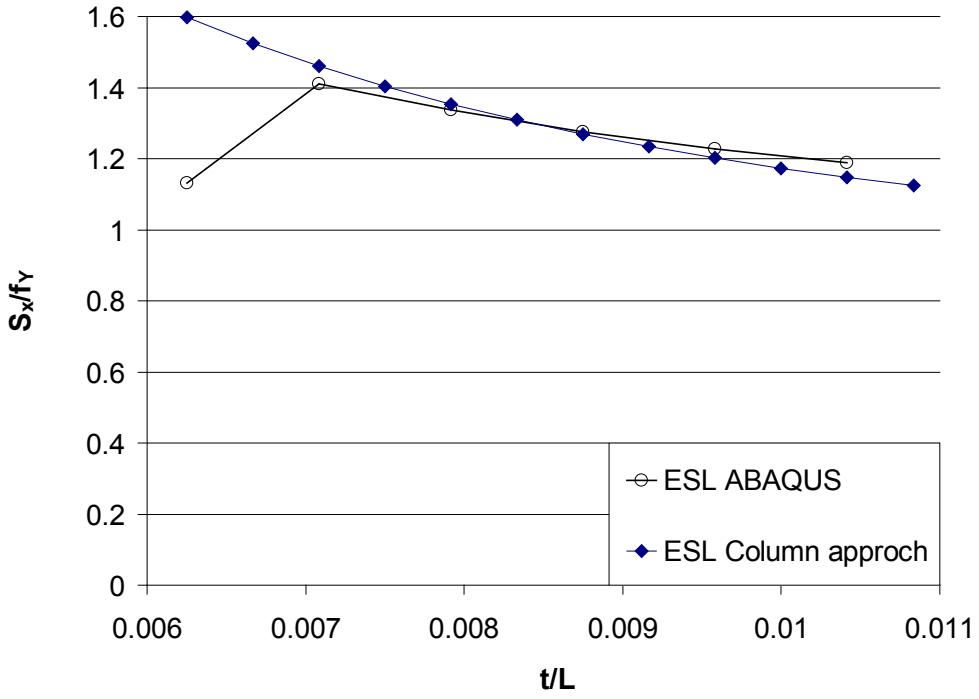

Figure 8.21: Comparison of the column approach, based on the Euler buckling stress, and the ABAQUS results for first linear elastic buckling stress. The thickness of the plate 3 is varied from $t = 15$ mm to $t = 26$ mm.

Chapter 9

Conclusion

9.1 General overview

Several different criteria for estimating ultimate strength (collapse) limit of unstiffened and stiffened plates with a free edge were developed in this thesis. The selected criteria for unstiffened and stiffened plates are consistent, giving a smooth transition from the unstiffened to the stiffened case. The selected plate criteria include a correction factor, for surface yielding, which is combined with the highest von Mises membrane stress in the plate. This correction factor is somewhat different for the unstiffened and stiffened case. A stiffener reduction, accounting for stiffener yielding, was also included for the stiffened cases.

The criteria were tuned to match ABAQUS results for both the unstiffened and stiffened case. This tuning was performed using the first elastic buckling mode as imperfection, and good estimates was obtained. An imperfection similar to the elastic first buckling mode will be expected for unstiffened plates because of the free edge. For the stiffened case the deformation shape is expected to be somewhat more complex in the transition from a global to a local elastic buckling shape. It is then natural to use a combination of a local and a global imperfection shape for the stiffened cases. This assures that the critical mode is easily triggered for all cases. Tests of the criterion for such combined imperfections were also done. The imperfections amplitudes used for combined imperfections was the same as used in the PULS code for the local and global mode of a simply supported stiffened plate. Strength estimates for combined imperfections was satisfactory for the test cases.

When testing the ultimate strength criteria in Chapter 5 a fixed imperfection amplitude of 5 mm is used. This imperfection amplitude was also used by Brubak [2]. The actual imperfection amplitude, in real structures, will depend on the thickness and slenderness of the plate. Thick stocky plates will be expected to have a very small imperfection, while thin slender plates will be expected to have a significant imperfection amplitude. These dependencies are not accounted for in the current work, since the main aspect is to develop a suitable criterion for strength (collapse) assessment. In Section 7.2 the effect of using model imperfections, combining a local and global mode, for stiffened plates is examined.

The local and global mode then includes the preferred/critical mode for all the plate cases. Imperfection amplitudes are then dependent on the stiffener spacing, s, and the length, L, of the plate. These amplitudes should probably also be dependent on the slenderness and thickness of the plate, but this is not addressed further here. The model imperfections are assumed to be in the preferred/critical mode of the plate, while real imperfection patterns for welded structures will be much more complex and random in nature. Using the preferred/critical mode should give conservative estimates of the ultimate strength in practical applications.

Torsional stiffness of stiffeners was also considered. This effect was tested by including the potential energy contribution due to St. Vernant torsion, into the equations of stationary potential energy. It will always be conservative to neglect the torsional rigidity of the stiffeners, since this reduces the overall stiffness of the system. The tests performed indicated that the effect was quite small. These observations motivate the exclusion of torsional stiffness of the stiffeners from the final model.

The uniformly applied load in combination with the parallel edge (uniform compression) assumption in the longitudinal direction implies a complex resultant load system. This resultant loading has to be a combination of a normal force and a moment and is implicitly included in the semi-analytical model. The assumption of a uniform compression is natural since the plate is connected to other plates, which are expected to give a uniform support along the connected edge. The actual loading distribution is probably somewhat more complex, and the uniform distribution used here is a simplification. It is still assumed that this distribution gives reasonable estimates for the ultimate strength limit.

The tests of model assumptions in Chapter 8 did not indicate any severe problems with regards to applications of the model. Further tests should still be conducted, due to the limited number of test cases, if general conclusions should be drawn.

9.2 Further work

The stiffened plate cases studied in this thesis are quite limited with respect to the stiffeners. It only includes longitudinal eccentric flat bar stiffeners. Both transverse stiffeners and other cross sectional profiles will be expected in real structures. Such stiffener profiles might be a T-bar, L-bar or bulb stiffener. The stiffener at the stiffened free edge will, in practical cases, often be symmetric. Including several types of stiffener profiles is a natural expansion of the current model. Inclusion of stiffeners with a T- or L-profile might give problems with the stiffener reduction scheme. Removing the flange of such profiles will imply a large change in stiffness and might give problems in the incremental calculations. Local buckling of the stiffener web might be present for stiffener profiles with a flange. The flange will, in such cases, have a large in-plane bending stiffness resisting sideways movement at the top of the web. Including symmetrically placed transverse (normal to the free edge) stiffeners should not give severe problems in the current formulation of the criterion. A symmetric stiffener at the free edge should also be easy to implement.

Further considerations regarding selection of the appropriate solution when the original

solution condition gives backward stepping (along the same curve) must be conducted. This problem was, as mentioned in Section 5.3.2 and discussed further in Appendix A.4, avoided by selecting the solution giving an increase in the end shortening for the problem plate cases. It is desirable to find an automatic procedure for selecting the correct solution along the path for all cases, if the model should be used for practical applications.

Computational time of the current model is high. The model and FORTRAN code must be improved to make the model practically relevant. Several things can be done to improve the calculation time and the following solutions are proposed here:

- *Scaling the arc length increment in the numerical algorithm.* The arc length increment should be set in accordance with the range of the expected ultimate strength limit. A long arc length increment will for instance be applicable when the elastic buckling stress is significantly higher than the yield stress. In such cases the response will be almost linear and large steps will give good results. The practical arc length increment will in the current model be dependent on the thickness of the plate, see Equation 3.32. A small plate thickness implies a small arc length increment. This is a natural correlation for unstiffened plates, but not necessarily for stiffened plates. The best way of improving the model, with respect to arc length increments, will be to include an procedure for selecting suitable arc length increments. Then a smaller number of increments will be used in ranges with almost linear response and a higher number of increments will be present when the response is non-linear.

- *Adjusting the number of terms in the displacement assumption.* In this thesis the number of terms used was selected to ensure reasonable estimates for all cases. It is possible to select the number of terms based on the expected deformation shape. This can be done by evaluating ratios between length and breadth, stiffener spacing and length etc. Such consideration could significantly reduce the calculation time, since the total number of degrees of freedom will be reduced. Considerations with regards to stress convergence should be carried out if this approach is investigated.

- *Changing the procedure for building matrices.* The non-linear matrices are built directly for each increment in the current code. This is not a computationally efficient way of calculating the matrices since a lot of loops will be repeated. The non-linear matrices consist of several constant matrix contributions, weighted with the current displacement amplitudes. Defining these constant matrix contributions up front and weighting them with the correct displacement amplitude for each increment will improve the efficiency significantly.

REFERENCES

[1] H.M. Eiding. Knekning av avstivede plater med variable randbetingelser (Buckling of stiffened plates with various boundary conditions), M.Sc. thesis, Mechanics Division, Department of Mathematics, University of Oslo, Norway, 2007, 87 pp.

[2] Lars Brubak. Semi-analytical postbuckling analysis of stiffend plates with a free edge, Research report in mechanics, No. 03-12, Mechanics Division, Dept. of Mathematics, University of Oslo, Norway, 2008, 98 pp

[3] Det Norske Veritas. Recommended practice DNV-RP-C201, Buckling strength of plated structures, Høvik, Norway, 2002

[4] E. Steen. Application of the perturbation method to plate buckling problems, Research Report in Mechanics, No. 98-1, Mechanics Division, Dept. of Mathematics, University of Oslo, Norway, 1998, 60 pp.

[5] Lars Brubak and Jostein Hellesland. Semi-analytical postbuckling and strength analysis of arbitrarily stiffened plates in local and global bending, Thin-Walled Structures, 2007; 45(6), 620–633

[6] Lars Brubak and Jostein Hellesland. Strength criteria in semi-analytical, large deflection analysis of stiffened plates in local and global bending, Thin-Walled Structures, 2008; 46(12), 1382–1390

[7] Det Norske Veritas. Nauticus Hull, User Manual, PULS Høvik, Norway, 2009

[8] E. Byklum. Ultimate strength analysis of stiffened steel and aluminium panels using semi-analytical methods, Dr. Ing. thesis, Norwegian University of Science and Technology, Trondheim, Norway, 2002

[9] Paik J, Thayamballi A, Lee S, Kang S. A semi-analytical method for the elastic-plastic large deflection analysis of welded steel or aluminium plating under combined in-plane and lateral pressure loads., Thin-Walled Structures, 2001; 39: 125–152

[10] J.K. Paik and M.S. Lee, A Semi-analytical method for the elastic-plastic large deflection analysis of stiffened panels under combined biaxial compression/tension, biaxial in-plate bending, edge shear, and lateral pressure loads, Thin-Walled Structures, 2005; 43(3): 375–410

[11] Z.P. Bažant and L. Cedolin. Stability of structures, Oxford University Press, 1991

[12] P.P. Benham, R.J. Crawford and C.G. Armstrong. Mechanics of Engineering Materials, Prentice Hall, Harlow, second edition, 1996, 641 pp

[13] Karl Rottmann. Matematisk formelsamling (Norwegian edition), Spektrum forlag, Oslo 9. edition, 2006

[14] K. Marguerre. Zur theorie der gekrümmten platte grosser formänderung, Proceedings of The 5^{th} International Congress for Applied Mechanics, 1938; 93–101

[15] R. D. Cook, D. S. Malkus, M. E. Plesha and R. J. Witt. Concepts and applications of finite element analysis, John Wiley & Sons, fourth edition, 2002, 719 pp

[16] D.O. Brush and B.O. Almroth. Buckling of bars, plates and shells, McGraw-Hill Book Company, 1975

[17] L. Brubak, J. Hellesland and E. Steen. Semi-analytical buckling strength analysis of plates with arbitrary stiffener arrangements, Journal of Constructional Steel Research, 2007; 63(4): 532–543

[18] Dassault Systèmes Simulia Corp., ABAQUS Documentation Manual 6.9, Providence, RI, USA, 2009

Appendix A

Strength criteria

A.1 Selection of the constant B for UP2

The value of B in criterion UP2, see Section 5.2.1, will be determined through tuning with finite element analyses. Two suitable values for B are presented in Figure A.1 for the different dimensions and thicknesses selected in Section 5.2.2. $B = 2$ is selected based on the results presented in Figure A.1.

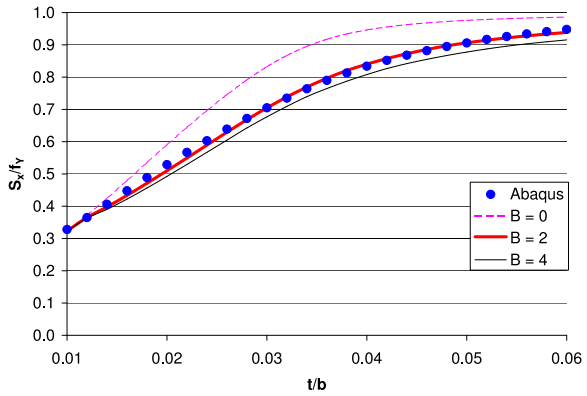

(a) 1000x1000

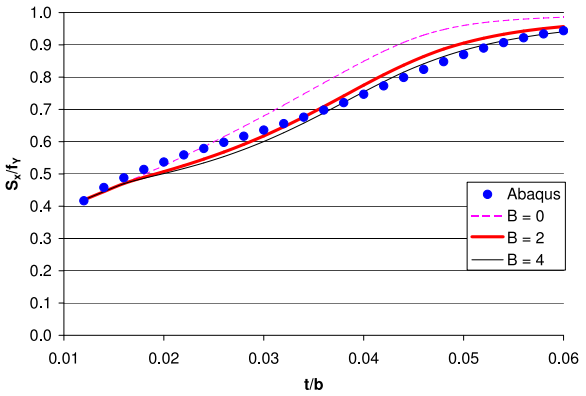

(b) 2000x1000

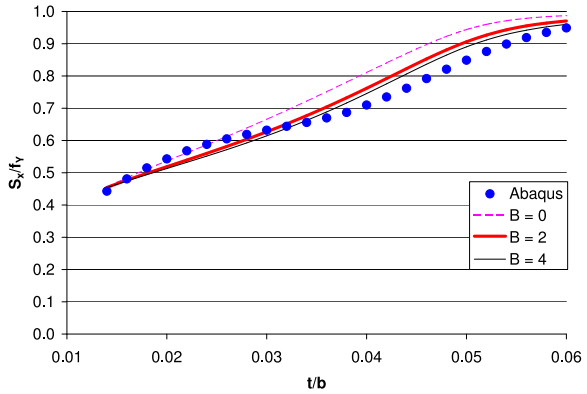

(c) 3000x1000

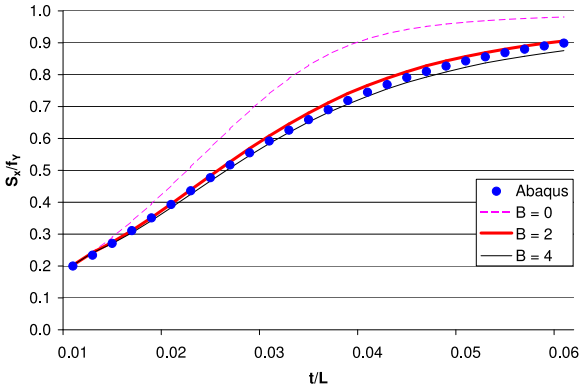

(d) 1000x2000

Figure A.1: Ultimate strength predictions, for plate cases in table 5.1, with criterion UP2 for different B values compared with ABAQUS predictions.

A.2 Selection of the constant c for UP3

The best value for c in criterion UP3, see Section 5.2.1, is found by tuning the results of the semi-analytical model with results from finite element analyses. The ultimate strength limit versus plate thickness for the two most suitable values of c is presented in Figure A.2. These plots shows that c = $\frac{1}{4}$ gives the best overall correspondence for the plates presented and this value of c is used in Section 5.2.3.

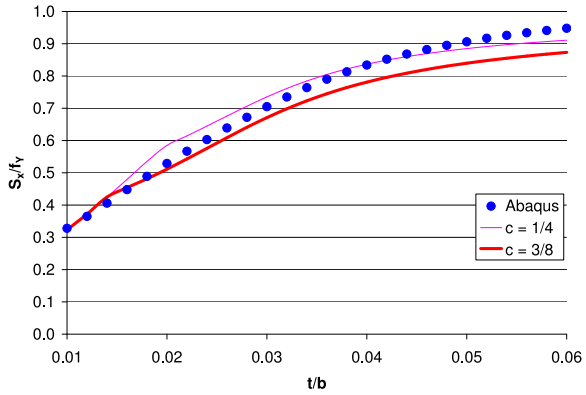

(a) 1000x1000

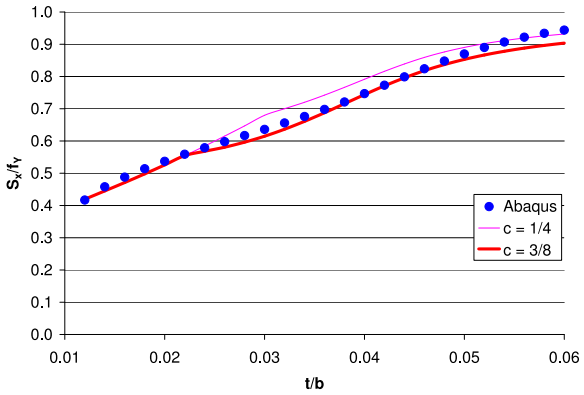

(b) 2000x1000

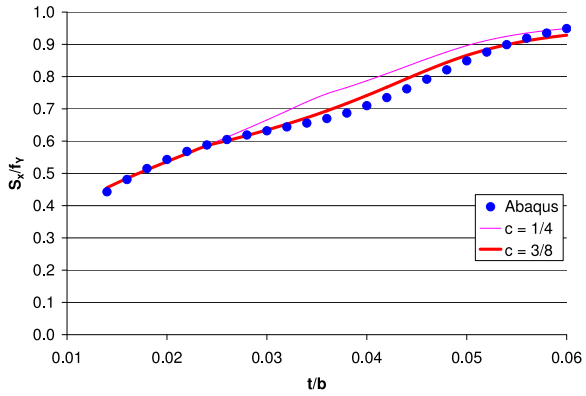

(c) 3000x1000

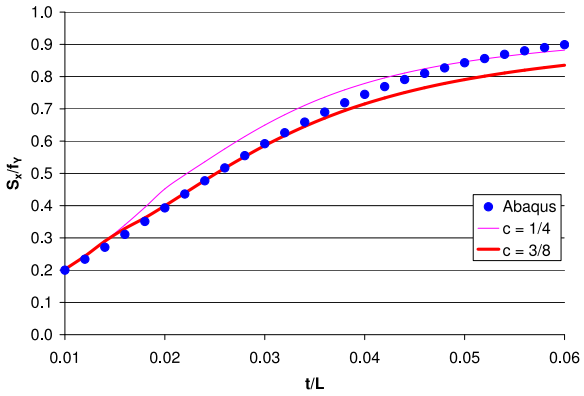

(d) 1000x2000

Figure A.2: Ultimate strength predictions, for plate cases in table 5.1, with criterion UP3 for different c values compared with ABAQUS predictions.

A.3 B_{mod} comparison

Comparison of the linear variation of B_{mod}, SP_LINEAR, and the selected variation, SP, is presented here for the plates cases in table A.1. Results with the original UP2 criterion is also included to motivate the need for $B_{mod} = B_{mod}(w_{t,edge}/w_{t,max})$. UP2 will, as for SP, be applied, separately, to the line(s) representing maximum Von Mises membrane stress along the edge at $y = 0$. The tests performed here will use the same number of terms as described in Section 5.3.3.

Figure A.3 shows the ultimate strength limit (USL) estimates for the different plate criteria combined with the reduced stiffener height criterion (SS1) presented in Section 5.3.2.

Plate	N_{stiff}	L (mm)	b (mm)	t (mm)	t_w (mm)	h_w (mm)
1000x1000$_3$	3	1000	1000	12	10	[16-116]
2400x2523$_3$	3	2400	2523	11	12	[45.5-205.5]

Table A.1: The plate cases selected when comparing the linear and selected B_{mod} with the original B value. Stiffeners are equally spaced and N_{stiff} gives the total number of stiffeners. The name convention used is LXB$_{N_{stiff}}$.

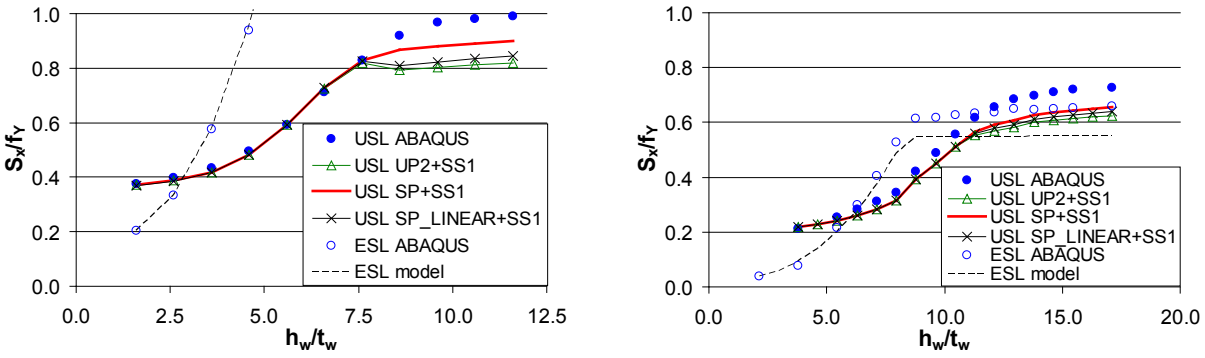

(a) 1000X1000$_3$ **(b)** 2400X2523$_3$

Figure A.3: Ultimate strength limits (USL) and elastic buckling strength limits (ESL) for (a) 1000X1000$_3$ and (b) 2400X2523$_3$(see table A.1). ABAQUS results are included for comparison.

It is seen that the selected B_{mod} variation, SP, gives the best accordance with ABAQUS results. This is natural due to the asymptotic behaviour of the selected B_{mod} variation as the free edges approaches a simply supported condition. The original UP2 criterion gives considerable conservative deviation especially for 1000X1000$_1$, indicating that a modification of B is necessary.

A.4 Problem with criterion for solution selection

Problem with tracing the load response behaviour was observed when a combination of the modified stress combination criterion (SP) and the reduced stiffener height (SS1) was applied to the cases with combined imperfections in Section 7.2. Two problem cases were observed. These problem cases both have two stiffeners, $L = 2400$ mm, $B = 2523$ mm, $t = 11$ mm and $t_w = 12$ mm, and the only difference between them is the stiffener height. The first problem case has $h_w = 65.5$ mm and the second one has $h_w = 75.5$ mm.

The incremental procedure produces two possible load rates, see Equation 3.32, and the smoothest one, with respect to all the displacements components, was selected by satisfying Equation 3.33. Results produced using the condition in Equation 3.33 to trace the solution will be denoted by Model A. Another model is also introduced, Model B, where the solution producing an increase in the x-direction end shortening is selected. Load-shortening curves for the two problem plates are given in Figure A.4 and Figure A.5. The unphysical behaviour for Model A, with reduced load factor and shortening, is avoided in Model B by selecting the load rate giving an increase in the shortening of the plate. Model B is then used for these two cases to ensure reasonable estimates, while Model A still will be used for all the cases where this problem is not present. Model A is used for the rest of the cases to ensure that snapping and similar physical behaviours can be modelled. Further considerations regarding the choice of solution should be performed if the model should be used in practical applications. The present version of the FORTRAN code will issue a warning if such unphysical behaviour is encountered.

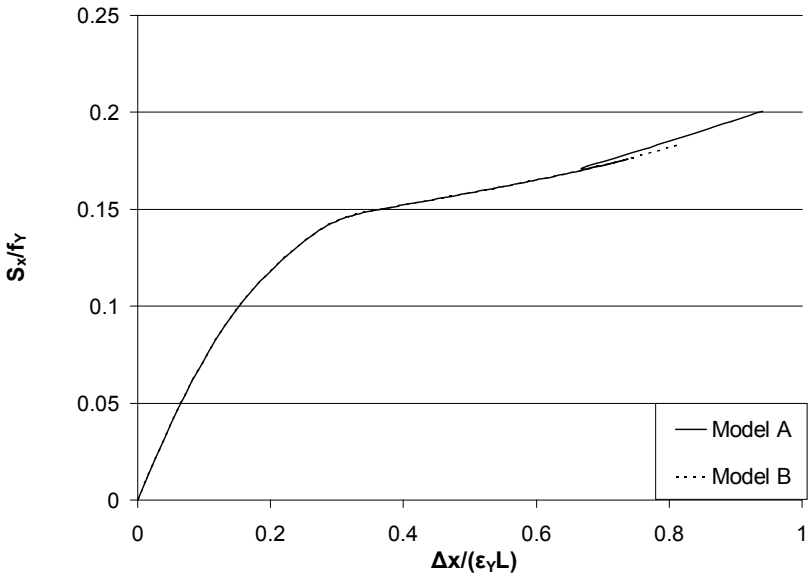

Figure A.4: Load-shortening curves for a case with two stiffeners, $L = 2400$ mm, $B = 2523$ mm, $t = 11$ mm and $t_w = 12$ mm and $h_w = 65.5$ with the original condition (Model A) and the shortening condition (Model B). The end-point of the curves gives the ultimate strength limit estimates.

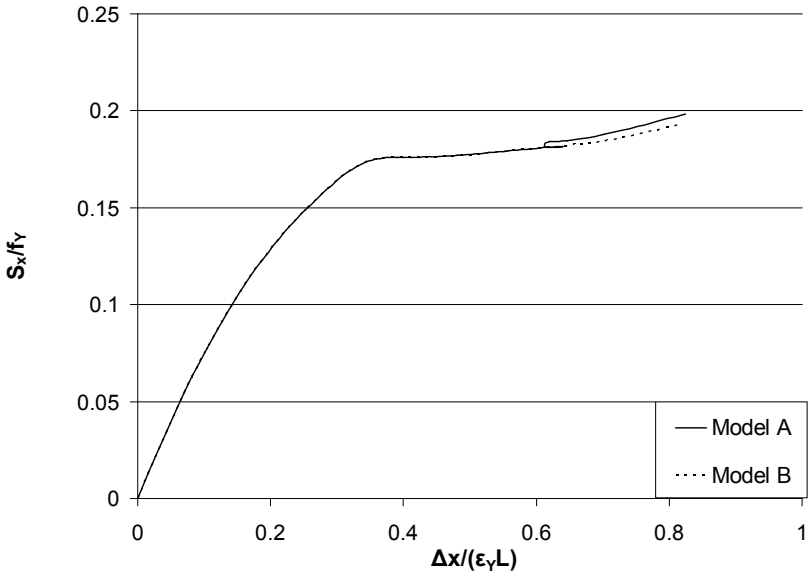

Figure A.5: Load-shortening curves for a case with two stiffeners, $L = 2400$ mm, $B = 2523$ mm, $t = 11$ mm and $t_w = 12$ mm and $h_w = 75.5$ with the original condition (Model A) and the shortening condition (Model B). The end point of the curves gives the ultimate strength limit estimates.

A.5 Testing of alternative stiffener criteria

Results for the modified stress combination criterion for the plate (SP) combined with the first yield criterion for stiffeners (SS2) and the interaction criterion for stiffeners (SS3) will be presented here. These results were not included earlier since they gave too conservative estimates, for small stiffeners, when compared to ABAQUS results. Ultimate strength limit (USL) estimates for the cases with one stiffener in table 5.2 will be presented here. The same parameters as in Section 5.3.3 is used.

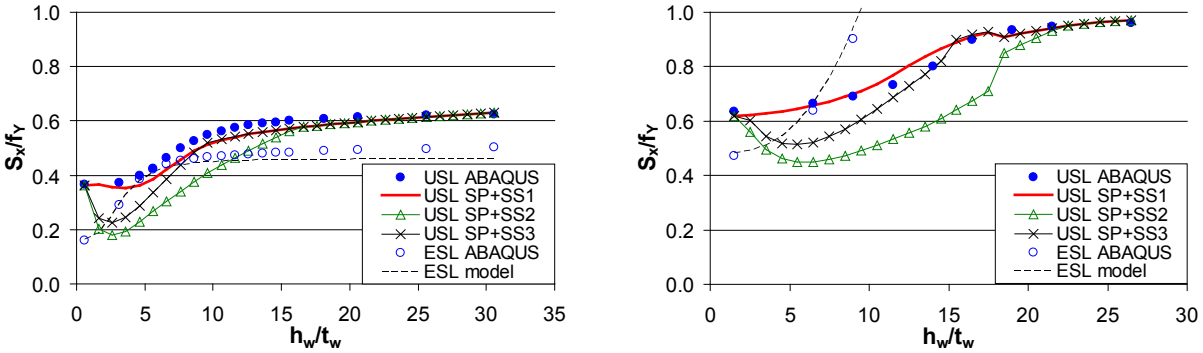

(a) $1000X1000_1$ **(b)** $2000X1000_1$

Figure A.6: Ultimate strength limits (USL) and elastic buckling strength limits (ESL) for (a) $1000X1000_1$ and (b) $2000X1000_1$ with the different stiffener criteria presented earlier (plate definitions are given in table 5.2). ABAQUS results are included for comparison.

Figure 5.7 includes all the stiffener criteria in combination with the modified stress combination criterion (SP) for the cases with one stiffener. It is observed that SS2 and SS3 give considerable conservative estimates for the approximately unstiffened cases with small stiffener. As the stiffened free edge approaches simply supported all the combined criteria give the same estimates. In such cases the stiffeners remain almost undeformed, due to the large bending stiffness of high stiffeners. Small deformations of the stiffener imply small stiffener bending stresses and limited, or no, yielding at the top of the stiffener. The ultimate strength limit (USL) estimates found using SS2 and SS3 decrease, for small stiffeners, as the stiffener height increases. This is a result of small stiffness contributions from the stiffeners, relative to the plate stiffness, implying an almost unstiffened case. For such cases the stiffener height will increase without a corresponding increase in the overall stiffness. This results in a reduction of first stiffener yield, for small stiffeners, as the stiffener height is increased. Conservative results for SS2 and SS3 is also observed for the other plate cases and the SS1 is then selected.

Appendix B

Incremental stiffness matrix due to St. Venant Torsion

The expressions for the incremental stiffness due to St Venant torsion in the stiffeners were not derived in Brubak [2]. The derivation of these expressions is therefore included in the following report.

The incremental stiffness matrix for the St. Venant torsion contribution for longitudinal stiffeners, $\mathbf{K^{sT,x}}$, will be subdivided in the same manner as the stiffness matrices derived in Brubak [2]. This gives the following structure:

$$\mathbf{K^{sT,x}} = \begin{bmatrix} \mathbf{K}_{uu}^{sT,x} & \mathbf{K}_{uv}^{sT,x} & \mathbf{K}_{uw}^{sT,x} \\ \mathbf{K}_{vu}^{sT,x} & \mathbf{K}_{vv}^{sT,x} & \mathbf{K}_{vw}^{sT,x} \\ \mathbf{K}_{wu}^{sT,x} & \mathbf{K}_{wv}^{sT,x} & \mathbf{K}_{ww}^{sT,x} \end{bmatrix} \tag{B.1}$$

The stiffness matrix (see Section 3.5.2) contribution due to St. Venant torsion of longitudinal stiffeners will be given by:

$$K_{ij}^{sT,x} = \frac{\partial^2 U^{sT,x}}{\partial d_i \partial d_j} \tag{B.2}$$

where $U^{sT,x}$ is the potential strain energy of a longitudinal stiffeners. The expression for the potential energy is restated here for simplicity:

$$U^{sT,x} = \frac{GJ}{2} \int_0^L w_{,xy}^2|_{y=y_s} dx \tag{B.3}$$

where y_s is the y-coordinate of the longitudinal stiffener. The assumed deflection shape, given in Section 3.2, is restated here for simplicity:

$$w(x,y) = w^a(x,y) + w^b(x,y)$$

where

$$w^a(x,y) = \sum_{i=1}^{M_{wa}} w_i^a \frac{y}{b} \sin(\frac{\pi i x}{L}) \tag{B.4}$$

and

$$w^b(x,y) = \sum_{i=1}^{M_{wb}} \sum_{j=1}^{N_{wb}} w_{ij}^b \sin(\frac{\pi i x}{L}) \sin(\frac{\pi j y}{b}) \tag{B.5}$$

It will necessary to necessary to find $w^a_{,xy}$ and $w^b_{,xy}$, since the energy expression in Equation B.3 contains $w_{,xy}$. Based on the assumed deflection shapes these derivatives will be:

$$w^a_{,xy}(x,y) = \sum_{i=1}^{M_{wa}} w_i^a \frac{1}{b} \frac{\pi i}{L} \cos(\frac{\pi i x}{L}) \tag{B.6}$$

$$w^b_{,xy}(x,y) = \sum_{i=1}^{M_{wb}} \sum_{j=1}^{N_{wb}} w_{ij}^b \frac{\pi i}{L} \frac{\pi j}{b} \cos(\frac{\pi i x}{L}) \cos(\frac{\pi j y}{b}) \tag{B.7}$$

The expression for potential strain energy, see Equation B.3, can be written as follows:

$$U^{sT,x} = \frac{GJ}{2} \int_0^L \left[(w^a_{,xy})^2 + 2 w^a_{,xy} w^b_{,xy} + (w^b_{,xy})^2 \right]_{y=y_s} dx \tag{B.8}$$

Using Equation B.6 and Equation B.7 the terms in the parentheses can be written as:

$$(w^a_{,xy}|_{y=y_s})^2 = \textstyle\sum_{i=1}^{M_{wa}} \sum_{j=1}^{M_{wa}} w_i^a w_j^a \frac{1}{b^2} \frac{\pi i}{L} \frac{\pi j}{L} \cos(\frac{\pi i x}{L}) \cos(\frac{\pi j x}{L})$$

$$2(w^a_{,xy} w^b_{,xy})|_{y=y_s} = 2 \textstyle\sum_{i=1}^{M_{wa}} \sum_{j=1}^{M_{wb}} \sum_{k=1}^{N_{wb}} w_i^a w_{jk}^b \frac{\pi i}{L} \frac{\pi j}{L} \frac{\pi k}{b} \frac{1}{b} \cos(\frac{\pi i x}{L}) \cos(\frac{\pi j x}{L}) \cos(\frac{\pi k y_s}{b})$$

$$(w^b_{,xy}|_{y=y_s})^2 = \textstyle\sum_{i=1}^{M_{wb}} \sum_{j=1}^{N_{wb}} \sum_{k=1}^{M_{wb}} \sum_{l=1}^{N_{wb}} w_{ij}^b w_{kl}^b \frac{\pi i}{L} \frac{\pi j}{b} \frac{\pi k}{L} \frac{\pi l}{b} \cos(\frac{\pi i x}{L}) \cos(\frac{\pi k x}{L}) \cos(\frac{\pi j y_s}{b}) \cos(\frac{\pi l y_s}{b})$$

Only integrals of the following form will be encountered when integrating these terms over the length of the stiffener:

$$\int_0^L \cos(\frac{\pi p x}{L}) \cos(\frac{\pi q x}{L}) dx = \frac{L}{2} \delta_{pq} \tag{B.9}$$

where δ is the Kronecker delta defined by:

$$\delta_{pq} = \begin{cases} 1, & p = q \\ 0, & p \neq q \end{cases} \tag{B.10}$$

To find the sub matrix $\mathbf{K}^{sT,x}_{ww}$ it is convinient to split this matrix into several new sub matrices:

$$\mathbf{K}^{sT,x}_{ww} = \begin{bmatrix} \mathbf{K}^{sT,x}_{wawa} & \mathbf{K}^{sT,x}_{wawb} \\ \mathbf{K}^{sT,x}_{wbwa} & \mathbf{K}^{sT,x}_{wbwb} \end{bmatrix} \tag{B.11}$$

where for instance:

$$\mathbf{K}^{sT,x}_{wawb} = \frac{\partial^2 U^{sT,x}}{\partial w_i^a \partial w_{jk}^b} = \begin{bmatrix} \frac{\partial^2 U^{sT,x}}{\partial w_1^a \partial w_{11}^b} & \frac{\partial^2 U^{sT,x}}{\partial w_1^a \partial w_{12}^b} & \cdots & \frac{\partial^2 U^{sT,x}}{\partial w_1^a w_{MwbNwb}^b} \\ \vdots & \vdots & & \vdots \\ \frac{\partial^2 U^{sT,x}}{\partial w_{Nwa}^a \partial w_{11}^b} & \frac{\partial^2 U^{sT,x}}{\partial w_{Nwa}^a \partial w_{12}^b} & \cdots & \frac{\partial^2 U^{sT,x}}{\partial w_{Nwa}^a w_{MwbNwb}^b} \end{bmatrix}$$

Using the integral in Equation B.9 and the sum formulations above the sub matrices of $\mathbf{K}_{ww}^{sT,x}$ can be written, in index notation, as follows:

$$\mathbf{K}_{wawa}^{sT,x}\dot{\mathbf{w}}^a = \frac{\partial^2 U^{sT,x}}{\partial w_i^a \partial w_j^a}\dot{\mathbf{w}}_j^a = \frac{GJ}{2}\sum_{i=1}^{M_{wa}}\sum_{j=1}^{M_{wa}}\frac{1}{b^2}\frac{\pi i}{L}\frac{\pi j}{L}\frac{L}{2}\delta_{ij}\dot{\mathbf{w}}_j^a = \frac{GJ\pi^2}{4Lb^2}\sum_{j=1}^{M_{wa}} j^2\dot{\mathbf{w}}_j^a \tag{B.12}$$

$$\mathbf{K}_{wawb}^{sT,x}\dot{\mathbf{w}}^b = \frac{\partial^2 U^{sT,x}}{\partial w_i^a \partial w_{jk}^a}\dot{\mathbf{w}}_{jk}^b = GJ\sum_{i=1}^{M_{wa}}\sum_{j=1}^{M_{wb}}\sum_{k=1}^{N_{wb}}\frac{\pi i}{L}\frac{\pi j}{L}\frac{\pi k}{b}\frac{1}{b}\cos(\frac{\pi k y_s}{b})\frac{L}{2}\delta_{ij}\dot{\mathbf{w}}_{jk}^b \tag{B.13}$$

Due to symmetry the matrix $\mathbf{K}_{wbwa}^{sT,x}$ will be given by:

$$\mathbf{K}_{wbwa}^{sT,x} = (\mathbf{K}_{wawb}^{sT,x})^T \tag{B.14}$$

$$\mathbf{K}_{wbwb}^{sT,x}\dot{\mathbf{w}}^b = \frac{\partial^2 U^{sT,x}}{\partial w_{ij}^b \partial w_{kl}^b}\dot{\mathbf{w}}_{kl}^b = \frac{GJ}{2}\sum_{i=1}^{M_{wb}}\sum_{j=1}^{N_{wb}}\sum_{k=1}^{M_{wb}}\sum_{l=1}^{N_{wb}}\frac{\pi i}{L}\frac{\pi j}{b}\frac{\pi k}{L}\frac{\pi l}{b}\cos(\frac{\pi j y_s}{b})\cos(\frac{\pi l y_s}{b})\frac{L}{2}\delta_{ik}\dot{\mathbf{w}}_{kl}^b \tag{B.15}$$

All of the non-zero sub matrices of $\mathbf{K}_{ww}^{sT,x}$ are now found. The rest of the sub matrices in Equation B.1 will be zero matrices since $U^{sT,x}$ only is dependent on $\mathbf{w}^a$ and $\mathbf{w}^b$ and not the rest of the displacement amplitudes in the $\mathbf{d}$ vector. This can be written as follows:

$$\begin{gathered}\mathbf{K}_{uu}^{sT,x} = \mathbf{0}, \quad \mathbf{K}_{\mathbf{uv}}^{\mathbf{sT,x}} = \mathbf{0}, \quad \mathbf{K}_{\mathbf{uw}}^{\mathbf{sT,x}} = \mathbf{0} \\ \mathbf{K}_{vu}^{sT,x} = \mathbf{0}, \quad \mathbf{K}_{\mathbf{vv}}^{\mathbf{sT,x}} = \mathbf{0}, \quad \mathbf{K}_{\mathbf{vw}}^{\mathbf{sT,x}} = \mathbf{0} \\ \mathbf{K}_{wu}^{sT,x} = \mathbf{0}, \quad \mathbf{K}_{\mathbf{wv}}^{\mathbf{sT,x}} = \mathbf{0}\end{gathered} \tag{B.16}$$